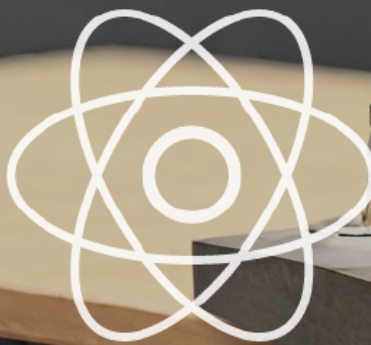


JOURNAL OF ENGINEERING RESEARCH & SCIENCES

JENRS



www.jenrs.com
ISSN: 2831-4085

Volume 1 Issue 10
October 2022

EDITORIAL BOARD

Editor-in-Chief

Prof. Paul Andrew
Universidade De São Paulo, Brazil

Editorial Board Members

Dr. Jianhang Shi

Department of Chemical and Biomolecular Engineering, The Ohio State University, USA

Dr. Sonal Agrawal

Rush Alzheimer's Disease Center, Rush University Medical Center, USA

Dr. Namita Lokare

Department of Research and Development, Valencell Inc., USA

Dr. Dongliang Liu

Department of Surgery, Baylor College of Medicine, USA

Dr. Xuejun Qian

Great Lakes Bioenergy Research Center & Plant Biology Department, Michigan State University, USA

Dr. Jianhui Li

Molecular Biophysics and Biochemistry, Yale University, USA

Dr. Atm Golam Bari

Department of Computer Science & Engineering, University of South Florida, USA

Dr. Lixin Wang

Department of Computer Science, Columbus State University, USA

Dr. Prabhash Dadhich

Biomedical Research, CellfBio, USA

Dr. Żywiłek Justyna

Faculty of Management, Czestochowa University of Technology, Poland

Prof. Kamran Iqbal

Department of Systems Engineering, University of Arkansas Little Rock, USA

Dr. Ramcharan Singh Angom

Biochemistry and Molecular Biology, Mayo Clinic, USA

Dr. Qichun Zhang

Department of Computer Science, University of Bradford, UK

Dr. Mingsen Pan

University of Texas at Arlington, USA

Editorial

This collection of research papers offers a rich tapestry of advancements across various fields, from sociopolitical frameworks to cutting-edge technology. The insights provided by these ten studies underscore the importance of interdisciplinary research in addressing complex challenges and driving innovation.

The first paper revisits the foundational principles of Dr. B.R. Ambedkar, focusing on his contributions to the Indian Constitution. It examines the reservation system, originally intended to create a classless and casteless society, and its implications in contemporary India. The paper critiques the current implementation of the reservation system, suggesting that it may now hinder economic and social development by perpetuating inequality. This critical analysis provides a platform for re-evaluating policies to better align with Dr. Ambedkar's vision of equality and justice [1].

In the realm of vehicle communication, the second paper introduces CANClassify, a method for decoding and labelling Controller Area Network (CAN) bus signals. By employing a novel convolutional interpretation method, CANClassify automates the process of interpreting raw CAN bus data. This innovation simplifies the complex task of signal decoding, offering a significant leap forward in automotive diagnostics and vehicle system monitoring [2].

The third paper addresses the challenges of high Peak-to-Average Power Ratio (PAPR) in Orthogonal Frequency Division Multiplexing (OFDM) modulation, a key technique for high-speed wireless communication. The researchers propose a Recursive Clipping and Filtering (RCF) technique to reduce PAPR, thereby enhancing Signal-to-Noise Ratio (SNR) and minimizing distortion. This work is crucial for improving the efficiency and reliability of modern communication networks, particularly in the context of AI, IoT, and 5G technologies [3].

Exploring agricultural productivity, the fourth paper evaluates soil fertility in Shirol Tehsil, Kolhapur district, Maharashtra, using a nutrient index approach. The study finds that the soil is fertile, with high potash levels contributing to superior sugarcane productivity compared to national averages. This comprehensive analysis of soil parameters provides valuable insights for developing sustainable agricultural practices and enhancing crop yields [4].

In the field of medical robotics, the fifth paper proposes a trajectory correction method for vertebral milling robots using force feedback. By defining motion description language atoms, the researchers address issues such as excessive milling and operator workload. The experimental results demonstrate the method's feasibility and effectiveness, marking a significant advancement in robotic surgery and precision medicine [5].

The sixth paper investigates the high-temperature properties of silicon carbide (SiC) ceramics with fractal lattices. Using molecular dynamics simulations, the study analyses the stress-strain behaviour and modulus changes of SiC crystals from room temperature to 1,250°C. The findings confirm the material's excellent high-temperature strength and thermal shock resistance, highlighting its potential for high-performance engineering applications [6].

The seventh paper explores the burgeoning field of smart physiotherapy, which aims to provide effective home-based exercise regimens for patients with physical anomalies. The study reviews recent advancements in automatic monitoring and guidance systems for physiotherapy exercises, identifying a gap in comprehensive applications. This research sets the stage for developing innovative solutions to support patient rehabilitation and improve healthcare outcomes [7].

Autonomous vehicles, the subject of the eighth paper, represent a transformative shift in road traffic management. The paper reviews recent advances in deep learning for autonomous vehicle research, offering insights into key technologies such as path planning, sensor fusion,

and data security. By identifying future research directions, this comprehensive review contributes to the ongoing development of safer and more efficient autonomous driving systems [8].

Finally, the ninth paper presents a fast method for constructing irregular pyramids in pattern recognition and image processing. By optimizing the selection of contraction kernels, the researchers enhance the efficiency of connected component labelling (CCL) and distance transform (DT) applications. This advancement in hierarchical structure processing has significant implications for managing the vast amounts of digital data generated daily [9].

Together, these papers illustrate the dynamic interplay between theory and application, showcasing how innovative research can drive progress across diverse fields. Whether addressing sociopolitical issues, enhancing technological capabilities, or improving healthcare and agricultural practices, these studies provide valuable contributions to our understanding and development of a better future.

References:

- [1] M.K. Ratanbhai, "Reservations - as a Step of Social Democracy: Review of Dr. Ambedkar's Principles," *Journal of Engineering Research and Sciences*, vol. 1, no. 10, pp. 1–4, 2022, doi:10.55708/js0110001.
- [2] P. Ngo, J. Sprinkle, R. Bhadani, "CANClassify: Automated Decoding and Labeling of CAN Bus Signals," *Journal of Engineering Research and Sciences*, vol. 1, no. 10, pp. 5–12, 2022, doi:10.55708/js0110002.
- [3] J. Singh, "An Approach for PAPR Reduction in OFDM System using RCF Technique," *Journal of Engineering Research and Sciences*, vol. 1, no. 10, pp. 13–18, 2022, doi:10.55708/js0110003.
- [4] C. Narvekar, M. Rao, "Assessment of Village-wise Soil Nutrients and their Effect on Sugarcane Productivity in Western Maharashtra, India," *Journal of Engineering Research and Sciences*, vol. 1, no. 10, pp. 19–25, 2022, doi:10.55708/js0110004.
- [5] W. Ding, Z. Liu, H. Wang, L. Cui, "Trajectory Correction Method of Motion Description Language of Vertebral Milling Robot based on Force Feedback," *Journal of Engineering Research and Sciences*, vol. 1, no. 10, pp. 26–35, 2022, doi:10.55708/js0110005.
- [6] S. Choi, E. Jekal, "Fractal Research to the Production of High-strength Materials," *Journal of Engineering Research and Sciences*, vol. 1, no. 10, pp. 36–44, 2022, doi:10.55708/js0110006.
- [7] A.A. Saleem, K. Zafar, M.A. Raza, Z. Kareem, M.- din, H.U.R. Siddiqui, S. Dudley, "IoT Based Smart Physiotherapy System: A Review," *Journal of Engineering Research and Sciences*, vol. 1, no. 10, pp. 45–55, 2022, doi:10.55708/js0110007.
- [8] J. Ren, R.N. Huang, J. Ren, H.A. Gabbar, "The Current Trends of Deep Learning in Autonomous Vehicles: A Review," *Journal of Engineering Research and Sciences*, vol. 1, no. 10, pp. 56–68, 2022, doi:10.55708/js0110008.
- [9] M. Banaeyan, W.G. Kropatsch, "Fast Labeled Spanning Tree in Binary Irregular Graph Pyramids," *Journal of Engineering Research and Sciences*, vol. 1, no. 10, pp. 69–78, 2022, doi:10.55708/js0110009.

Editor-in-chief

Prof. Paul Andrew

CONTENTS

<i>Reservations – as a Step of Social Democracy: Review of Dr. Ambedkar’s Principles</i> Mange Karan Ratanbhai	01
<i>CANClassify: Automated Decoding and Labeling of CAN Bus Signals</i> Paul Ngo, Jonathan Sprinkle, Rahul Bhadan	05
<i>An Approach for PAPR Reduction in OFDM System using RCF Technique</i> Juhi Singh	13
<i>Assessment of Village-wise Soil Nutrients and their Effect on Sugarcane Productivity in Western Maharashtra, India</i> Chhaya Narvekar, Madhuri Rao	19
<i>Trajectory Correction Method of Motion Description Language of Vertebral Milling Robot based on Force Feedback</i> Wei Ding, Zhaoming Liu, Hongwei Wang, Long Cui	26
<i>Fractal Research to the Production of High-strength Materials</i> Seoryeong Choi, Eunsung Jekal	36
<i>IoT Based Smart Physiotherapy System: A Review</i> Adil Ali Saleem, Kainat Zafar, Muhammad Amjad Raza, Zahid Kareem, Mui-zzud-din, Hafeez Ur Rehman Siddiqui, Sandra Dudley	45
<i>The Current Trends of Deep Learning in Autonomous Vehicles: A Review</i> Raymond Ning Huang, Jing Ren, Hossam A. Gabbar	56
<i>Fast Labeled Spanning Tree in Binary Irregular Graph Pyramids</i> Majid Banaeyan, Walter G. Kropatsch	69

Reservations - as a Step of Social Democracy: Review of Dr. Ambedkar's Principles

Mange Karan Ratanbhai *

Law Student, Parul Institute of Law, Parul University, Vadodara, 390025, India.

*Corresponding author: Mange Karan Ratanbhai, +91 9724788801, adv.karanmange@gmail.com

ABSTRACT: The paper aims to highlight the key frameworks of Dr. B.R. Ambedkar, his thoughts, philosophies, and goals behind the framing of the Indian constitution. Based on different theories and philosophies, the concept of the reservation system adopted by the Indian Constitution, and its relevance in today's scenario is being portrayed. Dr. Ambedkar's idea of a classless and casteless society is somewhat achieved but due to the undue advantages of the reservation system, the individuals are deprived of equality and equal opportunities. The rights of representation given to minors were for some time only but the parliament till today haven't changed this system which is a curse in the economic and social development of the nation.

KEYWORDS: Reservation, Minorities, Dr. Ambedkar Philosophies, Casteism, Indian Constitution, Right to representation

1. Introduction

The World's largest Written Constitution, the Indian Constitution is a bag of borrowings. The majority of the elements that are enshrined in the Constitution are taken from other countries. These countries were having different geographies, different societies, different classes of people, different cultural and religious practices, and altogether different ideologies. Being diverse, India borrowed the elements from these countries and molded them to frame the Indian Constitution.

After attaining freedom from the British, The Governance of the Whole Territory which was united to form the Union of India was in question. Indian at that point of time was in need of Legislation that will govern the nation and will protect the rights, integrity, and interests of the people of India. This legislation that will be the foundation of the Indian Government and regulatory systems, was the Indian Constitution. Framing of the Constitution for an Independent Nation that has attained its independence after years of struggle and countless sacrifices of the freedom fighters, needs to be done. For this purpose, in 1946, a Constituent committee was established under the chairmanship of Dr. Bhimrao Ambedkar, commonly known as Babasaheb [1].

Dr. Ambedkar always wanted equal representation and thus he adopted this system just to ensure that no unjust should be made to the underprivileged sections. They should get time and opportunities in order to come up and stand in the same row as other castes. Thus, Dr. Ambedkar was in favor of implementing reservation only and for 10 years only. But, In the Constituent Assembly on 25/08/1949, Objections of S. Nagappa and B. I. Muniswami Pillai were coming on the proposal of restricting the reservation of Scheduled Castes, Scheduled Tribes for only 10 years. They said that 10 years is a very short time period for the upliftment of these vulnerable sections of society. Dr. Ambedkar said I do not think that we should allow any change in this subject. If the status of Scheduled Castes does not improve in 10 years, it will not be beyond their intellect power to seek measures to achieve this protection [2].

2. Dr. Ambedkar's theory on Rights of Minorities

Dr. Ambedkar himself belongs to a Scheduled class where they were deprived of basic human rights. These classes were called and untouchables and there was a belief that they are not pure. If one touches them they will become impure, hence they use to live with many restrictions. They were not allowed to access public places; they were not a part of the society or township; they use to

reside in the outskirts of the village and had no dignified life. Exploitation, Ill-treatment, were rampant.

As per the formation of Ancient Indian societies, the people were divided on the basis of the occupation they are into. There used to be classifications based upon purity. The traders, soldiers, tailors, goldsmiths, zameendars, etc. belonged to a high classed society as the work they were doing was treated as pure. On the other hand, sweepers, cleaning persons, tribals, etc. were treated as impure based on the type of work they do. They were called Adivasis and Dalits (Shudras). These setting based upon occupation gave rise to the caste system in India. Generally, individuals belonging to a particular class or caste are found financially and socially vulnerable.

Thus to prevent the rights of these weaker sections of the society, Articles 15(3) and 16(4) were inserted that gave advantage to these sections for their equal representation [3], [4]. The rationale behind it was very simple, if you are not starting from the same line you cannot finish at the same line. The condition of these untouchables was brutal and they were constantly suppressed by the persons rich in caste. There was a huge gap in terms of education, wealth, and other privileges between classes.

The concept of minorities is way too far from what people think today. Dr. Ambedkar referred people under two classifications, such as privileged and underprivileged. Privileged are those who have sufficient means and can fulfill their necessities with ease. Underprivileged were those who were economically, socially, and educationally backward sections who if left untouched, will continue to remain the same, their exploitation will continue and they will be deprived of the dignified life.

3. Dr. B.R. Ambedkar's Philosophies

Dr. Ambedkar, a great scholar, a true visionary, a philosopher, and historian, was the only one who could lead the Constituent Assembly and after a fruitful hardship of 2 years, 11 months, and 17 days, finally, the first draft of the constitution was prepared. Dr. Ambedkar, a learned philosopher, having broad visions for Free India, drafted the Indian Constitution and his philosophies and progressive ideas are clearly traceable in many aspects of the Constitution.

Dr. Ambedkar believed that only the goods of a person should be seen and one should only intake the goods and must leave the evils. He also laid high emphasis on learning and believed that one should learn from the experiences of oneself as well as from others. These philosophies were followed in the framing of the constitution [5]. Different aspects were borrowed from different countries but only the good i.e. pros were taken. Now the question was how to evaluate the pros, for the

purpose, Babasaheb followed the Gandhian Philosophy. Mahatma Gandhi quoted that "If you make legislations, try to make them keeping in mind, its causes and benefits to the least privileged sects of the society, and you will never make mistake" [6]. Dr. Ambedkar, thus evaluated constitutions of different countries making no straight implications, instead, he analyzed the relevance of those aspects, measured the pros and the cons, and beautifully molded these aspects as per the relevance in the Indian Context.

The concept of fundamental rights taken from the US Bill of rights [7], being framed in Part 3 of the Indian Constitution are modified as per the suitability and practices of India and its people, because ultimately a nation is made by its citizens and they need to be protected, hence all the Articles framed are Human-Centric [8].

India, favored substantive equality which was adopted by Dr. Ambedkar by giving some special privileges and opportunities of recognition, in the form of reservation, to these group who was deprived of many rights as the question of their overall upliftment was concerned. If they were deprived of these reservations, then they will end up being in the same state of life and their exploitation will be continued.

Dr. Ambedkar believed in equal representation of each class of society at every level, hence for the protection of their right to representation, Dr. Ambedkar made reservations for these underprivileged and weaker sections of the society. Dr. Ambedkar being of a scheduled caste and after facing outrageous hate and indignity in his life, never favored casteism. He stated that If some people are residing on a piece of land, it doesn't become a country. There should be a feeling of nationality. Caste is against nationality. It creates indifferences between two persons belonging to the same nation but different castes. In social and economic life, discrimination breaks people and humanity is at stake. Dr. Ambedkar used to give more emphasis on the development and social harmony of the nation by rising above the caste system.

Here, Dr. Ambedkar classified minorities based on two types as Religious minority and Linguistic minority. Religious minorities mean the followers of a particular religion who were very few in number. Religious Minorities are given rights for the protection of religion. Being a secular nation all religions should be respected equally and everyone has the right to profess their religion with freedom. The Linguistic Minority means the people of different languages. A person having no knowledge of the language spoken in a particular state will surely face many difficulties to survive. Linguistic minors such as people belonging to a rural tribe or any other linguistic community having their own distinct language and are not able to communicate in the official languages need to

get some benefits. India, a diversified state with different languages and religions, is required to recognize the minorities to render them equal status [9].

4. Dr. B.R. Ambedkar's Ideology Rights to Representation

Aristotle said: *"It is an injustice to treat unequals as equals just as it is an injustice to treat equals as unequals"*

Dr. Ambedkar in his writings, used the term "Rights to representation", instead of reservation, enabling the representation of backward classes instead of reserving them. He always wanted a classless and casteless society. In Public Administration, He never favored the representation of candidates from scheduled castes who fails to fulfill the minimum required educational qualification, so he never wanted to compromise the quality of administration in public services. Representation was strictly based on the quantum of a population of scheduled castes corresponding to their proportion in the total population.

Most importantly, he did not bat for reservations in education, rather he merely states that the state should take care of financial assistance in education at every stage for the betterment of Scheduled Castes. This is a striking feature of Dr. Ambedkar's line of thinking.

Reservationists do not value the nation's supremacy of Dr. Babasaheb Ambedkar and have started doing politics of vote not adhering to Dr. Ambedkar's principle. There should be a deadline to give reservations so that the downtrodden can emerge. When the crushed people emerge under the prescribed limit of reservation, then the implementation of the reservation should be considered successful.

5. Conclusion

Reservation is a curse in the development of any nation. Today, if we want to take the country towards progress and to maintain the unity of the country, it is necessary to remove reservations and give equal opportunities in education, employment, welfare and all the means of social advancement. Therefore, to keep the development of the nation alive, reservation needs to be separated from politics. Today political parties in order to safeguard their vote bank promise reservations to the people.

Fondly remembering Dr. B.R. Ambedkar, Subhash Kashyap, former secretary-general of three Lok Sabha said, "Dr. Ambedkar did not spell out too many things but on the point of reservation for SC and ST, he had said that 10 years is too short a period and it should be 40 years, but thereafter the Parliament should have no power to extend reservation by law. He was against reservation in

perpetuity. He had said *'I would not want that symbol to continue in Indian society forever.'*" [10].

Dr. Ambedkar would be pained to see that these sections still need reservations. The concept of reservation was just to give a chance to a downtrodden section for their upliftment. But instead of upliftment, reservationists are using the reservations to get the unfair advantages and benefits that are associated with them. Dr. Ambedkar clearly stated that the reservations are only for the selected class of people who are exploited by the other. The concept was only to help them to stand along with other castes and contribute equally towards the growth and development of the nation. But in today's scenario, many of the classes are demanding the reservations for themselves, which is not at all an acceptable situation in long run. If reservations will be given to the majority of the classes, the whole system of equality of law, and equal opportunities will come to end.

Dr. Ambedkar stated that the reservations should be made available for a period of 40 years and after that, it will be the responsibility of the parliament to end the reservations and make laws that will be equally applicable to all. The role for which the reservations were made is still not achieved but the alternative method of providing benefits should be used. Equal opportunities on the basis of merit should be promoted. As per the current Indian Scenario, the benefits should be only given to those who are economically backward, and that too for their upliftment only. No undue advantages of these benefits should be made. Reservations should be based on merit and not on basis of religion or caste. Today all the classes and religions are economically stable and no need for reservation is felt, and those who are deprived must qualify to get these benefits.

As long as the unqualified people continue to play with the country with the help of reservation, neither the nation will benefit nor the society nor their caste. Reservation is the reason for the destruction of the country. Racism is breaking the country only through the politics of the vote bank, and the craving of some people. The day people of every caste will forget caste and will come forward on the strength of merit and on the basis of merit, will ensure the future of the country, the country will move on its own path of progress.

6. Recommendations

Dr. Ambedkar rightly said that, - *"However good a constitution maybe, if those who are implementing it are not good, it will prove to be bad. However bad a constitution maybe, if those who are implementing it are good, it will prove to be good."* [11]. Hence it solely depends on the people who are implementing the constitution. Thus we need to move towards equality by following Dr. Ambedkar's Philosophies and Principles to attain the growth and

development of the Nation. And It will happen only when casteism be overruled by Nationalism.

It is also true that the earlier societies oppressed the Scheduled classes and Tribes. It excluded them and exploited them at every stage. Reparations for historical injustices are just, but it cannot be endless and limitless. Its been 75 years since the reservation system is being practiced in India and if not changed will continue for decades. Dr. Ambedkar was very clear against offering majority seats to minorities. According to him, any such attempt would grossly commit an injustice to the majority. Baba Saheb Bhim Rao Ambedkar too became the creator of the constitution by his own merit and deeds and not from the reserved quota [2].

There was a need for the representation of the underprivileged sections in society, but now things have changed, there are rich and poor sects of people in all classes of society. No special protection is required anymore. Protection, if given, should be given based on the vulnerability and to only those who deserve it. In India today also there are many sects that are deprived of daily necessities. They should be given protection and protection here doesn't mean reservation. They should be provided with better opportunities just to improve their status of living. Beyond basic necessities, if reservations are made for any class based on minorities without considering their standard of living and resources available to them, it will be unjust. The reservation system if further carried on based upon the minorities and ignoring the standard of life and no. of opportunities will become a threat to both, economical development and social development.

References

- [1] V. Krishna, "November 1948: Ambedkar presents Draft Constitution, Indian Constitution-Making Shifts into High Gear" 2020, Online: <https://clpr.org.in/blog/november-1948-ambedkar-presents-draft-constitution-indian-constitution-making-shifts-into-high-gear/>
- [2] S. S. Singh, "Dr Ambedkar was the architect of social harmony", 2021, Online: <https://timesofindia.indiatimes.com/readersblog/dr-shanker-suwan-singh/dr-ambedkar-was-the-architect-of-social-harmony-31185>
- [3] Article 15 (3) in The Constitution Of India 1949 : Nothing in this article shall prevent the State from making any special provision for women and children. <https://indiankanoon.org/doc/609295/>
- [4] Article 16 (4) in The Constitution Of India 1949 : Nothing in this article shall prevent the State from making any provision for the reservation of appointments or posts in favor of any backward class of citizens which, in the opinion of the State, is not adequately represented in the services under the State. <https://indiankanoon.org/doc/211089/>
- [5] Outlook Web Desk "The Grammar of Anarchy", 2022, Online: <https://www.outlookindia.com/website/story/the-grammar-of-anarchy/289235>
- [6] M. K. Gandhi, "Essence of Democracy", 2022, Online: <https://www.mkgandhi.org/momgandhi/chap72.htm>
- [7] Wikipedia, "United States Bill of Rights", 2022, Online: https://en.wikipedia.org/wiki/United_States_Bill_of_Rights

- [8] Government of India, "THE CONSTITUTION OF INDIA", 2020, Online: <https://legislative.gov.in/sites/default/files/COI.pdf>
- [9] B. R. Ambedkar, "DR. BABASAHEB AMBEDKAR WRITINGS AND SPEECHES VOL. 1", 2014, Online: http://www.mea.gov.in/Images/attach/amb/Volume_01.pdf
- [10] S. Saigal, "Ambedkar would be pained to see that SC/ST still need reservation", 2021, Online: <https://www.thehindu.com/news/national/other-states/ambedkar-would-be-pained-to-see-that-scst-still-need-reservation/article37875984.ece>
- [11] M. Emmanuel, "'If hereafter things go wrong, we will have nobody to blame", Dr. Ambedkar's final speech in Constituent Assembly", Bar and Bench, 2018, Online: <https://www.barandbench.com/columns/dr-ambedkar-1949-constituent-assembly-speech>

Copyright: This article is an open access article distributed under the terms and conditions of the Creative Commons Attribution (CC BY-SA) license (<https://creativecommons.org/licenses/by-sa/4.0/>).



from ICSI.

MANGE KARAN RATANBHAJ has done his bachelor's degree in Business Administration and Management in 2020. He is pursuing Law degree from Parul Institute of Law, Parul University. He is also a Company Secretary Aspirant

He has co-authored Research Paper Titled - Three Dimensional View of Human Rights Through the Lens of Dr. B.R. Ambedkar, published in Journal of Research and Development – A Multidisciplinary International Level Referred and Peer Reviewed Journal.

Received: 19 July 2022, Revised: 20 September 2022, Accepted: 21 September 2022, Online: 10 October 2022

DOI: <https://dx.doi.org/10.55708/js0110002>

CANClassify: Automated Decoding and Labeling of CAN Bus Signals

Paul Ngo^{*1} , Jonathan Sprinkle² , Rahul Bhadani³ ¹University of California, Berkeley, Berkeley, California, USA, 94704²Vanderbilt University, Nashville, Tennessee, USA, 37212³The University of Arizona, Tucson, Arizona, USA, 85721*Corresponding author: Paul Ngo, ngopaul@berkeley.edu

ABSTRACT: Controller Area Network (CAN) bus data is used on most vehicles today to report and communicate sensor data. However, this data is generally encoded and is not directly interpretable by simply viewing the raw data on the bus. However, it is possible to decode CAN bus data and reverse engineer the encodings by leveraging knowledge about how signals are encoded and using independently recorded ground-truth signal values for correlation. While methods exist to support the decoding of possible signals, these methods often require additional manual work to label the function of each signal. In this paper, we present CANClassify — a method that takes in raw CAN bus data, and automatically decodes and labels CAN bus signals, using a novel convolutional interpretation method to preprocess CAN messages. We evaluate CANClassify’s performance on a previously undecoded vehicle and confirm the encodings manually. We demonstrate performance comparable to the state of the art while also providing automated labeling. Examples and code are available at <https://github.com/ngopaul/CANClassify>.

KEYWORDS External interfaces for robotics, Computing methodologies: Learning paradigms, Neural networks

1. Introduction

Modern vehicles are equipped with advanced sensors which record speed, detect and track nearby vehicles, and estimate fuel efficiency. Vehicles use Electronic Control Units (ECUs) and the CAN protocol to communicate the data among these sensors. While on the road, these sensors generate a large amount of information which is communicated through ECUs to be used for driver assistance, collision avoidance, fuel estimation, and general operation. However, this data is generally discarded after use. Vehicles are becoming increasingly digitized, resulting in a greater amount of data being communicated between ECUs. This CAN bus data is becoming increasingly important for many applications, including improving driving behavior [1], understanding and reducing traffic congestion [2], driver profiling [3], and improving fuel efficiency through human-in-the-loop CPS. CAN data is also a major source for general automotive data, which is evaluated to be worth between 450 and 750 billion USD by 2030 [4]. Due to the great potential of CAN bus data, decoding this data is becoming increasingly relevant in vehicle-related research. However, decoding CAN bus data is no trivial task. While a standardized protocol, SAE J1939 [5], for communication between ECUs has been developed, much of this data is encoded according to an encoding known only to each Original Equipment Manu-

facturer (OEM). Since these OEMs are generally unwilling to publicly release the encodings used for their CAN messages, it has become common to decode the CAN messages independently.

In the past, CAN signal decoding has largely been done by hand, though in recent years, new methods have been developed which support the automation of CAN signal decoding. Many of these methods use common features of encoded signals in order to detect the presence of signals and then refine their encodings. Signals are then correlated to ground truth signals, and the type of signal (e.g., wheel speed, brake pedal, etc.) is manually labeled by hand. In this paper, we present CANClassify, a method that both decodes CAN bus signals, as well as automatically labels them. We describe the problem in technical detail, discuss relevant research in the area, and present and evaluate our method. Finally, we discuss possible implications and future directions for this work.

2. Problem Statement

Modern vehicles use electrical buses following a protocol called CAN, in order to communicate between different sensors and processors on the vehicle. Sensors and processors interface directly with ECUs. Each ECU, also called a ‘node’, communicates a specific set of CAN messages to all other

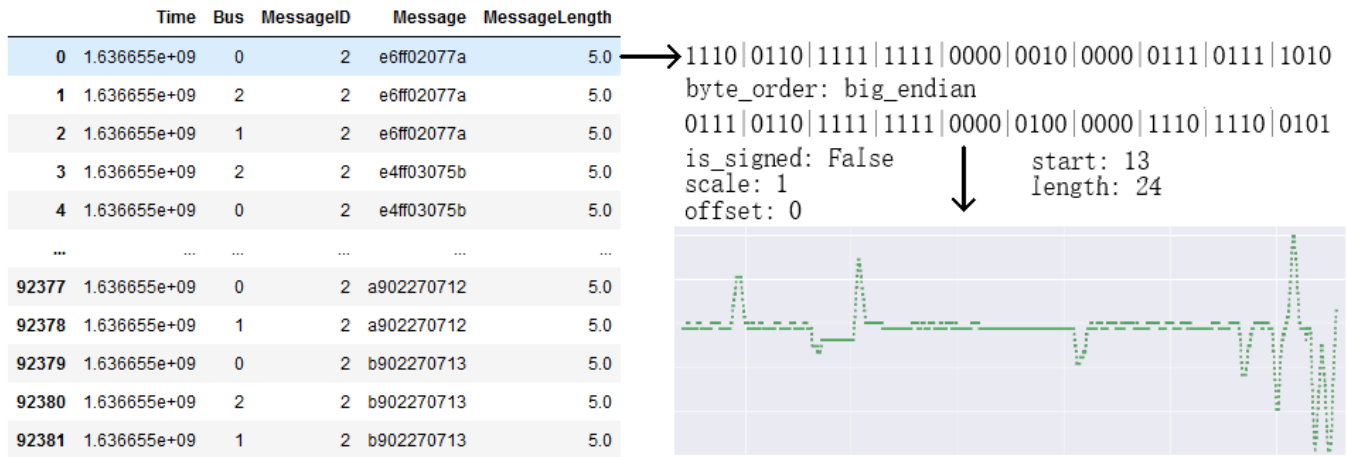


Figure 1: A CAN message is interpreted with specific bit boundaries and an encoding, generating a signal. A CAN message consists of a series of 64 bits that change every timestep. Bit boundaries delineate the start and end of a possible signal. A signal is interpreted using an endianness, signedness, scale, and offset. A final interpreted signal can then be generated.

ECUs on the same bus. Open-source tools can be used to interface with ports on the vehicle in order to read messages published on the CAN bus, or buses if there are multiple [6]. These CAN messages can be processed in real time (which can include real-time intercepting and modifying), or recorded for later analysis.

CAN messages contain an ID, which uniquely identifies a message on a bus and is related to the nature of the content of the message, and a payload. This payload, which generally ranges in length from 1 byte to 8 bytes, usually encodes multiple signals packaged together.

While sometimes a single CAN bus will contain all signals of interest, it is often the case that some signals of interest are broadcasted on separate CAN buses. Therefore, hardware that records or processes CAN bus messages generally must be able to do so on multiple buses simultaneously. However, for the work presented in this paper, we assume that a single unified set of CAN message data has been collected and stored with unique non-overlapping message IDs.

The goal of CAN signal decoding is to identify the presence of signals within CAN messages and reverse engineer their encodings. Within each CAN message payload, a signal is confined to a continuous stretch of bits. These bits can be interpreted with the correct endianness and signedness in order to get a decimal value. For this work, we assume that the encoding for any signal does not change and is always published on the same bits, e.g., signals are not multiplexed. This possibility is considered in the discussion on future work.

Once the correct bit boundaries, endianness, and signedness are identified for a signal, most of the decoding work is done. The final step is to determine the proper scale and bias to apply to the value to get the final signal in the desired unit, such as speed in km/hr. The solution presented in this paper automatically labels signals, so solving for the scale and bias of signals becomes the simple problem of obtaining a small number of data points on the relevant sensor.

Present work in the literature focuses heavily on identifying the correct bit boundaries for encoded signals, which is a major challenge for CAN signal decoding [7]–[8]. However,

for a decoded signal to be of use, it must also be labeled. Current CAN decoding methods find bit boundaries through common signal features, such as the rate of bits switching between 1 and 0, and finalize the encoding and signal label by correlating with an external ground-truth signal. For example, GPS sensors, Inertial Measurement Units (IMUs), or previously decoded CAN signals can be used to validate new signals [7]. Present methods commonly use such signals to validate the decoding of continuous signals, such as wheel speed. However, this requirement of having another external ground truth signal to validate and label signals becomes increasingly difficult to automate as the signals being decoded become more complicated. For example, obtaining a ground truth value for a gas pedal signal requires installing a physical sensor to detect when and how the gas pedal is pressed, or developing a dynamics model of the vehicle to calculate the gas pedal signal from other known values. Such signals must be decoded by hand or require specific equipment to record a ground truth. In this work, we demonstrate that it is not necessary to perform signal-specific work to label and decode a signal — instead, previous decoding knowledge can be used to further decode and label signals on new vehicles.

3. Related Work

3.1. LSTMs

LSTMs, Long Short-Term Memory neural networks, are a type of neural network which are able to learn long-term dependencies and relationships in data. They demonstrate excellent performance at predicting and classifying time series data [9, 10]. The solution presented in this work trains an LSTM to classify multiple convolutions of encoded CAN messages, which have continuous time-series-like behaviors. By reinterpreting the CAN decoding problem into this known form, we can leverage existing successes in the application of LSTMs.

Stacking multiple layers of LSTMs allows for the possibility of developing a latent space for higher order features of data, including different time scales and signal relationships

in time [11]. Developing a model of higher order features is useful for classifying signals even with incorrect bit boundary placements, which is demonstrated by our results in this paper.

3.2. CAN Signal Decoding

There exists a body of work related to decoding CAN messages from vehicles. Many methods in the literature are based on the work presented in READ [12]. READ segments CAN message payloads into sections by looking at bit flip rates. These sections are categorized into six different message types: UNUSED (an unused set of bits), CONST (constant values), MULTI (values that change but do not fall into other categories), COUNTER (clock- or counter-like signals), CRC (cyclic redundancy check signals), and PHYS (signals which represent a physical value). LibreCAN [13] is one method based on READ, which further attempts to gain accuracy with PHYS signals by using correlation to a known signal. CAN-D [14] presents another pipeline to decode CAN signals, notably generating a full set of decoding parameters (bit boundaries, endianness, signedness, scale, and offset). These CAN decoding methods seek to find commonalities between different signal encodings, increasing the accuracy of identifying the correct encoding by leveraging features such as bit flip rates, bit flip correlations, and other derived features. Our work approaches the decoding problem from a different point of view: our model attempts to learn the characteristic signature of specific types of PHYS signals, instead of identifying features relevant to all encoded signals.

Our work leverages known encodings in order to further assist in the decoding of new CAN vehicles. In this way, it is similar to the work presented in CANMatch [15]. CANMatch leverages frame matching, which relies upon vehicle manufacturers' re-use of the same Message IDs and signal encodings across multiple makes and models. The researchers discuss a possible mitigation to the success of their strategy, which is the scrambling of Message IDs and frames. We address this with CANClassify. By assessing the features of the signals themselves, our method can still find the same signals no matter which message they are published on, where they are within a message, and how they are encoded.

These other CAN decoding methods are generally evaluated for the methods' ability to predict signals on CAN messages, avoid predicting signals when there are none present in a range of bits, and find the correct encoding for identified signals. Therefore, methods are usually evaluated using a vehicle that has been fully decoded already. In this work, we evaluate on a vehicle that has not yet been fully decoded and verify the results manually. Another consideration is the time cost of decoding. For methods that decode CAN messages live, it is essential to keep decoding run times low, as high-speed CAN messages (as specified by ISO 11898-2) can transmit information at bit speeds at a rate of either 1 or 5 Mbit/s. For offline decoding, as with CANMatch and CANClassify, it is not as necessary to decode as quickly; however, the worst case runtime performance should be bounded by the time it takes to interpret

all possible signal encodings (on the order of 10^6 encodings) and score each signal interpretation with a correlation to a ground-truth signal. On a modern 5 GHz processor, this brute force method takes on the order of days to process the information from an hour-long drive. However, it is more common to compare to the present state of the art, which takes on the order of minutes and hours.

4. Solution

We present two primary contributions in the area of CAN signal decoding, which form the CANClassify method. The first is the method of interpretive convolutions, a novel way to generate a feature vector for encoded binary signals. This technique is used to preprocess data for input to an LSTM-based CAN signal decoding network. This enables the network to both decode and label continuous CAN signals. The second contribution is the masking and filtering method used to decode using the neural network.

4.1. CAN Classifier Network

Data were collected using the comma.ai [6] panda black OBD-II interface and Libpanda [16] on two vehicles: the 2021 Toyota RAV-4 and 2017 Honda Pilot. The following signals were selected for classification, based on their relevance to driving behavior, traffic conditions, and fuel usage:

- v_x , velocity in the forward direction
- a_x , acceleration in the forward direction
- a_y , acceleration in the horizontal direction
- θ_s , the angle of the steering wheel
- ω_s , the rate at which the steering wheel turns
- p_b , continuous value for how much the brake pedal is pressed
- p_g , continuous value for how much the gas pedal is pressed
- *radar-long*, longitudinal radar signal
- *radar-lat*, latitudinal radar signal
- *radar-rel-vel*, radar signal tracking relative velocity in the forward direction
- *radar-rel-acc*, radar signal tracking relative acceleration in the forward direction

In order to generate the training set for the classification network, the relevant bits for each of the above signals were taken from 3 hours of recorded CAN data. Algorithm 1 was used to generate randomized messages from these relevant bits.

Algorithm 1 Generate Randomly Positioned Messages

```

randomized_messages ← []
for s in can_signals do
  start_positions ← random(0...64, 10 times)
  for p in start_positions do
    s_1 ← place s at p, pad=random(0, 1)
    s_2 ← place s at p, pad=0
    randomized_messages ← s_1
    randomized_messages ← s_2
  end for
end for

```

Algorithm 2, interpretive convolutions, were then used to generate a signal of the correct input size for the CAN classification network. This algorithm is similar to what Convolutional Neural Networks [17] do for images, but instead are interpretive convolutions for CAN messages. Differing sizes of bit widths are used to interpret the same message across all possible positions in the message. This generates a vector of varying bit boundaries, byte orders, and sign values used to interpret the message. Interpreting CAN signals with bit widths similar to the true bit width of a signal will generate time series signals which have similar behavior to the true signal, allowing the LSTM to learn from signal behaviors relevant to each type of signal. This behavior similarity is visually demonstrated in Figure 2.

Algorithm 2 Interpretive Convolutions

Require: msg is 64 bits

```

out ← []
for i from 1 to 61 do
  out ← interpret(msg, i:i+4, big, +)
  out ← interpret(msg, i:i+4, little, -)
end for
for i from 1 to 57 do
  out ← interpret(msg, i:i+8, big, +)
  out ← interpret(msg, i:i+8, little, +)
  out ← interpret(msg, i:i+8, big, -)
  out ← interpret(msg, i:i+8, little, -)
end for
for i from 1 to 53 do
  out ← interpret(msg, i:i+12, big, +)
  out ← interpret(msg, i:i+12, little, +)
end for
for i from 1 to 49 do
  out ← interpret(msg, i:i+16, big, +)
  out ← interpret(msg, i:i+16, little, +)
  out ← interpret(msg, i:i+16, big, -)
  out ← interpret(msg, i:i+16, little, -)
end for

```

Convolutionally interpreted signal vectors are then scaled and shifted according to the training set means and ranges of the vectors, placing the vector values to be between the values of -1 and 1. This enables the network to identify signature patterns for each type of signal regardless of the signal's order of magnitude, which is directly related to the length of the interpretation.

The final preprocessing step samples the convolutionally

interpreted signals every 100 time-steps for a total of 100 samples. This sampling value was fixed because the data rates of broadcasted CAN messages reflect the relative rate at which the CAN signals on the message change in time. Various other sampling strides and sample counts perform similarly.

The layers of the CAN classification neural network model were as follows:

- Fully Connected, 500 units
- LSTM, 256 units
- LSTM, 256 units, dropout 0.1
- Fully Connected, 100 units, dropout 0.1
- Fully Connected, 50 units
- Fully Connected, 12 units, sigmoid activation

The model's objective was to correctly predict the presence of 11 signals from 100 sampled values from a convolutionally interpreted CAN message. All data were preprocessed according to the described algorithms. A prediction is only correct if the model predicts the presence of the relevant signal and the absence of all other signals.

An 80:20 train-test split was used to train and evaluate the model. The model was trained for 6 epochs on CAN message data collected from 3 hours of driving. The model achieved 0.8118 training set accuracy after 6 epochs of training, which took 3 hours on a 4.3 GHz processor (with multi-threading disabled). The model achieved 0.8170 test set accuracy.

4.2. Using CAN Classifier for Decoding

The CAN classifier network can be used to both detect specific signal types, as well as decode the exact bit boundaries of detected signals. CAN messages are first preprocessed according to Algorithm 2. The model can then predict the signal types transmitted on each message. Only signals which are predicted to be present with a probability of 80% or greater are accepted.

The bit boundaries of the signal can then be found using Algorithm ??, which iteratively masks the signal to evaluate which part of the message contributes to the prediction of the class of interest. This algorithm generates scores for each possible starting and ending bits of a signal. The left bit boundary is encoded as a peak in the starting scores, and the right bit boundary is encoded as a peak in the ending scores. Each boundary combination, endianness, and signedness are interpreted for each signal. Finally, these interpretations are filtered based on three criteria. First, the interpretations scored based on continuity. Continuity is approximated by counting the number of differences in value between two timesteps which are within 10% of the range of a signal, as shown in Equation 1. Only signals which have a continuity score of greater than 50% are accepted. Signals are then scored based on the rate at which they vary, which is the number of times the value changes — the highest score is accepted as the encoding. Finally, counter signals are filtered out [13]. The ultimate output from this filtering process is an endianness, signedness, and signal type label for each detected signal.

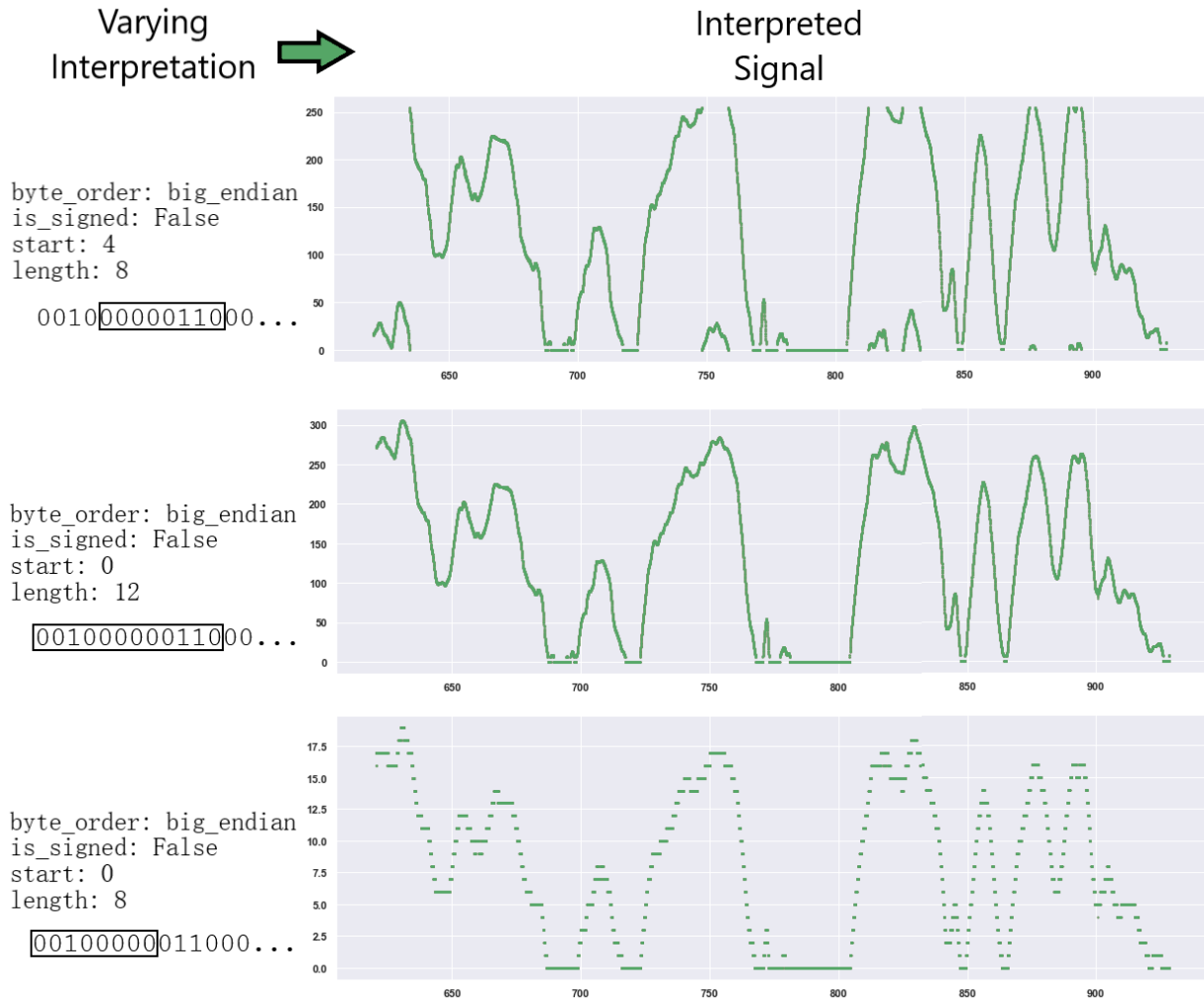


Figure 2: Similar but varying bit widths at the same bit positions in a binary-encoded signal generates signals with similar behaviors. Signal shapes, relative peak heights, and signal rates of change are similar.

$$\text{score} = \frac{1}{\text{count}(\text{diff}(\text{signal}) > 0.1 * \text{range}(\text{signal})) + 1} \quad (1)$$

A raw signal value can be obtained by interpreting the original CAN message with the signal boundaries, endianness, and signedness from this decoding process. Figure 3 shows an example of this decoding workflow.

5. Results

CANClassify was evaluated on a previously undecoded vehicle, a 2020 Nissan Rogue Sport. The data was collected by interfacing with the ADAS module located in the passenger rear quarter panel. All messages on a single CAN bus were recorded over a 5 minute period. This shows the power of the model to identify useful signals even with small amounts of data. CANClassify identified, decoded, and labeled seven signals, of which two were *radar-long* signals, one was a *radar-lat* signal, one was a p_b signal, one was an a_x signal, and two were v_x signals. In the final filtering stage, two of these seven signals were filtered out as counter signals.

The non-radar signals found were manually verified using Strym [18] and mapped to valid signal labels. The wheel speed signal was independently decoded on the vehicle using bit flipping techniques as described in previous literature. The model predicted the same encoding for the wheel speed signal as was found manually. Figure 3 illustrates the decoding process as applied to the wheel speed signal.

The model was also successful at learning the signal behavior of more complicated signals, such as acceleration- and pedal-related signals. Figure ?? shows a signal that the model classified as a brake pedal signal. This signal is more likely to be associated with acceleration, but the model and decoding process obtained a sufficiently close labeling result, as braking is closely related to acceleration. This example demonstrates that CANClassify is able to learn signal features such as braking without having to individually define physical signal relationships (e.g., calculating an acceleration signal by differentiating wheel speeds and searching for signals that correlate with the differentiated value).

A single-core 4.3 GHz processor was used for evaluating the runtime of CANClassify. The time taken to decode using CANClassify is linearly correlated to the number

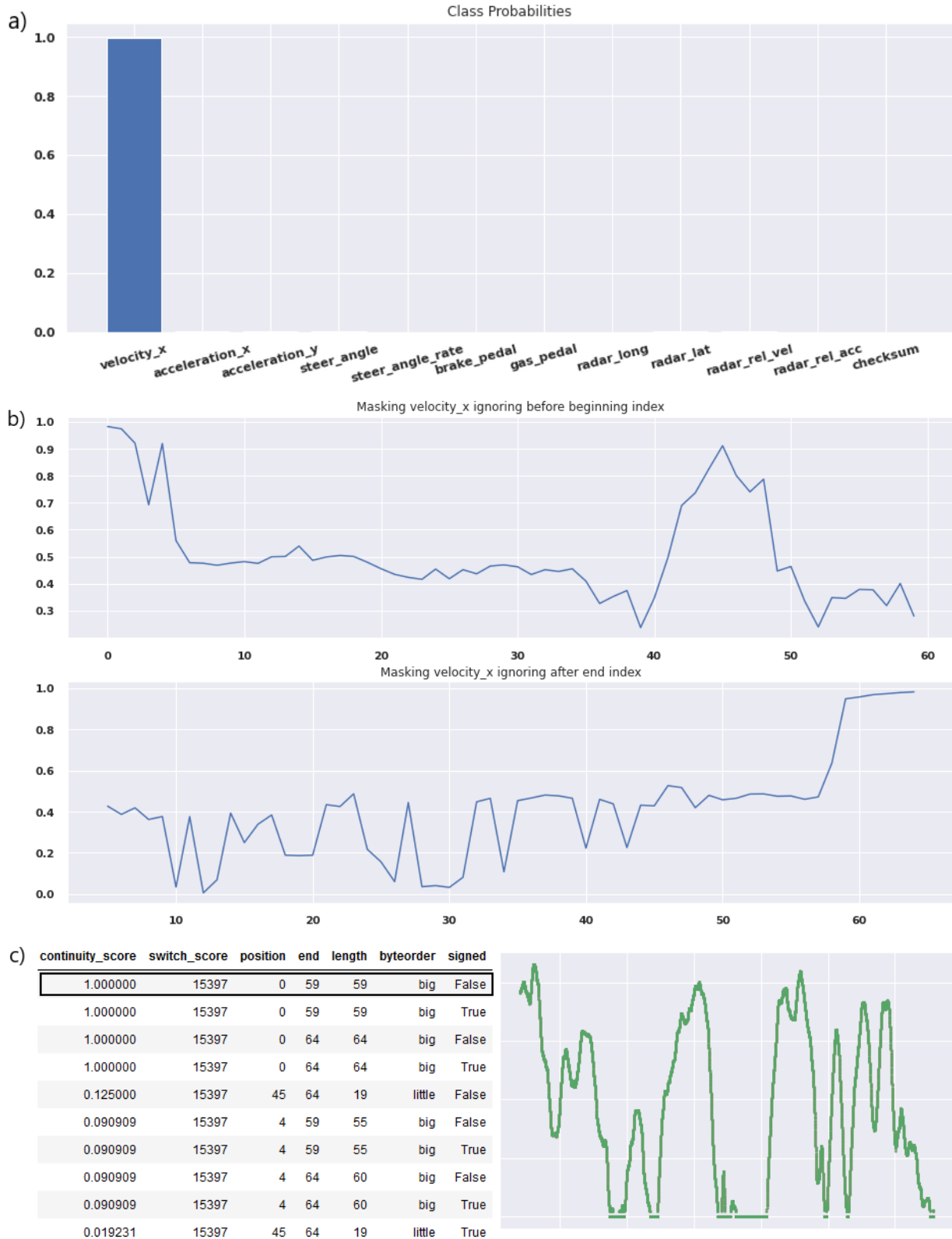


Figure 3: Bit boundary masking for likely wheel speed signal on test Nissan data. a) The model predicts the CAN message to only contain a velocity signal. b) The masking process generates peak values at possible beginning and ending bit positions. c) Through the scoring process, an encoding is chosen. The encoding is applied to view the raw velocity signal.

of messages and the length of the CAN data because the same convolutions are evaluated regardless of the message. Therefore, CANClassify will take the same time to decode any vehicle make and model, assuming the previous factors are constant. We evaluated on data from a five-minute drive, recording 129 CAN messages, where each message published at a rate of 400 bytes per second on average. CANClassify took 55 seconds to preprocess and classify all messages without decoding. The bit decoding process took 165 seconds per message on the same hardware. Notably, the CANClassify method for decoding can be entirely parallelized across messages, across time, and across bit masks during bit decoding. With the same hardware and 16-threads, CANClassify only takes 3 seconds to classify all messages, and 10 seconds per message (on which a signal of interest is detected) to identify the correct encoding. Therefore, we conclude that CANClassify is competitive with the current state of the art while achieving the additional task of labeling discovered signals.

6. Discussion

In this work, we presented an alternative approach to CAN signal decoding. Many current CAN decoding methods, such as LibreCAN [13] and CAN-D [14], use signal-independent features such as bit flipping rates to identify and decode signals, and then rely on manual work and correlation with labeled ground truth signals to label the decoded signals. While there has been previous work that leverages known decodings to further decode CAN signals [15], there has been no corresponding work to automate the labeling of these signals. Our solution, CANClassify, leverages known encodings and labels to further accelerate both decoding as well as labeling.

However, more efficient CAN decoding brings up some concerns about the security and safety of these methods. As vehicles become more interconnected, it becomes increasingly likely that infrastructure is created for inter-vehicle communication. Adversarial attacks on physical CAN systems in conjunction with these new inter-vehicle communication protocols [19] could allow adversaries to remotely decode additional vehicles, or interfere with intra-vehicle CAN messages. Accelerated CAN decoding could also allow attackers to more easily identify the CRC bits packaged with CAN signals, which act as a checksum and a way to detect modified or invalid CAN signals. Such an attacker could maliciously inject or modify CAN signals by correctly setting CRC signals to valid values.

Some intrusion detection methods have been developed to detect such attacks [20, 21]. Another simple solution to secure CAN data is the use of encryption. Encryption solutions have been demonstrated to be both feasible and fast enough to be used on modern CAN buses [22]. While signals could still be detected through power analysis, the true encoding, as well as the underlying value of the CAN signals, would be obfuscated — such a solution could only be defeated through a cryptographic attack.

7. Conclusion

We presented a novel method for decoding CAN signals from vehicle driving data by leveraging existing knowledge of CAN message encodings and signal dynamics. Instead of identifying features about the signal encodings themselves, we use our network to identify features about signal behaviors. By using convolutional interpretations of CAN messages, our model can learn from known encodings and be used to identify the encodings of unknown signals. It is able to do so even with a small amount of driving data — a trained network is able to quickly decode signals as well as label them, a task that would normally require manual work for each type of signal.

Our solution was validated by evaluating the model on signals recorded from a previously undecoded vehicle. Encodings were validated by independently decoding the same signals using present techniques and using correlations to ground truth values.

Future directions for work include training on additional signal types. With our current method, COUNTER and CRC signals are sometimes detected as other PHYS signals (though they are ultimately filtered out of the output). By including these types of signals in the training set for the model, these over-detections can be mitigated. Additionally, we assume a consistent encoding for each signal. However, some signals are multiplexed in time over the same set of bits, where a single bit or a small number of bits are used to specify which signal is transmitted over the rest of the bits. By assessing the evolution of prediction probabilities across time, CANClassify has the potential to detect multiplexed signals and individually classify each multiplexed signal. However, additional work must be done to identify the multiplexing selection bit or bits.

Conflict of Interest The authors declare no conflict of interest.

Acknowledgment This material is based upon work supported by the U.S. Department of Energy's Office of Energy Efficiency and Renewable Energy (EERE) award number CID DE-EE0008872. The views expressed herein do not necessarily represent the views of the U.S. Department of Energy or the United States.

References

- [1] M. Nice, S. Elmadani, R. Bhadani, M. Bunting, J. Sprinkle, D. Work, *CAN Coach: Vehicular Control through Human Cyber-Physical Systems*, p. 132–142, Association for Computing Machinery, New York, NY, USA, 2021.
- [2] E. Baschab, S. Ball, A. Vazzana, J. Sprinkle, *Safer Adaptive Cruise Control for Traffic Wave Dampening*, p. 231–232, Association for Computing Machinery, New York, NY, USA, 2021.
- [3] S. Jafarnejad, "Machine learning-based methods for driver identification and behavior assessment: Applications for can and floating car data", 2020.
- [4] M. Bertinello, "Monetizing car data", 2017.
- [5] "Sae j1939 standards collection", 1994.

- [6] Comma.ai, “opendbc: The project to democratize access to the decoder ring of your car”, 2021.
- [7] J. de Hoog, T. Bogaerts, W. Casteels, S. Mercelis, P. Hellinckx, “Online reverse engineering of can data”, *Internet of Things*, vol. 11, p. 100232, 2020, doi:<https://doi.org/10.1016/j.iot.2020.100232>.
- [8] M. E. Verma, R. A. Bridges, J. J. Sosnowski, S. C. Hollifield, M. D. Iannacone, “CAN-D: A Modular Four-Step Pipeline for Comprehensively Decoding Controller Area Network Data”, *arXiv e-prints*, arXiv:2006.05993, 2020.
- [9] S. Siami-Namini, N. Tavakoli, A. Siami Namin, “A comparison of arima and lstm in forecasting time series”, “2018 17th IEEE International Conference on Machine Learning and Applications (ICMLA)”, pp. 1394–1401, 2018, doi:10.1109/ICMLA.2018.00227.
- [10] F. Karim, S. Majumdar, H. Darabi, S. Chen, “Lstm fully convolutional networks for time series classification”, *IEEE Access*, vol. 6, pp. 1662–1669, 2018, doi:10.1109/ACCESS.2017.2779939.
- [11] R. Pascanu, C. Gulcehre, K. Cho, Y. Bengio, “How to construct deep recurrent neural networks”, 2014.
- [12] M. Marchetti, D. Stabili, “Read: Reverse engineering of automotive data frames”, *IEEE Transactions on Information Forensics and Security*, vol. 14, no. 4, pp. 1083–1097, 2019, doi:10.1109/TIFS.2018.2870826.
- [13] M. D. Pesé, T. Stacer, C. A. Campos, E. Newberry, D. Chen, K. G. Shin, “Librecan: Automated can message translator”, “Proceedings of the 2019 ACM SIGSAC Conference on Computer and Communications Security”, CCS ’19, p. 2283–2300, Association for Computing Machinery, New York, NY, USA, 2019, doi:10.1145/3319535.3363190.
- [14] M. E. Verma, R. A. Bridges, J. J. Sosnowski, S. C. Hollifield, M. D. Iannacone, “Can-d: A modular four-step pipeline for comprehensively decoding controller area network data”, 2020, doi:10.48550/ARXIV.2006.05993.
- [15] A. Buscemi, I. Turcanu, G. Castignani, R. Crunelle, T. Engel, “Canmatch: A fully automated tool for can bus reverse engineering based on frame matching”, *IEEE Transactions on Vehicular Technology*, vol. 70, no. 12, pp. 12358–12373, 2021, doi:10.1109/TVT.2021.3124550.
- [16] M. Bunting, R. Bhadani, J. Sprinkle, “Libpanda: A high performance library for vehicle data collection”, “Proceedings of the Workshop on Data-Driven and Intelligent Cyber-Physical Systems”, DI-CPS’21, p. 32–40, Association for Computing Machinery, New York, NY, USA, 2021, doi:10.1145/3459609.3460529.
- [17] K. Fukushima, “Neocognitron: A self-organizing neural network model for a mechanism of pattern recognition unaffected by shift in position”, *Biological Cybernetics*, vol. 36, no. 4, pp. 193–202, 1980, doi:10.1007/BF00344251.
- [18] R. Bhadani, M. Bunting, M. Nice, N. M. Tran, S. Elmadani, D. Work, J. Sprinkle, “Strym: A python package for real-time can data logging, analysis and visualization to work with usb-can interface”, “Proceedings of the 2nd Workshop on Data-Driven and Intelligent Cyber-Physical Systems”, 2022.
- [19] J. Kleylein-Feuerstein, F. Joas, R. Steinhilper, “Remanufacturing of electronic control units: An rfid based (service) interface”, *Procedia CIRP*, vol. 29, pp. 168–172, 2015, doi:<https://doi.org/10.1016/j.procir.2015.02.163>, the 22nd CIRP Conference on Life Cycle Engineering.
- [20] M. Markovitz, A. Wool, “Field classification, modeling and anomaly detection in unknown can bus networks”, *Veh. Commun.*, vol. 9, pp. 43–52, 2017.
- [21] M. H. Shahriar, Y. Xiao, P. Moriano, W. Lou, Y. T. Hou, “Canshield: Signal-based intrusion detection for controller area networks”, 2022.
- [22] O. Avatefipour, H. Malik, “State-of-the-art survey on in-vehicle network communication (can-bus) security and vulnerabilities”, 2018, doi:10.48550/ARXIV.1802.01725.

Copyright: This article is an open access article distributed under the terms and conditions of the Creative Commons Attribution (CC BY-SA) license (<https://creativecommons.org/licenses/by-sa/4.0/>).



PAUL NGO completed his bachelor’s degree from the University of California, Berkeley, in 2021. He obtained his Masters degree from the University of California, Berkeley in 2022.

His research interests and experience are in applying machine learning methods to approach problems in the field of cyber-physical systems. He applies his experience in machine learning, and electrical engineering, and software engineering.



JONATHAN SPRINKLE is a Professor of Computer Science at Vanderbilt University since 2021. Prior to joining Vanderbilt he was the Litton Industries John M. Leonis Distinguished Associate Professor of Electrical and Computer Engineering at the University of Arizona, and the Interim Director of the Transportation Research Institute. In 2020 he was named a Distinguished Scholar of the University of Arizona.

His research interests and experience are in model-based approaches to cyber-physical systems, and he teaches courses ranging from systems modeling and control to mobile application development and software engineering.



RAHUL BHADANI obtained his PhD in Electrical and Computer Engineering from the University of Arizona.

He studies the driving behavior of vehicles in human-autonomous vehicles mixed traffic through simulation and field experiments; quantum information theory; and statistical modeling of physical and biological systems. His research is built on the foundation of cyber-physical systems, software engineering principles, and control engineering.

An Approach for PAPR Reduction in OFDM System using RCF Technique

Juhi Singh *

Department of Electronics and communication, GLA University, Mathura, India

*Corresponding author: Juhi Singh, juhisi.94@gmail.com

ABSTRACT—OFDM is one of the important modulation techniques for wireless communication which is the advanced version of FDM. Now-a-days congestion networking is growing like AI, IoT, 5G etc. so there is a need of high data rate with low BER. For such a network there is requirement of high-speed secured data transmission that is multicarrier technique OFDM. This modulation technique is useful for current and future scenario. One of the major issue in OFDM is high PAPR and this is happened due to large amount of input data bits. High PAPR results in distortion in bands and power inefficiency using power amplifier. RCF is the technique used in this paper to reduce the PAPR and analyze the results with and without applying PAPR reduction technique. In this paper, after application of 4 clip and filter SNR is improved along with decrement of CCDF of PAPR which is desired.

KEYWORDS—BER, OFDM, PAPR reduction, RCF

1. Introduction

Power efficiency and low BER is the high demand in the field of communication that requires high data rates, large BW, low congestion [1]. Multi carrier OFDM is the solution for 4G technologies and beyond 4G techniques like 5G or beyond 5G communications that provide high-speed secured data transmission [2]. Single carrier system is the oldest way in the field of transmission of data that compromising with distortion of signals and high cost of frequency selection. There is no need of compromising with bit error performance, OFDM is currently used as multi-carrier modulation scheme. In this scheme large number of sub-carriers are closely spaced and orthogonal to each other that carries modulated data over parallel data streams or sub-channels [3]. In OFDM, each sub-carrier is modulated in conventional way with low symbol rate. The BW of each subcarrier is so small that on adding the BW of subcarrier is smaller than conventional modulation BW hence it doesn't suffer from frequency selective fading but extremely suffers from PAPR [4] The advantage of OFDM is that spectral efficiency increases as subcarriers are overlapped to each other such that they maintain orthogonality between each other [5]. Due to the presence of power amplifiers which is a non-linear element that distorts the signal [6].

The difficulty of OFDM is high PAPR that results in high bit error rate and this is happened due to variation in amplitude of large number of sub-carriers. This also results in increment of cost of the system.

The paper is organized as follows: system model which describes the important terms and method. To verify the terms and method simulation result are presented and finally conclusion is done at last.

2. System Model

2.1 About OFDM

In OFDM, complete channel bandwidth is divided into multiple sub-carriers which are orthogonal to each other OFDM is widely used in DAB and DVB as it has several advantages over traditional modulation schemes like spectral efficiency is high, tolerance to interference, robustness to channel fading.

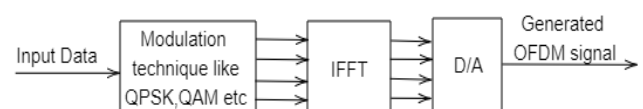


Figure 1: Transmitting side of OFDM system

Figure 1 represents block diagram of transmitter of OFDM system. Input is given to modulation schemes like QAM, QPSK which is used to map the input data

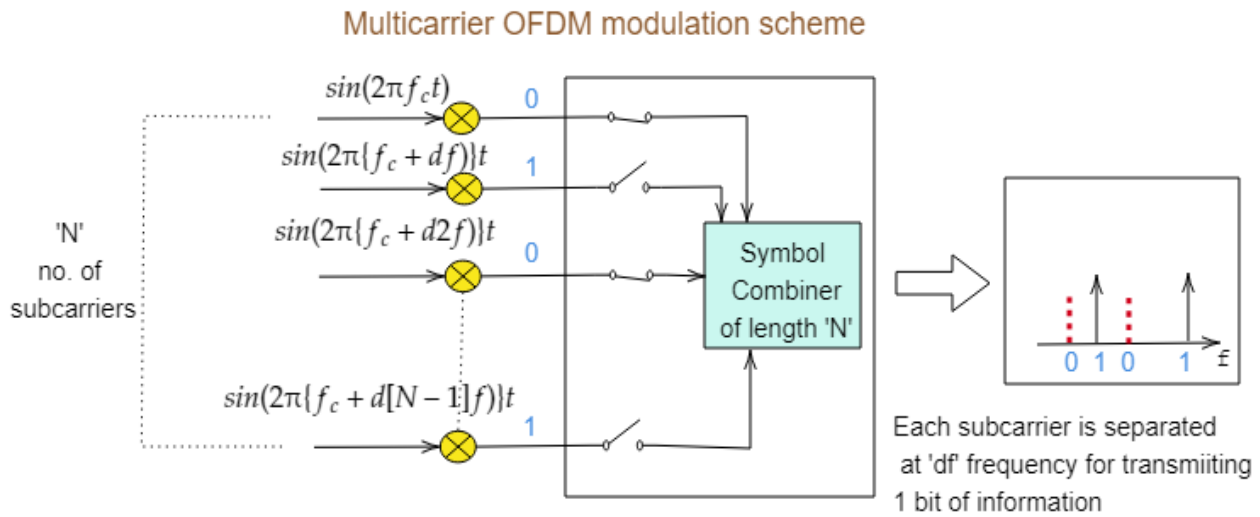


Figure 2: Illustration of generation of OFDM samples

for constellation representation. IFFT is used to multiplex the symbols over different sub-carriers by generating time domain OFDM samples which is defined as:

$$x(t) = \sum_{m=0}^{N-1} X(m) e^{j2\pi mft} \tag{1}$$

where, $X(m)$ = m^{th} symbol

f = fundamental frequency

N = total number of symbols

B = total bandwidth, $f = B/N$

Maximum frequency component of $x(t)$ is given by:

$$f_{\max} = \frac{B}{2}$$

Using Nyquist Rate, sampling rate = $2f_{\max} = B$

and sampling interval $T = \frac{1}{B}$

for n^{th} instant sample,

$$x(t) = \sum_{m=0}^{N-1} X(m) e^{j2\pi mft} \tag{2}$$

$$\Rightarrow x(nT) = \sum_{m=0}^{N-1} X(m) e^{j2\pi mfnT} = \sum_{m=0}^{N-1} X(m) e^{j2\pi mn \left(\frac{B}{N}\right) \left(\frac{n}{B}\right)} \tag{3}$$

$$\Rightarrow x(n) = \sum_{m=0}^{N-1} X(m) e^{j\frac{2\pi mn}{N}} \tag{4}$$

This makes the system digital as each bit is transmitted at equally spaced time interval T which is illustrated as:

2.2 PAPR Reduction

PAPR of any signal in continuous time domain is defined as the ratio of peak value of instantaneous output power of signal to its average power. PAPR for signal let say $x(t)$ is defined as:

$$PAPR_x(t) = \frac{p_{\text{peak}}}{p_{\text{av}}} = \frac{\max_{t \leq T} |x(t)|^2}{p_{\text{av}}} \tag{5}$$

where p_{peak} represents maximum output power and p_{av} average output power of sample in OFDM symbol.

For discrete signal $x(n)$, PAPR is given for length 'L' as:

$$PAPR_x[n] = \frac{p_{\text{peak}}}{p_{\text{av}}} = \frac{\max_{n \leq NL} |x[n]|^2}{E[|x[n]|^2]} \tag{6}$$

In dB it given as:

$$PAPR_x[n] \text{ at dB} = \frac{p_{\text{peak}}}{p_{\text{av}}} = 10 \log_{10} \frac{\max_{n \leq NL} |x[n]|^2}{E[|x[n]|^2]} \tag{7}$$

where. $E[.]$ is the expectation operator, the PAPR of baseband signal is nearly half to passband signal [7].

PAPR is also defined in terms of CF which says that ratio of peak value of OFDM signal $x(t)$ root-mean square value of the waveform. That is:

$$CF = \frac{\max |x(t)|}{E[|x(t)|]} = \sqrt{PAPR} \tag{8}$$

Oversampling is used to approximate the continuous time domain OFDM signal into discrete time domain OFDM signal. This is done by performing LN point IFFT whereas $(L-1) * N$ is the zero padding. Hence PAPR is computed for 'L' times oversampling and 'N' is the total number of subcarriers. $x[n]$ is given as:

$$x[n] = \frac{1}{\sqrt{N}} \sum_{k=0}^{NL-1} X_k e^{j\frac{2\pi kn}{LN}}, 0 \leq n \leq (NL-1) \tag{9}$$

CCDF is the complementary of CDF which is a tool for PAPR evaluation that is used for estimation of minimum number of redundancy bits [2]. CCDF for PAPR reduction of OFDM signal can be given as:

$$P(PAPR > PAPR_0) = 1 - (1 - e^{-PAPR_0})^2 \tag{10}$$

$PAPR_0$ is the clipping level. This equation explains about the probability that PAPR of symbol block exceeds $PAPR_0$.

2.3 PAPR Distribution

Distribution of PAPR plays vital role in order to design and develop PAPR reduction technique effectively. It is also important for designing the whole OFDM system. PAPR distribution is used to calculate BER and achievable rate [8].

In OFDM, if real and imaginary part of $x[n]$ are uncorrelated and orthogonal then data stream of input signal must be i.i.d. Real and imaginary part of input are i.i.d. for large number 'N' using central limit theorem that is Gaussian random variable each with zero mean and variance. [z]

$$\sigma^2 = \frac{E[|x[n]|^2]}{2}$$

For 'N' OFDM signals, Gaussian probability distribution is given as:

$$P[x(n)] = \frac{1}{\sqrt{2\pi\sigma^2}} \exp\left(-\frac{x^2[n]}{2\sigma^2}\right) \quad (11)$$

where σ^2 is variance of $[x(n)]$.

Rayleigh distribution is followed by the amplitude of OFDM signal and its PDF is given by:

$$P[x(n)] = \frac{2|x(n)|}{\sigma^2} \exp\left(-\frac{|x(n)|^2}{\sigma^2}\right) \quad (12)$$

Chi-square distribution is followed by power of OFDM signal. CCDF is a probability that describes real-valued random variable $X \geq x$

If $F(y)$ is the CDF of OFDM signal then where y is the reference level i.e.,

$F(y) = 1 - \exp(-y)$ then CCDF is given as:

$$\begin{aligned} P(\text{PAPR} > y) &= 1 - P(\text{PAPR} \leq y) \\ &= 1 - F(y)^N \\ &= 1 - (1 - \exp(-y))^N \end{aligned} \quad (13)$$

2.4 Factors Affected PAPR [9]

Number of subcarriers: Complex base band signal for one symbol in multi-carrier system can be expressed as:

$$x(t) = \frac{1}{\sqrt{N}} \sum_{n=1}^N a_n e^{-j\omega_n t} \quad (14)$$

where 'N' is the modulating symbol and also number of sub-carriers. $X(t)$ tends towards Gaussian distribution for large number of MPSK. These subcarriers are out of phase a high PAPR is produced.

Order of Modulation: Due to high order of modulation, high data B.W. efficiency can be achieved for example QAM. PAPR is increased when signal get integrated while higher order of modulation. One of the advantage of OFDM is that sub-carriers can adopt channel condition as modulation works independently for these sub-carriers.

Constellation Shape

Constellation shape helps in reducing PAPR. This is done by additional processor associated with encoding and decoding.

Pulse Shaping

Pulse shaping is very popular in terrestrial communications specially for baseband signals which is used to decrease the BW of the transmitted signal. Due to this, overshoot problem arises which increases PAPR.

2.5 Clipping and filtering

Clipping and filtering is the easiest way for OFDM reduction. At a defined level, clipping limits the maximum amplitude of OFDM signal. It is the easiest way to implement such method.

In clipping method, some parts of the amplitude are clipped off which are above the defined level. Clipping equation is given as follows:

$$C(x) = \begin{cases} x, & |x| \leq Z \\ Z, & \& |x| > Z \end{cases} \quad (15)$$

where Z is the clipping level and also a positive number. Usually clipping is done at transmitter side. The correct estimation is required for clipping the OFDM signal and there are two parameters i.e., location and size of the clip. Clipping produces two problems into OFDM signals one is in band distortion and second one is out of band radiation. Filtering is one of the method which is used to reduce the out of band radiation.

2.5.1 Drawbacks of clipping and filtering method

- It produces in band signal distortion which degrades BER performance.
- It produces out-of-band radiation which enhances aliasing problem.
- Out of band radiation can be reduced by filtering process but peak re-growth arises.

To reduce the overall peak re-growth, repeated clipping and filtering is used which increases the overall cost of the system.

2.6 RCF Method

This technique is useful to cure the OOB distortion but in-band distortion can't be removed. Input vector is first converted from frequency domain to time domain. 'N' is the number of subcarriers in each OFDM symbol. By adding zeros in the middle of the input vector, the input vector is extended. Through this interpolation is done at time domain signal [10]. When input signal is consisting of integral frequencies over FFT window then perfect trigonometric interpolation is obtained in case of OFDM.

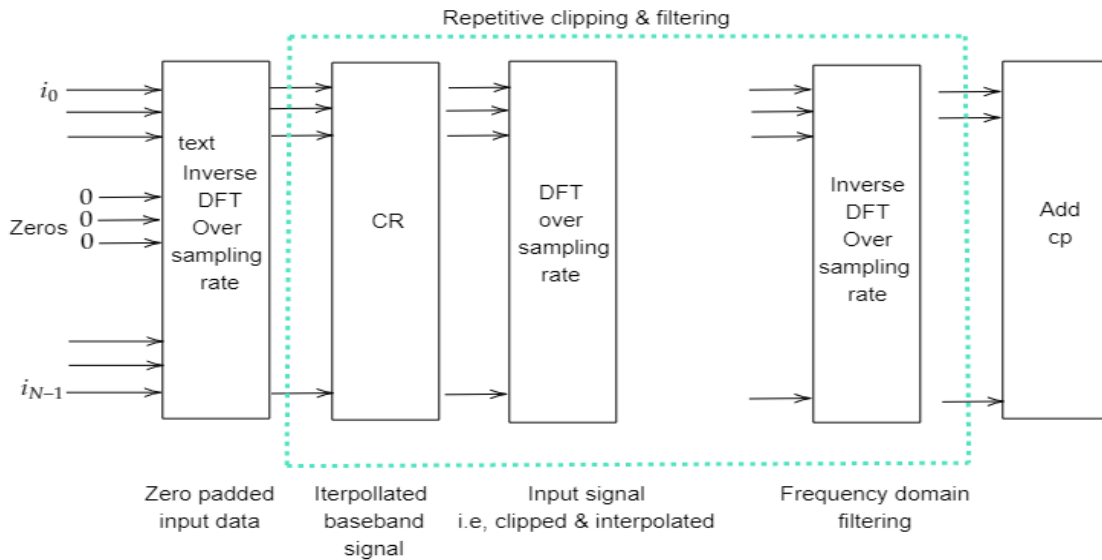


Figure 3: Block diagram of RCF method

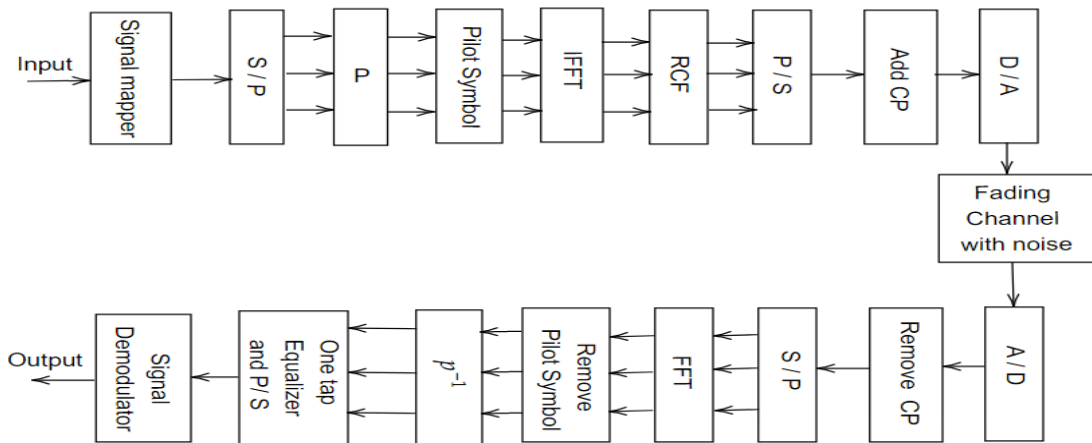


Figure 4: RCF Implemented OFDM model

The time domain signal is clipped and described as follows:

$$C = \begin{cases} \sqrt{c_{ratio} * E[|x|^2]}, & \text{if } |x|^2 > c_t \\ x, & \text{if } |x|^2 \leq c_t \end{cases} \quad (16)$$

Where C is the output of the time domain signal. The above equation signifies that clipping is done in the amplitude of discrete time domain signal. Amplitude is reduced whenever the signal exceeds the clipping level without changing the phase.

c_t is the threshold clipping level and it is given as:

$$c_t = c_{ratio} * E[|x|^2] \quad (17)$$

$|x|^2$ is the signal power, $E[|x|^2]$ is the expected mean and

c_{ratio} is defined the ratio of clipping level to mean power of the unclipped baseband signal.

Frequency domain filtering is done after time domain filtering to reduce OOB distortion.

3. Simulation Result

It is necessary to CCDF and BER of OFDM system when none PAPR technique is applied. From figure 5 and 6, without using PAPR technique CCDF of the system is equal to 10.95dB while PAPR is equal to 25.812 dB and SNR at BER 10^{-4} is 9.5612 dB

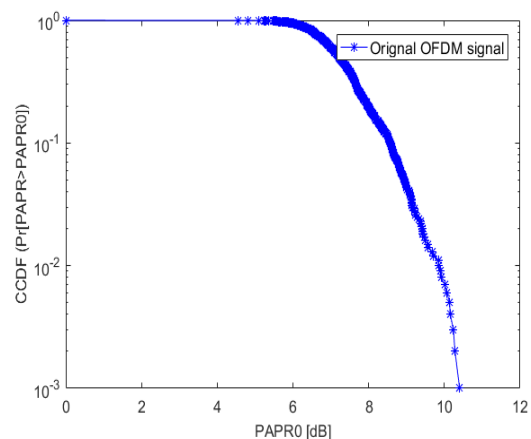


Figure 5: CCDF of OFDM system without using PAPR techniques

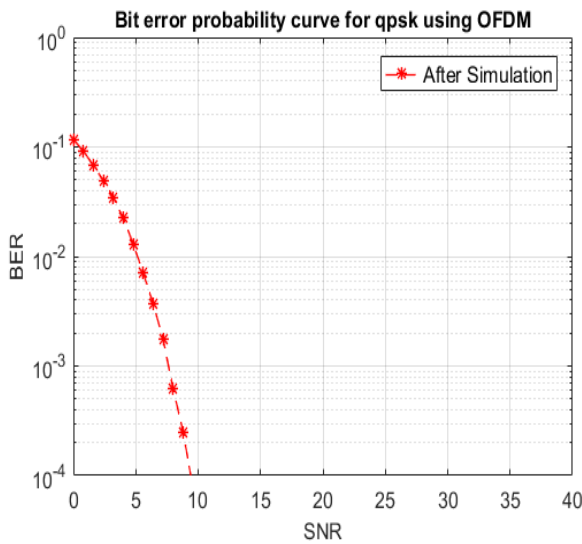


Figure 6: BER of OFDM system without using PAPR technique

From above it is clear that PAPR of system is quite high. So to reduce the PAPR of OFDM system PAPR reduction technique is applied i.e., RCF and RFC. These method useful BER is improved by filter while PAPR is improved by clipping method.

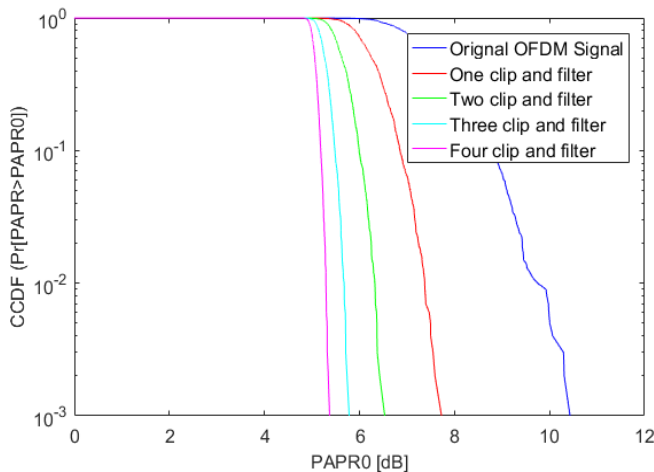


Figure 7: Effect of RCF on PAPR (CR=3 & I=2)

Table 1: CCDF and SNR

Technique	CCDF of PAPR	SNR
One clip and filter	7.681dB	8.6718dB
Two clip and filter	6.6426dB	9.412dB
Three clip and filter	5.818dB	12.231dB
Four clip and filter	5.502dB	14.335dB

From figure 7, 8 and 9, It shows for CR=3 and I=2, PAPR is improving and SNR also increasing which is shown below SNR is improved when PAPR reduction

technique is applied. It is also found SNR and CCDF of PAPR shows opposite relationships.

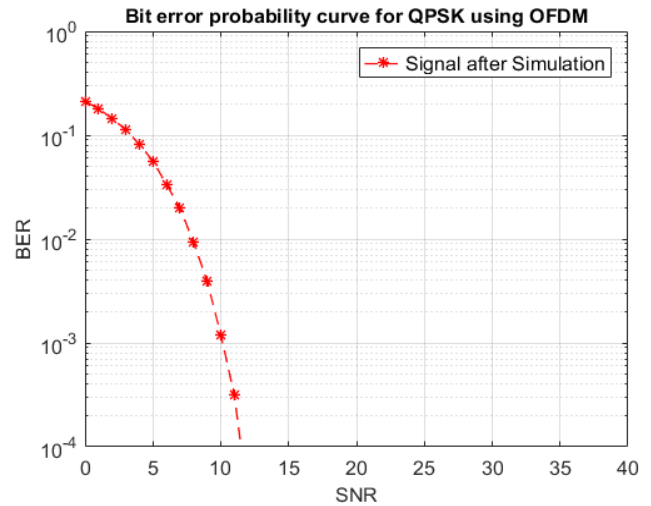


Figure 8: SNR vs BER curve after PAPR reduction applied on original OFDM signal

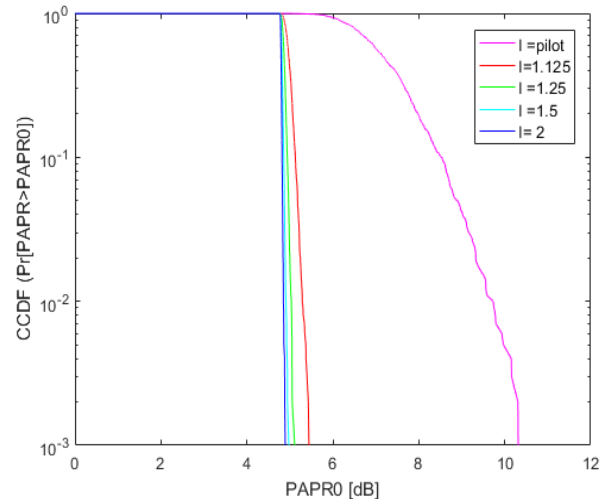


Figure 9: CCDF of OFDM method for different values of 'I' (oversampling)

Table 2: CCDF of PAPR

I	CCDF of PAPR
pilot	11.365dB
1.125	5.306dB
1.25	4.968dB
1.5	4.895dB
2	4.776dB

On increasing the values of 'I', PAPR of OFDM decreases except I=pilot. CCDF improves when I increase and CR decreases.

4. Conclusion

Performance of OFDM is degraded due to high value of PAPR. This drawback is minimized by RCF method. CCDF of PAPR of original is found to be

7.681dB with SNR 8.6718dB which is reduced by using repeated clipping method and it is reduced up to 5.502dB with increased SNR 14.335dB value also BER also improved along with. Reduction in PAPR helps in performance improvement of OFDM system.

References

- [1]. S. A. Mondal, S. Chakraborty, S. Mondal, R. Ghosh, M. Samanta, and P. Mukherjee, "Approach to reduce PAPR in Orthogonal Frequency Division Multiplexing Technique," *Turk. J. Comput. Math. Educ.*, vol. 12, no. 10, pp. 4480-4484, 2021.
- [2]. R. Musabe, M. B. Lionel, V. M. Ushindi, M. Atupenda, J. Ntaganda, and G. Bajpai, "PAPR reduction in LTE network using both peak windowing and clipping techniques," *J. Electr. Syst. Inf. Technol.*, vol. 6, no. 3, 2019. doi: 10.1186/s43067-019-0004-1.
- [3]. V. Ghode, S. Gawande, and S. Tiwari, "A review study on orthogonal frequency division multiplexing," *Paripex-Indian J. Res.*, vol. 10, no. 1, Jan. 2021.
- [4]. B. Kotade, A. B. Nandgaonkar, and S. L. Nalbalwar, "Peak-to-average power ratio reduction techniques in OFDM: A review and challenges," in *2018 International Conference On Advances in Communication and Computing Technology (ICACCT)*, pp. 319-324, 2018.
- [5]. M. D. Martín-Sacristán, J. F. Monserrat, J. Cabrejas-Peñuelas, D. Calabuig, S. Garrigues, and N. Cardona, "On the way towards fourth-generation mobile: 3GPP LTE and LTE-advanced," *EURASIP J. Wirel. Commun. Netw.*, vol. 2009, 2009. doi: 10.1155/2009/354089.
- [6]. S. Srikanth, V. Kumarn, C. Manikandan, and M. Murugesapandian, "Orthogonal frequency division multiplexing: is it the multiple access system of the future?," AU-KBC Research Center, Anna University, Chennai, India, 2018.
- [7]. C. Choudhary and V. Gupta, "A Study of Performance Enhancement Schemes for Multicarrier Transmission," *Int. J. Comput. Appl.*, vol. 68, no. 5, pp. 50-54, Apr. 2013.
- [8]. H. D. Joshi, "Performance augmentation of OFDM system," Ph.D. dissertation, Jaypee Univ. of Engineering and Technology, India, May 2012.
- [9]. R. W. Bäuml, R. F. H. Fischer, and J. B. Huber, "Reducing the peak-to-average power ratio of multicarrier modulation by selected mapping," *IEEE Electron. Lett.*, vol. 33, pp. 2056-2057, Oct. 1996.
- [10]. R. Prasad. OFDM for Wireless Communications Systems. Artech House Publishers, August 2004.

Copyright: This article is an open access article distributed under the terms and conditions of the Creative Commons Attribution (CC BY-SA) license (<https://creativecommons.org/licenses/by-sa/4.0/>).

Abbreviations

AI	Artificial Intelligence
BER	Bit Error Rate
BW	Band Width
CCDF	Complementary Cumulative Distribution Function
CF	Crest Factor
CR	Clipping Ratio
DAB	Digital Audio Broadcasting
DVB	Digital Video Broadcasting
HPA	High Power Amplifier
IFFT	Inverse Fast Fourier Transform
i.i.d.	Independent identically distributed
IoT	Internet of Things
mPSK	Minimum Phase Shift Keying
OFDM	Orthogonal Frequency Division Multiplexing
OOB	Out-of-Band distortion
PAPR	Peak-to-Average Power Ratio
QAM	Quadrature Amplitude Modulation
QPSK	Quadrature Phase Shift Keying
RCF	Repeated clipping and frequency domain filtering
RFC	Repeated frequency and clipping domain filtering

Assessment of Village-wise Soil Nutrients and their Effect on Sugarcane Productivity in Western Maharashtra, India

Chhaya Narvekar ^{1*}, Madhuri Rao ²

¹ Information Technology Department, Xavier Institute OF Engineering, Mumbai,400016 , India

² Information Technology Department, Thadomal Shahani College OF Engineering, Mumbai,400050 , India

*Corresponding author: Chhaya Narvekar, Mahim, Mumbai, 8097181363, chhaya.n@xavier.ac.in

ABSTRACT: Soil fertility needs to be assessed to develop strategies for long-term agricultural productivity. A study has been undertaken at Shirol tehsil, Kolhapur district, Maharashtra state, India to evaluate the fertility status of soil using nutrient index approach. For the present study PH, organic carbon, and EC were chosen as potential markers of soil quality along with primary nutrient potash and phosphorous. Objectives of this research are i) To provide nutrient availability index, ii) To assess soil fertility status and sugarcane productivity in the study area. Based on the soil parameters analysis, it is found that the soil is fertile. Sugarcane is the most cultivated crop in this area and the productivity of sugarcane is observed to be higher in study area as compared to national productivity. The nutrient index values for PH, Organic carbon and Phosphorous were normal, EC was low, and Potash was high. It is also observed that all ten years of study potash is high. Productivity change as well as nutrient values change over a period of time tested with standard t- test approach.

KEYWORDS: Fertility, Micronutrients, Nutrient index value, Productivity

1. Introduction

1.1. Soil nutrient

Nutrient management based on soil tests has become a major problem in attempts to boost agricultural productivity. The sustainability of Indian agriculture is a subject of growing concern due to declining soil fertility. In general, soil quality and soil health are synonymous with soil fertility, or the soil's reserve of agricultural nutrients. It is important to acquire a single number for each nutrient in order to compare the levels of soil fertility between different areas. Nutrient Index Value (NIV) is one of the approach [1]. Soil analysis aids farmers and agricultural producers in determining which fertilizers are required and in what quantities they should be applied to the plant to generate a profitable crop [2]. The 5th of December is designated as "World Soil Day." India joins the rest of the world in recognizing the importance of soil and its role in our country's overall growth and well-being. To produce crops, farming combines manufactured agricultural equipment, natural capital soil, and human capital such as farmer expertise. The presence of currently used pesticides in the agricultural regions is found to be of major concern in many countries, indicating the need for

long-term monitoring programs, particularly in regions with intensive agricultural activities, to determine the fate and accumulation of currently used pesticides in reality [3, 4]. Soil fertility is a dynamic natural quality that changes as a result of both natural and human-induced influences. Figure 1 depicts the nutrient available in soil.

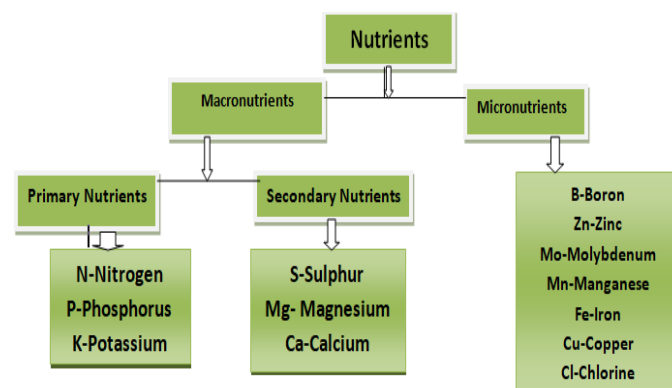


Figure 1: Nutrients available in soil

Soil chemical properties are one of the factors that influence soil fertility. The ability of the soil to naturally provide plants with the right kinds and amounts of nutrients is referred to as soil fertility [5,6,7]. Soil productivity refers to a soil's ability to produce crops

under specified management regimes and is measured in yields. Fertile soils are found in all productive soils [8-10].

A soil test is a chemical method for estimating the nutrient-supplying power of soil. The primary objective of soil testing is its ability to determine the nutrient status of the soil before the crop is planted. If the soil has an adequate supply of nutrients, it refers to the soil's ability to support life, generate economically valuable crops and sustain soil health without deterioration [11].

The Physico-chemical parameters analyzed in this research are: PH-The most significant property of soil is its PH level. Its effects on all other parameters of soil are profound. Electrical conductivity is another essential feature of soil that is used to determine its quality. It is a metric for the number of ions in a solution. When the concentration of ions in a soil solution rises, so does its electrical conductivity. Phosphorus is an essential component of every living cell. It's one of the most crucial macronutrients for plant development. Potassium is involved in a variety of plant metabolism events, including the generation of cellular structural components, photosynthetic regulation, and the production of plant sugars that are required for a variety of plant metabolic demands. The foundation of soil fertility is organic carbon in the soil. It releases nutrients for plant growth, helps to maintain soil structure and biological and physical health, and acts as a buffer against dangerous elements. Increasing soil organic carbon has two advantages: it aids in climate change mitigation and enhances soil health and fertility [12, 13]. Plants require thirteen vital nutrients as shown in Figure 1, which they obtain from the soil . Macronutrients are the six nutrients that plants require classified as primary nutrients N-P-K stands for Nitrogen, Phosphorus, and Potassium, and secondary nutrients are Calcium, Magnesium, and Sulphur. Micronutrients are the other nutrients that are only required at trace levels. Soil chemical properties are linked to properties that have a direct impact on plant nutrition.

1.2. Description of study area

In this research, five soil parameters are analysed for twenty villages as discussed in the second section, by calculating nutrient index values for the Shirol Tehsil, Kolhapur district, Maharashtra. Shirol Taluka of Kolhapur district is gifted by the presence of natural irrigation potential on account of five major rivers, i.e., Krishna, Panchaganga, Warana, Dudhganga, and Vedganga. The soil type here is alluvial. Normal rainfall is from June-October, with 1019.5 mm. The top three crops cultivated are sugarcane at 113.9 ('000 ha), paddy rain-fed at 113.8 ('000 ha), and groundnut at 57.4 ('000 ha) . India is the world's second-largest producer of sugarcane after Brazil. Sugarcane is grown in all of India's states and at various times of the year.

1.3. Methods and material

Soil fertility Status in India and measure taken

There are different types of soil in India, from the alluvial of the Indo-Gangetic plains to the dark red and black soils of the Deccan Plateau. The Government of India continues to have serious concerns about the health and quality of the soil. The Soil Health Card (SHC) programme launched in February 2015, is one of many soil health monitoring programmes being run by the Government of India. Under this programme, uniform standards are followed across all States for soil analysis. According to this plan, soil health condition is evaluated in relation to 12 significant soil factors, which depicted in Figure 2

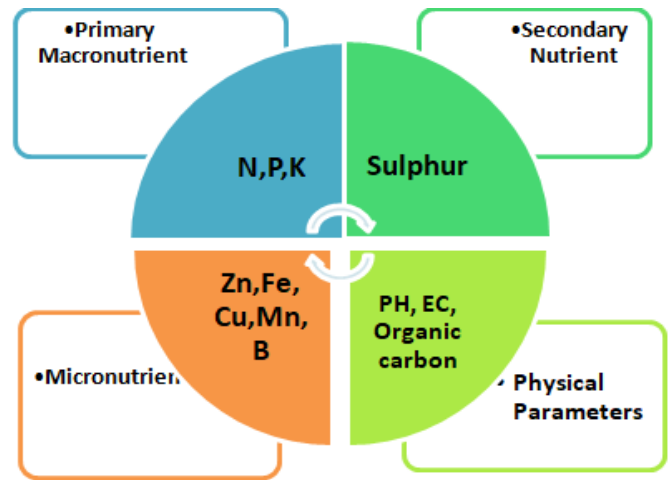


Figure 2: Significant soil parameters in SHC

State-wise Soil Nutrient Indices - Macro and Micro Nutrient for the Maharashtra State are as in Table 1 for two cycles. That clearly indicates potash is increased, nitrogen and Organic carbon are low.

Table 1: Maharashtra State Nutrient Indices

First Cycle- (2015-17)			Second Cycle (2017-19)		
L	M	H	L	M	H
B, Fe, S, Zn, OC, N	P, Cu, Mn	K	N, B, Fe, S, Zn	P, OC, Cu, Mn	K

1.4. Agricultural Practices in the study area

In India, small and marginal farmers follow basic fertilizer recommendations for N, P, and K, which rarely match soil fertility needs and frequently ignore secondary and micronutrients [14-16]. Aiming to sustain soil health and agricultural output, the Indian government is pushing integrated nutrient management (INM).

2. Material

Soil testing data is made available for research purposes by Shree Dutta Sugar Factory Shirol. Sugar mill provide soil testing facility to farmers to motivate them to

test their soil. Temporal time window is of ten years of data from the years 2010–2020. The data description is shown in Table 2.

Table 2: Descriptive Statistics of the Whole dataset

Descriptive	PH	EC	OC	P	K
Mean	7.51	0.65	0.75	27.84	543.96
Standard Error	0.00	0.01	0.00	0.26	2.32
Median	7.55	0.46	0.75	17.00	504.00
Mode	7.50	0.30	0.60	7.50	1120.00
Standard Deviation	0.41	0.92	0.30	26.59	239.12
Sample Variance	0.16	0.84	0.09	707.06	57178.72
Kurtosis	17.52	189.5	547.7	10.73	3.95
Skewness	-1.83	10.77	13.17	2.00	1.12
Range	8.00	27.97	14.76	476.62	2689.70
Minimum	0.60	0.03	0.04	0.38	0.30
Maximum	8.60	28.00	14.80	477.00	2690.00
Sum	79469	6888	7977	294494	5754524
Count	10579	10579	10579	10579	10579

2.1. Method

The nutrition index (N.I) value is a measurement of the soil's ability to give nutrients to plants. The nutrient index approach introduced by Parker and adopted and modified by many researchers Nutrient index is used to evaluate the fertility status of soils based on the sample classification. Sample are divided into three categories, low, medium and high. Region wise nutrient index can be calculated using the following formula [17]:

$$\text{Nutrient Index (N.I.)} = (L \times 1 + M \times 2 + H \times 3) / \text{TOTAL}$$

where,

L: Count of sample with low nutrient status.

M: Count of sample with medium nutrient status

H: Count of sample with high nutrient status

TOTAL: This is total number of samples taken for a given area.

The total number of samples analyzed in this research is 10579.

Table 2 presents the descriptive statistics for the all sample and corresponding parameters. For the period of study (2010-2020) year wise nutrient index is calculated for the soil parameters under study. Twenty sample villages from Shirol Tehsil, western Maharashtra were selected for assessing village-wise average parameters. Ten year parameter wise nutrient status in the study area is shown in Table 3-Table 6 and Figure 1 through Figure 5.

For selected village all farmers data used for calculation of village soil property status for ten years from 2010-2020. Yearly nutrient index is calculated combining all twenty village samples for that year, which is indicated in Table 7. Samples are classified as per Table 6. Figure 4 shows NIV trends over ten years. Table 6 gives overall soil nutrient status of study area.

As sugarcane is dominating crop of the study area, sugarcane production for the same temporal window is used for finding the productivity of the region. Sugarcane production data is made available by Shree Dutta Sugar Factory Shirol [18]. Production is recorded with six features such as farmer name, gat number, area, irrigation mode, cane variety and compute type, etc. number of records are 287475, recorded from the year 2010 to 2020. By using this dataset village-wise sugarcane cultivated area and total production from that further derived feature is the productivity of a particular village. Study area productivity is calculated per year as shown in Figure 5, this data is derived from all village productivity. Soil parameters and sugarcane productivity analysis is done for same time window, so tried to see a correlation between nutrient index value and productivity. This study found a positive correlation but less. Compute type is a crop cultivation method based on the season which is impacting the production and maturity and also has an effect on production.

2.2. Classification of Nutrient Index Value

Based on the macronutrient Nutrient index value calculated for the study area, which is a fertility indicator of soil. Soil parameters and their nutrient indices for ten years are as shown in Table 7. Figure 4 clearly observe potash is excess during all the years this is tested with T-test for testing hypothesis H_0 Potash in study area is above normal range, and accepted the null hypothesis. This could be due to excess fertilizer use. Electrical conductivity is towards lower border. Most of the soil samples are alkaline as PH is on the higher side. Organic carbon is observed normal, phosphorus is fifty percent normal, rest is below normal. Soil fertility status was calculated from all samples and labeled into three classes as per Table 6, and labels are shown in Table 8.

Table 3: Village-wise Ten Year Phosphorous status mg kg⁻¹

Village Name	2010-11	2011-12	2012-13	2013-14	2014-15	2015-16	2016-17	2017-18	2018-19	2019-20
AKIWAT	10.81	10.89	14.55	28.00	21.10	32.16	17.84	11.05	57.68	51.99
ARJUNWAD	14.30	10.59	15.62	16.80	21.33	18.74	14.12	9.55	37.88	58.57
BORGAON	8.00	11.13	11.60	21.00	23.30	15.49	14.47	8.40	30.55	47.11
CHAND-	10.67	6.89	11.76	17.50	16.50	43.01	12.97	7.10	29.51	61.34
CHINCHWAD	11.02	14.43	16.58	23.53	21.10	25.52	7.01	6.36	42.88	50.84
DATTANAGAR	10.21	15.70	13.43	18.00	38.00	32.99	11.64	6.42	32.28	56.03
JAMBHALI	9.25	11.29	13.51	25.29	32.60	28.63	15.21	9.59	42.61	53.85
JANWAD	5.00	8.88	12.28	18.18	44.20	15.32	14.71	6.21	30.04	64.17
KURUNDWAD	11.37	12.71	12.94	20.56	24.23	33.88	13.59	10.58	53.24	55.50
MANGAVATI	7.21	10.09	15.74	26.00	34.90	36.66	12.42	8.66	26.87	57.82
NANDANI	16.21	13.59	14.77	13.57	21.74	36.15	13.91	11.20	36.34	54.93
RAJAPUR	6.97	10.64	15.10	18.25	16.80	31.81	7.00	7.47	41.12	49.55
SHAHAPUR	9.31	8.50	13.28	21.97	32.60	33.56	15.34	8.96	24.98	47.70
SHEDBAL	6.83	5.78	5.95	19.25	18.60	14.36	8.95	7.89	33.62	55.30
SHIRATI	11.12	10.36	15.08	19.89	16.10	26.22	18.34	8.36	29.18	60.24
SHIRDHON	16.92	7.35	11.46	15.05	20.43	37.16	15.36	9.75	43.48	62.89
SHIROL	10.24	10.17	13.60	22.74	22.62	25.23	17.23	9.45	41.79	66.71
TAKALI	9.11	8.03	10.48	18.00	32.60	29.17	12.75	9.73	49.65	52.84
TERWAD	15.80	14.14	7.68	21.67	10.00	16.15	12.85	7.98	40.66	44.67
UDGAON	10.43	7.82	12.35	22.15	12.15	33.72	8.29	9.65	35.14	53.89

 Table 4: Village-Wise Ten Year Potash Status Mg Kg⁻¹

Village Name	2010-11	2011-12	2012-13	2013-14	2014-15	2015-16	2016-17	2017-18	2018-19	2019-20
AKIWAT	367	417	525	392	319	328	670	516	597	367
ARJUNWAD	417	427	451	691	547	473	578	663	635	417
BORGAON	277	319	358	414	706	454	453	519	545	277
CHAND-SHIRADWAD	310	350	542	429	498	439	461	615	572	310
CHINCHWAD	515	578	869	468	577	553	740	696	648	515
DATTANAGAR	423	397	503	715	347	457	529	781	547	423
JAMBHALI	335	415	477	565	480	433	709	725	654	335
JANWAD	415	426	470	529	829	613	531	606	771	415
KURUNDWAD	238	326	643	353	907	452	492	628	594	238
MANGAVATI	324	366	459	479	631	421	664	558	485	324
NANDANI	405	419	566	657	717	502	433	669	703	405
RAJAPUR	498	684	570	573	755	494	567	624	623	498
SHAHAPUR	278	504	339	347	862	484	398	770	661	278
SHEDBAL	286	371	379	439	720	426	621	626	565	286
SHIRATI	300	336	440	477	829	514	538	660	605	300
SHIRDHON	454	339	563	607	717	468	580	668	682	454
SHIROL	381	403	525	530	549	555	501	615	643	381
TAKALI	437	391	454	376	577	443	596	640	566	437
TERWAD	505	414	510	324	347	582	747	740	722	505
UDGAON	433	457	460	405	535	531	605	604	666	433

Table 5: Village-wise Ten Year Organic Carbon % Status

Village-> Year	2010-11	2011-12	2012-13	2013-14	2014-15	2015-16	2016-17	2017-18	2018-19	2019-20
AKIWAT	0.55	0.67	0.57	0.90	0.87	0.75	0.68	0.78	0.67	0.86
ARJUNWAD	0.64	0.71	0.58	0.62	0.61	0.72	0.91	0.84	0.77	0.73
BORGAON	0.51	0.55	0.54	0.50	0.48	0.66	0.79	0.88	0.74	0.77
CHAND-SHIRADWAD	0.53	0.65	0.48	0.38	0.60	0.56	0.60	0.79	0.68	0.81
CHINCHWAD	0.60	0.81	0.72	0.65	0.69	0.74	0.84	0.84	0.81	0.86
DATTANAGAR	0.50	0.54	0.65	0.55	0.90	0.72	0.84	0.83	0.75	0.74
DHARANGUTTI	0.63	0.64	0.63	0.67	0.82	0.78	0.81	1.03	0.82	0.82
JAMBHALI	0.71	0.70	0.66	0.63	1.92	0.73	0.87	0.86	0.92	0.84
JANWAD	0.49	0.64	0.70	0.49	1.05	0.68	0.67	0.85	0.77	0.80
KURUNDWAD	0.60	0.68	0.67	0.51	0.59	0.69	0.88	0.94	0.76	0.83
MANGAVATI	0.66	0.59	0.61	0.57	0.81	0.72	0.94	0.76	0.69	0.75
NANDANI	0.67	0.99	0.64	0.71	0.45	0.81	0.81	0.93	0.79	0.89
RAJAPUR	0.57	0.60	0.56	0.64	0.48	0.68	0.65	0.66	0.72	0.81
SADALGA	0.55	0.55	0.57	0.56	0.77	0.73	0.82	0.82	0.79	0.88
SHAHAPUR	0.93	0.60	0.64	0.51	1.05	0.64	0.69	0.90	0.81	0.80
SHEDBAL	0.45	0.62	0.58	0.53	0.78	0.65	0.81	0.75	0.74	0.88
SHIRATI	0.63	2.53	0.75	0.62	0.84	0.82	0.82	0.80	0.81	0.85
SHIRDHON	0.58	0.74	0.59	0.68	0.51	0.90	0.80	0.78	0.72	0.84
SHIRGUPPI	0.72	0.58	0.54	0.58	0.45	0.49	0.81	0.73	0.86	0.75
SHIROL	0.60	0.64	0.62	0.58	0.84	0.76	0.84	0.84	0.78	0.83
TAKALI	0.64	0.61	0.70	0.51	0.60	0.62	0.83	0.87	0.75	0.70
TERWAD	0.59	0.63	0.58	0.40	0.72	0.80	0.76	0.70	0.82	0.68
UDGAON	0.33	0.64	0.64	0.65	0.57	0.87	0.91	0.91	0.85	0.83

Table 6: Nutrient Index Value- Classification.

Nutrient Class	Nutrient Index Value
LOW	< 1.66
MEDIUM	1.67-2.33
HIGH	>2.33

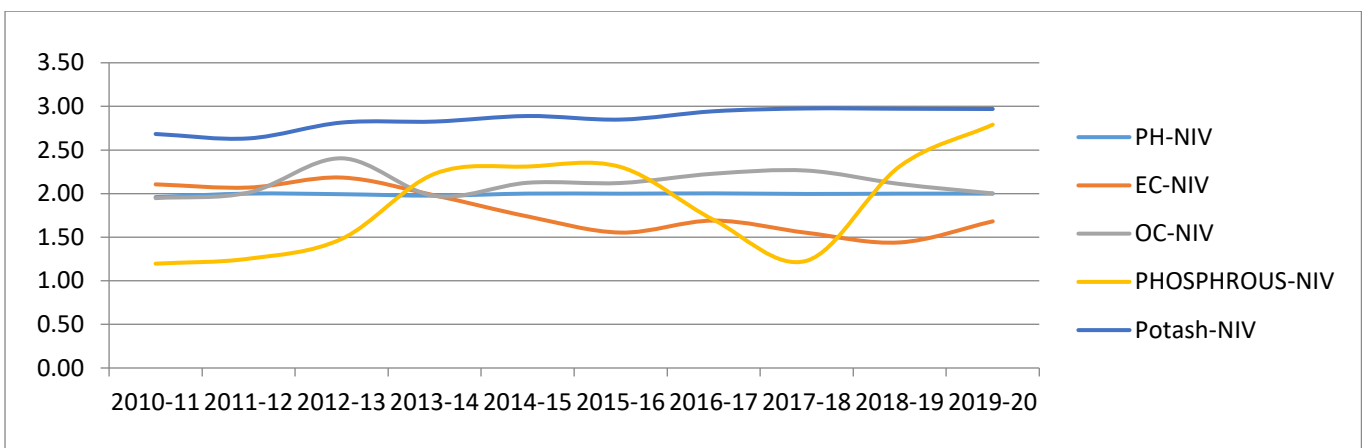


Figure 4: The trend in Nutrient Index value in the study area

Table 7: Nutrient Indices for ten years

YEAR	PH-NIV	EC-NIV	OC-NIV	PHOSPHROUS-NIV	Potash-NIV
2010-11	1.96	2.11	1.95	1.20	2.68
2011-12	2.00	2.07	2.01	1.25	2.63
2012-13	1.99	2.18	2.40	1.48	2.81
2013-14	1.98	1.98	1.97	2.23	2.83
2014-15	2.00	1.74	2.12	2.31	2.89
2015-16	2.00	1.55	2.12	2.30	2.85

2016-17	2.00	1.69	2.23	1.70	2.94
2017-18	2.00	1.55	2.26	1.23	2.98
2018-19	2.00	1.44	2.11	2.31	2.97
2019-20	2.00	1.68	2.00	2.79	2.97
2010-20	2.00	1.63	2.33	2.13	2.89

Medium is the acceptable range for many crops. We can say soil is fertile but needs proper nutrition management to avoid deficiency as well toxicity of soil.

Table 8: Percentage- NIV –Shirol Tehsil

Soil Property	L	M	H	NIV	Fertility Index
PH	0.53	99	0.09	2.00	Medium
EC-dsm-1	57	22	20	1.63	Low
OC %	9	49	42	2.33	Medium
PHOS- mg kg-1	28	30	42	2.13	Medium
Potash- mg kg-1	0.72	10	89	2.89	High

Productivity column is added for unit area production. Average productivity for the period of study in the study area is 99.6, which is greater than Maharashtra state productivity.

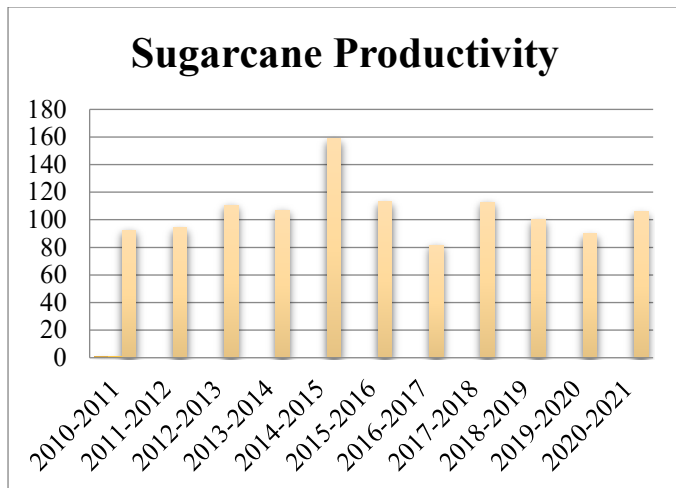


Figure 5: Sugarcane Productivity of study area in tons

3. Results and discussion

Dataset had outliers as well as missing values; those records are not considered for analysis. Based on available data and parameters following observations were noted. From Table 6 pH of soils is normal (99% Samples). Electrical conductivity was low (57 % samples). Organic carbon was found to be normal. The nutrient index value for major nutrients phosphorus normal and potash was found to be high. Average sugarcane productivity in India is 70-80, the average sugarcane

productivity in Maharashtra is 80.72, , and the average productivity of the study area is 99.6. Hypothesis is tested with standard test. H0 - Productivity of the region is increasing. From test statistics H0 is rejected and Ha is accepted as in productivity there is not much change over a period of study. This indicates soil is fertile and productive. Soil type is Black Soil, and from the nutrient index observation it is fertile as well. Black soils can be used for a variety of crops because of their high moisture content, which makes them ideal for growing cotton. Black cotton soil is another name for it in common usage. However, a wide variety of other crops, including rice, sugar cane, wheat, jowar, linseed, sunflower, cereal crops, citrus fruits, tomatoes, tobacco, groundnut, any crops, and millets and oilseeds, can be cultivated on these soils.

4. Conclusions

Understanding the consequences of existing farming practices and assessing the suitability of these soils for future policy formulations will help to ensure that this resource gives farmers the most benefit. This research will facilitate improved decisions for most of the stakeholders of the agriculture industry such as farmers, agriculture managers, and government bodies involved in policy-making for improvement in the economic production of agricultural products. Soil fertility index will help in nutrient management and fertilizer application. The soil nutrient index provides an index of nutrient availability for fertilizer recommendation and evaluation of soil fertility. According to soil fertility crop recommendation is possible. Soil health leads to the health of plants which gives healthy nutritious food for all living beings, so healthy life on the planet.

Acknowledgement

The authors are highly grateful to Shree Dutta Sugar Factory, Shirol, and the soil testing laboratory, for providing the necessary data to carry out this research and thankful to Thadomal Shahani Engineering College, Bandra, Mumbai, India.

References

- [1]. G. Singh, M. Sharma, J. Manan, and G. Singh, "Assessment of soil fertility status under different cropping sequences in District Kapurthala," *J. Krishi Vigyan*, vol. 5, no. 1, pp. 1-9, 2016. doi: 10.5958/2349-4433.2016.00023.4.
- [2]. A. Archana, V. S. Sankari, and S. S. Nair, "An economically mobile

- device for the on-site testing of soil nutrients by studying the spectrum," *Mater. Today: Proc.*, 2021. doi: 10.1016/j.matpr.2021.05.620.
- [3]. S. Sabzevari and J. Hofman, "A worldwide review of currently used pesticides' monitoring in agricultural soils," *Sci. Total Environ.*, 2021. doi: 10.1016/j.scitotenv.2021.152344.
- [4]. B. Rammoorthy and J. Bajaj, "Available N, P and K status of Indian soils," *Fertil. News*, vol. 14, no. 8, pp. 24-26, 1969.
- [5]. S. R. Kashiwar, M. C. Kundu, and U. R. Dongarwar, "Assessment and mapping of soil nutrient status of Sakoli tehsil of Bhandara district of Maharashtra using GIS techniques," *J. Pharmacogn. Phytochem.*, vol. 8, no. 5, pp. 1900-1905, 2019.
- [6]. M. T. Gedamu, "Assessment of soil quality index for agricultural purpose in Agamsa sub-watershed, Ethiopia," *AGBIR*, vol. 37, no. 2, pp. 102-107, 2021.
- [7]. J. Idowu, R. Ghimire, R. Flynn, and A. Ganguli, "Soil Health: Importance, Assessment and Management," *Cooperative Extension Service, College of Agriculture, Consumer and Environmental Sciences, Circular 694B*, 2019. [Online]. Available: http://aces.nmsu.edu/pubs/_circulars/CR694B/welcome.html. [Accessed: Dec. 9, 2021].
- [8]. T. Pandiaraj, P. P. Srivastava, S. Das, and A. K. Sinha, "Assessing soil fertility status of tasar host plants growing soils in Purulia district of West Bengal state," *J. Pharmacogn. Phytochem.*, vol. 7, no. 2, pp. 2966-2970, 2018. doi: 10.54026.203587108.
- [9]. [9] S. R. Kashiwar, M. C. Kundu, and U. R. Dongarwar, "Soil fertility appraisal of Bhandara block of Maharashtra using geospatial techniques," *Int. J. Chem. Stud.*, vol. 8, no. 2, pp. 2570-2576, 2020. doi: 10.22271/chemi.2020.v8.i2am.9136.
- [10]. B. Hermiyanto, S. Winarso, and W. Kusumandaru, "Soil Chemical properties index of tobacco plantation land in Jember District," *Agric. Agric. Sci. Procedia*, vol. 9, pp. 181-190, 2016. doi: 10.1016/j.aaspro.2016.02.118.
- [11]. S. S. Rana, *Principles and Practices of Soil Fertility and Nutrient Management*, Department of Agronomy, Forages and Grassland Management, CSKHPKV, Palampur, 2012. doi: 10.13140/RG.2.2.30430.02888.
- [12]. D. R. Montgomery and A. Biklé, "Soil health and nutrient density: beyond organic vs. conventional farming," *Front. Sustain. Food Syst.*, vol. 5, 2021. doi: 10.3389/fsufs.2021.699147.
- [13]. H. Pathak, "Trend of fertility status of Indian soils," *Curr. Adv. Agric. Sci.*, vol. 2, no. 1, pp. 10-12, 2010. [Online]. Available: <https://www.semanticscholar.org/paper/Trend-of-fertility-status-of-Indian-soils-Pathak/53540356>. [Accessed: May 20, 2024].
- [14]. F. W. Parker, W. L. Nelson, E. Winters, and I. E. Miles, "The broad interpretation and application of soil test information," *Agron. J.*, vol. 43, no. 3, pp. 105-112, 1951. doi: 10.2134/AGRONJ1951.00021962004300030001X.
- [15]. A. Reddy, "Impact study of soil health card scheme," *National Institute of Agricultural Extension Management (MANAGE)*, Hyderabad, 2018. doi: 10.31220/osf.io/n3d2m.
- [16]. N. R. Krishna, P. Chandravamshi, and L. B. Ashok, "Soil Fertility Status of Major Nutrients, Micronutrients and Mapping in Nicchapura-2 Micro Watershed of Davanagere District, Karnataka," *Int. J. Curr. Microbiol. Appl. Sci.*, vol. 6, no. 9, pp. 1178-1186, 2017. doi: 10.20546/ijcmas.2017.609.142.
- [17]. ICAR_CRIDA_NICRA, "Chapter 2: Soil Health and Nutrient Management," 2017. [Online]. Available: https://mospi.gov.in/documents/213904/0/b14_Chapter+2+%282%29.pdf/432d7ade-8bea-52eb-9eb1-ffe8ba9c475b?t=1612935861353.
- [18]. Website: <http://dattasugar.co.in/>

Copyright: This article is an open access article distributed under the terms and conditions of the Creative Commons Attribution (CC BY-SA) license (<https://creativecommons.org/licenses/by-sa/4.0/>).

CHHAYA NARVEKAR received the B.Tech. degree in Information Technology in 2001 from SNDT University, Mumbai and, M.E Degree in Computer Engineering from Mumbai University in 2008. She is currently working as Assistant Professor in the Department of Information Technology, at Xavier Institute Engineering, Mumbai, India. She has eighteen year of experience. Her current research interests include AI/ML/DL, Computer Vision, Machine learning, Cryptography & Network Security. She has published papers in IEEE conferences. She is a life member of ISTE and IETE.

DR. MADHURI RAO has done her PhD, and currently working as Professor and Head Of Department of AI & DS department. She has published research papers in various conferences and journals. Her area of research includes, Big Data Analytics, Software Project Management, Data Warehousing Mining and Business Intelligence, Software Engineering, Database technologies, Parallel Computer Architecture, Management Information System, Machine Learning

Trajectory Correction Method of Motion Description Language of Vertebral Milling Robot based on Force Feedback

Wei Ding¹, Zhaoming Liu², Hongwei Wang², Long Cui^{*2}

¹Shenyang Institute of engineering, Department of Communication, College of Automation, Shenyang, 110136, China

²Shenyang Institute of Automation, Chinese Academy of Sciences, State Key Laboratory of Robotics, Shenyang, 110016, China

*Corresponding author: Long Cui, No.114 Nanta Street, Shenhe District, +8602423970992 & Email: cuilong@sia.cn

ABSTRACT: In the real-time control procession of the vertebral milling robot, there are problems such as heavy workload of the operator, long working time, operational tremble and complicated procession. In order to solve the clinical practical basic problems such as avoiding excessive milling and force perception control of vertebral milling robot, this paper proposes a method of trajectory correction of motion description language of milling robot based on force feedback. The task of trajectory correction of the milling robot oriented to force feedback, on the basis of ensuring the atom relationship of motion description language, defines seven motion atoms for the function of avoiding excessive milling during the actual operation of the milling robot. A milling robot experimental system is built with a force feedback control handle and a milling robot. Experiments are carried out on the trajectory correction method of the milling robot based on the motion description language. The experimental results verify the feasibility and effectiveness of this method. The innovation of this paper is reflected in the following two aspects. The use of force feedback to define and model motion description language atoms is an innovation, and the application of motion description language trajectory correction method to the field of vertebral milling robots is an application innovation.

KEYWORDS: Milling robot, Motion description language, Force feedback, Trajectory correction, Vertebral lamina milling

1. Introduction

1.1. Vertebral milling robot

This template, In recent years, with the rapid development of society, the problem of aging population structure has become more and more serious. Spinal stenosis represented by lumbar disc herniation is a relatively common back pain caused by long-term compression of the medial spinal nerve by the spinal canal. The incidence of diseases, especially elderly people, is particularly high [1].

As people get older, the physiological functions of the human spine gradually degenerate, such as spinal hyperplasia and lamina thickening, which can cause the spinal canal space to become smaller and compress the spinal nerves. The degenerative condition can cause numbness and pain in the lower limbs of the patient, and in severe cases, it can lead to paralysis [2]. The most effective surgical treatment for this disease is lamina

decompression, and vertebral milling is an important step in the process of lamina decompression [3].

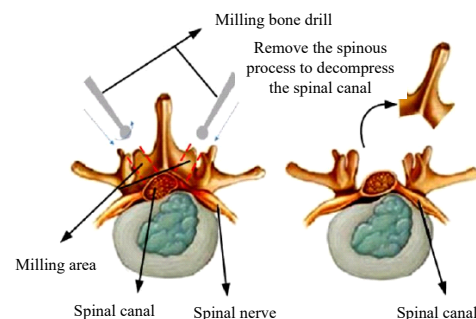


Figure 1: Schematic diagram of the "double window" of laminectomy

Vertebral lamina milling requires the doctor to mill the lamina of the lesion area and remove the spinous process with the aid of positioning and navigation, and mill the V-shaped groove on one or both sides of the spinous process of the spine, as shown in Figure 1. Expand the space and scope of the spinal nerves in the spinal canal, so that the

compression of the vertebral lamina wall on the nerves and blood vessels can be released, and the "single window" or "double window" operation of the vertebral lamina can be realized [4], so that the spinal nerves and vertebrae joints return to normal functions.

As we all know, the blood vessels and nerves that connect the brain and various organs are scattered around the spinal canal, and the risk of spinal surgery is higher. Improper operation during the surgery may damage the nerves and blood vessels around the spinal canal. The small residual amount of milling the lamina may damage the nerves in the spinal canal, and the excessive residual amount may not achieve the effect of decompression of the spinal nerves [5]. During the milling operation, the doctor basically relies on the operating experience to control the strength and feed depth of the milling. Therefore, doctors lacking experience in hand manipulation and strength cannot guarantee the success rate of surgery, and may cause surgical injury to patients. Medical surgery hospitals urgently need more advanced assistive robotic equipment to improve the current surgical situation [6].

In the field of orthopedic robots, the United States and Europe are at the leading level, and various countries in Asia and Europe are actively investing and developing. Common doctor operations in spinal surgery include drilling and milling. As early as 1992, French Sautot et al. used CT images to drill nail and used PUMA spinal surgery assistant robots to assist doctors in drilling nail path. In 2003, the second-generation Renaissance spine assist robot system developed by Israel's Mazor company realized automatic posture adjustment to assist doctors in drilling nail path [7]. In 2006, the VectorBot spine surgery robot system developed by Ortaier at the German Aerospace Center can realize the drilling and milling operations.

In China, the research on orthopedic surgical robots is still in the initial stage of accumulation, lagging behind Europe and the United States. In 2006, Wang of Beijing University of Aeronautics and Astronautics developed a spinal surgery milling system, which determined the state of vertebral milling by monitoring the force change of the bone drill when milling the vertebrae. In 2019, Li of Harbin Institute of Technology independently developed clinical-oriented SRAS image navigation, data acquisition and other software systems, and achieved many results in robotic laminar surgery planning methods.

1.2. Control method of surgical milling robot

Human spine bone is divided into two types, cortical bone and cancellous bone. The milling operation of spinal decompression and the drilling operation of screw insertion are both the inner cortical bone as a safe surgical restraint to avoid damage to the nerves and spinal cord in the spinal canal of the patient [8-9].

In recent years, scholars from various countries had also proposed a variety of effective control methods for the surgical operation of vertebral milling robots. Deng of the University of Hamburg used fuzzy control to adjust the feed depth and speed of the milling head in the process of vertebral milling, which improved the quality and efficiency of milling [10]. Wang used a parametric modeling method to identify the bone layer, but this method was based on the milling force data, and the difference in environmental parameters may cause the identification results to be inaccurate [11].

Compared with doctor operation, medical milling robot has many advantages such as anti-fatigue, anti-radiation and good stability [12]. In summary, the research on the control of medical milling robots is still in the accumulation stage. It is necessary to further improve the milling robot modeling and milling control methods.

2. Force Feedback and Motion Description Language

2.1. Force feedback

At this stage, with the practical application of milling robots, force feedback technology has become a very important information interaction technology for milling robots [13-15]. The introduction of force feedback into the milling robot system will increase the amount of information feedback and the milling accuracy of the doctor, which in turn will improve the milling quality, reducing misoperation, and shortening the milling operation time [16]. There are two types of force feedback methods for milling robots, direct feedback and perception substitution [17]. The direct feedback method is that the force sense information is directly fed back to the operator through the tactile device [18-19]. In short, we use the operation control unit with force feedback function to perform force perception, which can increase the immersion and realism of the doctor during the operation.

2.2. Motion Description Language

The basic physical model of the Motion Description Language (MDL), is also known as the motion state machine model. The motion state machine model is to form a mapping relationship from the state space to the output space. The motion state machine model definition [20-21] is:

$$\begin{aligned} \dot{x} &= G(x)(u + k(y)) \\ y &= h(x) \end{aligned} \quad (1)$$

Among them, x , y and u are the vector functions of the time variable t , G is the matrix, and h and k are the mapping of the vector space.

Under the framework of motion description language control theory, the control process and state process of a complete control system can be decomposed into several

small segments and sub-processes. Each sub-process is expressed by a triple (u, k, t), this triple is called a motion atom, where u is the control input, k is the control law, and t represents time. Represent a continuous state system in segments, and then use parameterized motion atoms (u, k, t) to represent each sub-process, and reconstruct the original continuous system in the form of a sequence of motion atoms, we can use a set of discrete motion atom symbol sequences to drive the original continuous system.

The triples (u_i, k_i, T_i) are called "motion atom", and the set consisting of these triples is called the "motion alphabet". The robot control process program is a symbol string composed of motion atoms to realize the drive and control of the robot. Representing a continuous system in segments, and then expressing each segment with parameterized motion atoms, a sequence of discrete symbols can be used to drive the continuous system.

It is described by the spatial kinematics of the robot of end tool coordinate system. If the end of robot moves along a curve in space, the general form of the curve equation [22] is:

$$\begin{cases} F_1(x, y, z) = 0 \\ F_2(x, y, z) = 0 \end{cases} \quad (2)$$

This curve is simplified as F(X)=0, where X=(x,y,z)^T,

$$\textcircled{\otimes} \mathbf{F}(\mathbf{X}) = \begin{pmatrix} F_1(x, y, z) \\ F_2(x, y, z) \end{pmatrix} \quad (3)$$

If the initial state of the robot is x₀=x(t₀), after receiving the combination of motion atoms (u₁, k₁, T₁) (u₂, k₂, T₂)...(u_n, k_n, T_n), the system state motion law can be expressed as:

$$\begin{aligned} \dot{x} &= G(x)(u_1 + k_1(y)); & t_0 \leq t < t_0 + T_1 \\ \dot{x} &= G(x)(u_2 + k_2(y)); & t_0 + T_1 \leq t < t_0 + T_1 + T_2 \\ & \vdots & \vdots \\ \dot{x} &= G(x)(u_n + k_n(y)); & t_0 + \sum_{i=1}^{n-1} T_i \leq t < t_0 + \sum_{i=1}^n T_i \end{aligned} \quad (4)$$

In the above formula, u, X, and y are functions of t. u is the system input function. X is the n-dimensional system state function. y is the output function of the system, and k is the n-dimensional state feedback.

From the perspective of bionics and artificial intelligence, robot behavior is defined as a collection of continuous actions of a robot with certain characteristics. The design of the motion description language atom function is used to express a certain behavioral feature of the robot, and the robot's behavior is corresponding to the motion atoms of the motion description language. Designing a set of symbol strings composed of motion atoms is called motion planning of a robot. The structure of the robot control system based on the motion description language method is shown in Figure 2. Overall, the robot controller is responsible for path

planning and motion description language atom sequence generation.

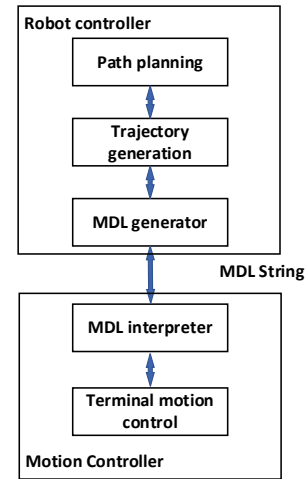


Figure 2: Control system configuration of MDL framework

The compiler receives a sequence combination of motion atoms, and then the compiler translates this sequence into segments and maps the motion segment group. The slave robot can autonomously complete the motion segment expressed by the atom. The master operator organizes the motion control program sequence according to the robot's motion alphabet, and the slave robot actuator generates the actual motion to complete the robot's planning task.

2.3. Motion Description Language Model of the Vertebral Milling Robot based on Force Feedback

The medical milling robot is applied to the milling process of human vertebral laminae, and its expected movement path has been clarified. However, due to the large differences in the stiffness and hardness of human tissue, cortical bone and cancellous bone, the robot may encounter different resistance and impedance conditions during real-time operations. In the task of orthopedic milling operations, the robot is required to have a certain degree of compliance with the force of the human tissue to avoid excessive damage. Therefore, this article refers to forming an admittance model between the robot and the force feedback sensor, and modeling the working environment as a spring system model [23].

The impedance factor and force feedback are used as the control reference factors for adjusting the robot trajectory. In the MDL control process, not only the position and posture, but also the resistance factor must be considered. That is, the force feedback has an influence on the MDL control process, forming an admittance factor, and achieving force-based feedback MDL control. Due to the effects of various organizations and resistances, the robot's planned path deviates from the actual path, and the robot's posture needs to be adjusted to achieve the desired trajectory planning [24].

Admittance control is a control method based on the dynamic relationship between force and speed or position. The admittance model can be regarded as the inverse process of the impedance model [25].

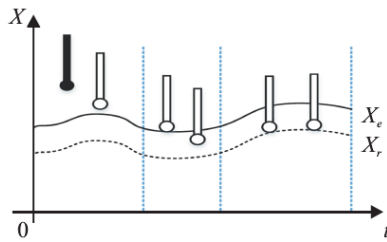


Figure 3: The contact diagram of the robot end with the environment

The contact process between the milling robot and the environment can be divided into two stages, (1) non-contact and no-load spatial movement; (2) constrained spatial movement after contact with the environment [26]. The contact procession is shown in Figure 3. X_e represents the position of the working environment, X_r represents the actual position of the end effector of the milling robot [27-28].

In this paper, the control algorithm adopts the admittance control method to realize the control process of the contact force. The control block diagram is shown in Figure 4. The model of force-sensing milling robot system is simplified to a "spring-damping" second-order system model, and the working environment model is simplified to a first-order spring model [29-30].

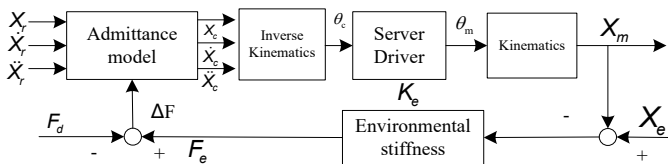


Figure 4: Control block diagram of position-based force tracking admittance model

In Figure 4, the meaning of each variable is shown in Table 1. In general, position control satisfies the variable $X_c=X_m$, and the error between the expected reference trajectory and the actual trajectory of the robot is $E=X_m-X_r=X_c-X_r$.

Table 1: Variable Table of Admittance Control Model

NO.	Variable name	Variable meaning
1	X_m	The actual track position of the milling robot
2	X_c	Trajectory position command sent to the milling robot
3	X_r	The trajectory position variable corresponding to the desired tracking force at the end of the milling robot
4	K_e	Environmental stiffness
5	X_e	Environment location variables
6	F_d	Desired tracking power
7	F_e	The actual contact force obtained by the sensor
8	ΔF	Force error of robot
9	E	Trajectory deviation

Through the above-mentioned environmental model analysis, the working environment of the milling robot is assumed to be a first-order spring model [31-32]. Then the contact force between the milling robot and the environment is $F_e=K_e(X_e-X_m)=K_e(X_e-X_c)$, and the deviation between the robot's expected tracking force and the actual contact force obtained by the sensor is $\Delta F=F_e-F_d$.

In the admittance control model shown in Figure 4, the expression of the admittance control model is the second-order function $K(s)=1/(Ms^2+Bs+K)$, that is, the robot force error ΔF and trajectory error E are the second-order differential system of "spring-damping", the expression is as follows,

$$M \frac{d^2 E(t)}{dt^2} + B \frac{dE(t)}{dt} + KE(t) = \Delta F(t), \tag{5}$$

In the above formula, K , M and B represent stiffness coefficient, mass coefficient and damping coefficient, respectively.

According to the force error ΔF , the track position X_c sent to the milling robot can be obtained by calculation, expressed as $X_c=X_r+E=X_r+\Delta F \cdot K(s)$.

At this time, $E=X_c-X_e$, analyzing the impedance characteristics of unidirectional force error and position error, $e=x_c-x_e$, Suppose the estimated value of environmental position $\hat{x}_e=x_e-\delta x_e$, after calculation, its corresponding trajectory position error $\hat{e}=e+\delta x_e$, and obtain the equation

$$f_e - f_d = m\ddot{\hat{e}} + b\dot{\hat{e}} = m(\ddot{e} + \delta\ddot{x}_e) + b(\dot{e} + \delta\dot{x}_e), \tag{6}$$

Among them, f_e and f_d are time-varying functions, and the force tracking error is a time-varying function.

The problem of trajectory correction based on force feedback is the most basic practical problem in the clinical application of vertebral milling robots. Converting it into an experimental task can be summarized as follows, the vertebral milling robot moves on a planned trajectory, performs milling operations on the outer layer of cancellous bone. If reaches the inner layer of cortical bone according to the force feedback handle feedback exceeding the admittance parameter threshold, then switch the MDL atoms to modify the trajectory according to the current movement situation to achieve the effect of protecting the nerves in the vertebrae.

Based on the analysis of the above operation tasks, this article defined seven control atoms, which described the movement of the vertebral milling robot along the space linear motion correction, the plane circular motion correction, and the space circular motion correction under the description of the tool coordinate system atoms, their motion atoms and motion alphabet definitions are shown in Table 2.

Table 2: Description Table of Milling Robot Motion Atoms

No.	Behavior classification	MDL atoms	Switching conditions
1	Linear motion regression correction	(u_1, k_1, δ_1)	The feedback force is greater than the threshold value F_1
2	Plane left circular motion correction	(u_2, k_2, δ_2)	Right plane circular motion, the feedback force is greater than the threshold F_2
3	Plane right circular motion correction	(u_3, k_3, δ_3)	Left plane circular motion, the feedback force is greater than the threshold F_3
4	Correction of the forward movement of the left circle of the three-dimensional cylinder	(u_4, k_4, δ_4)	The rightward three-dimensional cylindrical arc backward movement, the feedback force is greater than the threshold F_4
5	Correction of the forward movement of the right circle of the three-dimensional cylinder	(u_5, k_5, δ_5)	The backward movement of the three-dimensional cylinder arc to the left, the feedback force is greater than the threshold F_5
6	Three-dimensional cylindrical left arc backward motion correction	(u_6, k_6, δ_6)	Three-dimensional cylindrical arc forward motion to the right, the feedback force is greater than the threshold F_6
7	Three-dimensional cylindrical right arc backward motion correction	(u_7, k_7, δ_7)	Leftward three-dimensional cylindrical arc forward motion, the feedback force is greater than the threshold F_7

The motion atom $\sigma_1=(u_1, k_1, \delta_1)$ is "the vertebral milling robot moves back and forth along a straight line in the tool coordinate system". When the operator performs milling tasks through the robot system, the interaction force between the end effector of the milling robot and the lamina tissues that he cares about is greater than the threshold, which means, the milling force is too large, and corresponding corrections and adjustments is needed. Therefore, the linear motion of the robot in the tool coordinate system is defined as the control atom.

If the direction vector of the end effector along a straight line in the tool coordinate system is $s=(m,w,p)^T$ and $m \neq 0$, then the linear motion equation [33-34] can be expressed as

$$\begin{cases} F_1(x, y, z) = wx - my \\ F_2(x, y, z) = px - mz \end{cases} \quad (7)$$

The system state equation based on MDL can be expressed as formula (4),

$$u_1 := \xi_{\pm,1} \cdot ({}^T J(\theta))^{-1} \cdot (m \ w \ p \ 0 \ 0 \ 0)^T \quad (8)$$

$$k_1 := -\xi_{\pm,1} \cdot ({}^T J(\theta))^{-1} \cdot \begin{pmatrix} w & -m & 0 & 0 & 0 & 0 \\ p & 0 & -m & 0 & 0 & 0 \end{pmatrix}^T \begin{pmatrix} wx-my \\ px-mz \end{pmatrix} \quad (9)$$

$$y = (x_c, \dot{x}_c, \ddot{x}_c)^T \quad (10)$$

$\Delta f=f_e-f_d$, $u=(\Delta f)$ is the control input, y is the control system output. $k_1(u, y)$ is the control law of u_1 atom, and its expression is as follows,

$$k_1(u, y) := \begin{cases} \ddot{x}_c(f) = \ddot{x}_c(f) + \frac{1}{m} [\Delta f(f) - b(f)(\dot{x}_c(f) - F) - \dot{x}_c(f)] \\ \dot{x}_c(f) = x_c(f) - F + \dot{x}_c(f) \times F \\ x_c(f) = x_c(f) - F + \dot{x}_c(f) \times F \end{cases} \quad (11)$$

δ_1 is the execution condition function of the atom (u_1, k_1, δ_1) . It is a function defined in the output space of the system. The value range is $\{0,1\}$. When $\delta_1(y)=0$, it means (u_1, k_1, δ_1) continues to act on the control system, and when $\delta_1(y)=1$, it means that the slave robot system will execute the next motion control atom [35]. δ_1 is defined as,

$$\delta_1(y) = \begin{cases} 0, & \text{if } \rho_1(y) - \rho_1 < 0 \\ 1, & \text{if } \rho_1(y) - \rho_1 \geq 0 \end{cases} \quad (12)$$

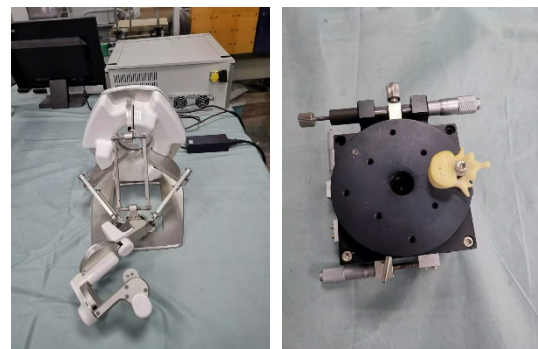


Figure 5: Vertebral milling robot control handle (left) and vertebral operation platform (right)

Among them, $q_1(y)$ is the feedback force of the end mechanism motion when the atom σ_1 is executed, and q_1 is the given feedback force threshold F_1 . In the same way, define $(u_2, k_2, \delta_2), \dots, (u_7, k_7, \delta_7)$, and the basic parameter variables can be deduced by analogy. When the milling robot approaches the desired trajectory in the advancing direction, the robot azimuth angle θ will tend to the desired straight line. When the force feedback is greater than the threshold value F_1 , the backlash correction is performed immediately, and the K_1 control law is switched, and finally back to the planned trajectory to avoid damage to the vertebra due to excessive milling. δ_1 is a function defined on the output space of the robot. $(u_2, k_2, \delta_2), (u_3, k_3, \delta_3), \dots, (u_7, k_7, \delta_7)$ for symbol definition and function description refer to (u_1, k_1, δ_1) .

3. MDL Trajectory Correction Experiment of Vertebral Milling Robot based on Force Feedback

3.1. Experimental Platform of Vertebral Milling Robot

The milling robot system is mainly composed of two parts, a three-dimensional force feedback handle and a milling robot platform. The platform uses a three-dimensional force feedback handle to control the milling robot. The control handle adopts the force feedback sensing device independently developed by this group, as shown in Figure 5.

The control handle of the robot adopts an enhanced three-dimensional structural design, which integrates the spatial perception display method of three-dimensional force perception and three-dimensional force feedback. The platform implements the terminal handle enhancement control function for the force feedback handle, which can realize the high-precision control of the handle and the expression function of multi-dimensional force feedback information.

The experimental platform of the milling robot is shown in Figure 6. Its control handle has the function of direction control of up, down, left and right. It also includes the function of controlling forward and backward of the controlled object. It sends console commands to the milling robot. The interactive information of the milling environment can be fed back to the operating handle, so as to make corresponding adjustments according to actual needs.

Robot behavior planning refers to the rational definition of robot action atom set and optimization of the atom set to achieve the balance between the completion of the work task and the underlying motion control for robot.



Figure 6: Experimental platform for vertebral milling based on force feedback control handle

3.2. Experiment and Analysis of Trajectory Correction of Vertebral Milling Robot Motion Description Language based on Force Feedback

Through the above analysis of the functional requirements of the milling robot, the motion of the milling robot is mainly divided into three categories: linear motion, plane motion and spatial arc motion, which

also conform to the characteristics of the three-dimensional motion atoms of the milling robot. The control method of the milling robot adopts the basic behavior set up, down, left and right, and its characteristic behavior set is, straight line k_1 retreat correction, plane left arc k_2 correction, plane right arc k_3 correction, three-dimensional space arc k_4 forward motion correction and three-dimensional space circular arc k_5 retreat motion correction. Seven action atoms are formed, (u_1, k_1, δ_1) , (u_2, k_2, δ_2) , (u_3, k_3, δ_3) , ... , and their movement description language atom table is shown in Table 2.

The meaning of atom (u_1, k_1, δ_1) is shown in section 2.3. Among them, v_0 is a constant parameter, u and k are functions of the direction vector of the milling robot's motion trajectory, and δ is the state digital quantity of whether the milling robot's motion trajectory exceeds the threshold, and it is a function defined in the robot output space. The definition and function description of (u_2, k_2, δ_2) ... (u_7, k_7, δ_7) refer to atom (u_1, k_1, δ_1) . According to the definition of the above atoms, the movement alphabet of the milling robot is obtained, $\Sigma = \{(u_1, k_1, \delta_1), (u_2, k_2, \delta_2), (u_3, k_3, \delta_3), (u_4, k_4, \delta_4), (u_5, k_5, \delta_5), (u_6, k_6, \delta_6), (u_7, k_7, \delta_7)\}$.

Through the above behavior planning of the vertebral milling robot, it can realize the atom switching and trajectory correction when the force feedback is greater than the threshold, and realize the protection of the spinal canal, soft tissue and nerves. This is the great advantage of the motion description language control model.

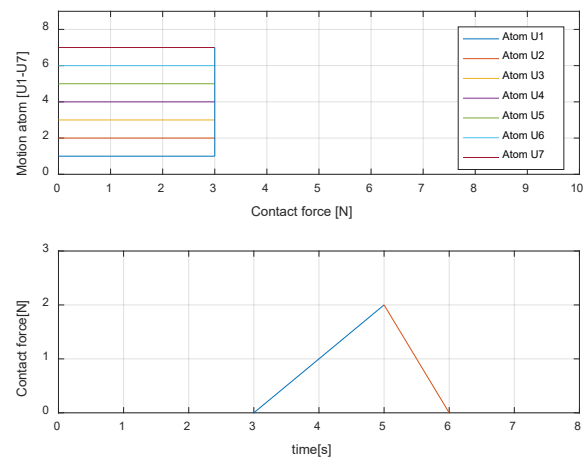


Figure 7: Milling robot force feedback control function diagram and atom relationship diagram

In the operating environment of the vertebral milling robot, the force threshold is set by the value of the force feedback. When the contact force is greater than the threshold, the motion description language atom is triggered to modify the trajectory, and the contact force between the end of robot and the tissue drops immediately. As shown in Figure 7(below). When the robot moves with the U_1 atom, it interacts with the boundary vertebra. When the interaction force is greater

than the force threshold, the robot switches to the U_m atom for corrective movement. When the U_n atom movement interacts deeply with the vertebra, continue switch other correction atom to form a robot MDL atom correction strategy based on the force feedback threshold, as shown in Figure 7(above). Therefore, the force-constrained switching trajectory correction function is a characteristic function of the MDL control method.

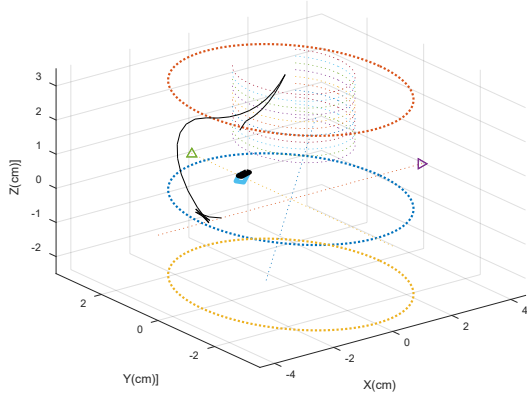


Figure 8: Basic element switching trajectory correction function based on motion description language (movement after correction)

The force feedback threshold and the motion description language atoms are used for switching correction to realize the dynamic trajectory correction of the milling robot. The Matlab2016 simulation platform is used to simulate the trajectory correction based on MDL. Starting from the initial point, the milling robot moves in three-dimensional space with a planned path, as shown in Figure 8. When the robot moves to the vertebra for milling, while the feedback force is greater than the threshold, the MDL atom trajectory is corrected immediately, and the movement continues after switching to adjust the control law to the planned trajectory, as shown in Figure 8. Therefore, it can be seen that the motion atom switching correction based on MDL can realize the robot trajectory correction function based on force feedback in three-dimensional space and trajectory control based on constraints.

The working environment parameters are described as follows, in the milling and processing vertebra environment, the space environment of the milling robot is restricted to a cylindrical area with a radius of $R=3\text{cm}$. The cylindrical area above $(-2, -2, 0)$ is the position of the vertebra. When the initial position of the robot end is $(-2, 0, 0)$ and the posture is toward the Y-axis side, as shown in Figure 8, the task of trajectory correction is realized by switching the MDL atoms based on force feedback.

The experiment procession and analysis are as follows, the experiment uses seven atoms to describe the behavior of the milling robot, and conducts the milling robot control experiment. The MDL atom table is shown in Table 2. During the control procession, the control angle can be

adjusted according to the position and posture of the milling robot. The three-dimensional motion curve of the milling robot is shown in Figure 9 and Figure 10. The experiment includes manual control mode and MDL correction mode to compare the advantages and disadvantages of the two control modes.

In the manual control mode, the running trajectory of the end of the milling robot is shown in Figure 9. It can be seen that in the manual control mode controlled by the handle controller, the running trajectory has fluctuations and discontinuities, and the trajectory is determined by operator through visual feedback and force feedback, so there are problems such as inaccurate control and hand tremble. In addition, the use of visual feedback to control the milling robot has the problem of information delay from the controller to the robot, which will also cause fluctuations and discontinuities in the end trajectory of the milling robot. Therefore, the manual control method still has obvious shortcomings.

The trajectory correction method based on the MDL is shown in Figure 10. The end of the milling robot moves upward to the edge of the vertebra in the forward direction of the planned trajectory. After the force feedback is greater than the threshold, the k_5 correction atom is used to perform backward motion. Then move to the vertebral processing area in the forward direction of the planned trajectory. Finally, the end of robot uses k_5 atom to correct the trajectory, completing the task of using force feedback to correct the trajectory.

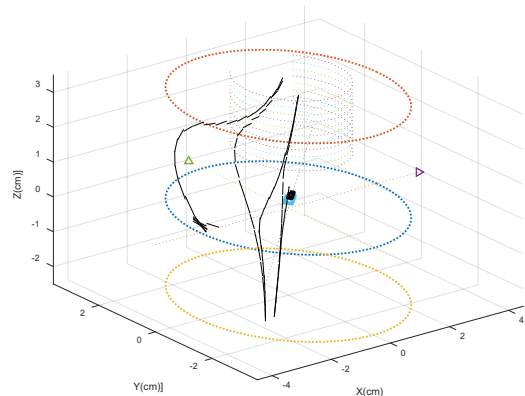


Figure 9: End motion of milling robot based on manual control

The motion trajectory of the milling robot based on the MDL method is shown in Figure 10. The solid line starts from the initial point $(-2, 0, 0)$. For the convenience of experimental visual observation, the movement procession of the end of the milling robot is mapped to the XOY two-dimensional plane in real time, so as to observe its real-time position and movement procession.

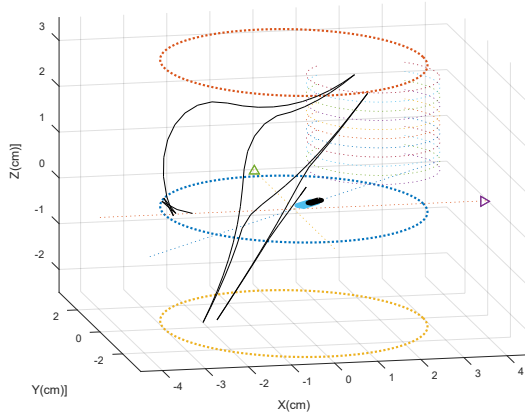


Figure 10: End motion of milling robot based on motion description language

Compare the manual control mode and the MDL control mode, and analyze from the two aspects of accuracy and time of control. Since the MDL trajectory correction belongs to the automatic control of the underlying motion, the motion trajectory of the MDL correction is continuous and the control accuracy has a high level. In the manual control mode, humans make judgments through actual vision, and there are disadvantages such as trembles at the end of the robot and discontinuous motions with time delay. From the aspect of the workload of the operator, the manual mode requires the operator to control and judge the whole control procession, and the operator is easy to operate fatigue. While in the MDL method to correct the trajectory, automatic trajectory correction can be realized through force feedback to ensure the milling operation safety. Therefore, the trajectory correction method of the milling robot based on MDL has obvious advantages.

It can be seen from Figure 10 that the trajectory correction MDL method of the vertebral milling robot can well complete the trajectory correction task under the constraint condition. It is verified by experiments that the trajectory correction method of the milling robot based on MDL is accurate and effective.

4. Conclusion

Based on the characteristics of the operation of the vertebral plate milling robot, based on the data processing of the force feedback, a motion atom planning correction model based on the motion description language and force feedback is proposed. Atom planning ensures that the motion description language can meet the trajectory correction requirements of the milling robot. Compared with the real-time control of the traditional milling robot, it reduces the risk of excessive milling operation, improves the safety performance of the milling robot, and provides a more effective trajectory correction that conforms to the operating characteristics for the use of the milling robot. The method improves the safety and reliability of the vertebral milling robot. The limitations of the trajectory

correction method of the laminar bone milling robot proposed in this paper are mainly reflected in the high accuracy requirements of the force sensor.

In the actual clinical application, the restriction condition of prohibiting switching within 1-2 seconds should be added to the switching conditions of the atoms, which has prevented the too frequent switching of the correction atoms. If the correction atom is frequently triggered within 1-2 seconds, the local space micro-vibration of the milling robot will be formed, and the long-term micro-vibration is not conducive to the stable control of the robot. Therefore, in order to ensure the stability and safety of the milling robot system, atom switching constraints should be added.

A milling robot control system was established with a milling robot and an experimental platform. Aiming at the task of vertebral milling based on force feedback, a reasonable behavior model of the milling robot is constructed. Through the space motion simulation experiment and comparison, the feasibility and effectiveness of the trajectory correction method based on the motion description language are verified. Future research will mainly focus on introducing the force feedback and visual feedback functions of the milling robot at the same time to assist the operation tasks of the milling robot.

Conflict of Interest

The authors declare no conflict of interest.

Acknowledgment

This paper was funded by the National Natural Science Foundation of China Cooperation Program (U2013208) and the Young and Middle-aged Science and Technology Innovation Talent Plan of Shenyang City (RC210314).

References

- [1] L. Wang, Y. Sun, R. Q. Wang, X. Z. Qi, "Kinematics analysis and trajectory planning of lamina decompression surgical robot," *Machinery Design and Manufacture*, vol.05, pp. 281-284, May 2020, doi: 10.19356/j.cnki.1001-3997.2020.05.068.
- [2] H. Y. Jin, Y. Hu, P. Zhang, W. Tian, B. Li, "Safety analysis and control of a robotic spinal surgical system," *Mechatronics*, vol.24, no.1, pp: 55-65, 2014, doi:10.1016/j.mechatronics.2013.11.008.
- [3] T. Osa, C. F. Abawi, N. Sugita, H. Chikuda, M. Mitsuishi, "Autonomous penetration detection for bone cutting tool using demonstration-based learning," *Proc. IEEE International Conf. Robotics and Automation*, pp.290-296,2014, doi:10.1109/ICRA.2014.6906624.
- [4] D. Yu, X. Yuan, J. Zhang, "Milling state identification based on vibration sense of a robotic surgical system," *IEEE Trans. Industrial Electronics*, vol.63, pp. 6184-6193, 2016, doi: 10.1109/tie.2016.2574981.
- [5] F. Liu, W. Wang, L. Wang, G. Wang, C. Yun, "Effect of contact wheel's deformation on cutting depth for robotic belt grinding," *Journal of Mechanical Engineering*, vol.53, no.5, pp.86-92, 2017, doi: 10.3901/JME.2017.05.086.
- [6] C. M. Wani, S. R. Deshmukh, R. R. Ghorpade, "Studies on stress

- analysis of hip prosthesis implant," *Journal of Engineering Research and Sciences*, vol.1, no.8, pp. 01-11,2022, doi:<https://dx.doi.org/10.55708/jrs0108001>.
- [7] C. Stüer, F. Ringel, M. Stoffel, A. Reinke, M. Behr, B. Meyer, "Robotic technology in spine surgery: current applications and future developments," *Acta Neurochirurgica Supplement*, vol.109, pp. 241-245, 2011, doi: 10.1007/978-3-211-99651-5_38.
- [8] T. Inoue, N. Sugita, M. Mitsuishi, T. Saito, K. Tanimoto, "Optimal Control of Cutting Feed Rate in the Robotic Milling for Total Knee Arthroplasty," *IEEE Proc. Ras and Embs International Conf. Biomedical Robotics and Biomechatronics*, pp.215-220, 2010, doi: 10.1109/BIOROB.2010.5626940.
- [9] H. Y. Tran, T. M. Bui, T. L. Pham, V. H. Le, " An Evaluation of 2D Human Pose Estimation based on ResNet Backbone," *Journal of Engineering Research and Sciences*, vol. 1, no.3, pp.59-67, 2022, doi: <https://dx.doi.org/10.55708/jrs0103007>.
- [10] Z. Deng, H. Jin, Y. Hu, Y. He, P. Zhang, W. Tian, J. Zhang, "Fuzzy force control and state detection in vertebral lamina milling," *Mechatronics*, vol.35, pp. 1-10, 2016, doi: 10.1016/j.mechatronics.2016.02.004.
- [11] L. Fan, P. Gao, B. Zhao, Y. Sun, X. Xin, Y. Hu, S. Liu, J. Zhang, "Safety Control Strategy for Vertebral Lamina Milling Task," *Caai Trans. Intelligence Technology*, vol.1, pp.249-258, 2016,doi: 10.1016/j.trit.2016.10.005.
- [12] T. Wang, B. Pan, Y. L. Fu, S. G. Wang, "Gravity compensation for the force reflection manipulator of minimally invasive surgical robot," *Robot*, vol.42, pp. 525-533, 2020, doi: 10.13973/j.cnki.robot.190547.
- [13] M. Lu, Y. Zhao, Y. Jiang, "Design of Master-Slave Operation Robot Based on Impedance Control in Minimally Invasive Spinal Surgery," *Robot*, vol.39, pp. 371-376, 2017, doi: 10.13973/j.cnki.robot.2017.0371.
- [14] X. Zhao, X. Tan, B. Zhang, "Development of soft lower extremity exoskeleton and its key technologies," *Robot*, vol.42, pp. 365-384, 2020, doi: 10.13973/j.cnki.robot.190474.
- [15] Y. Huang, G. J. Xiao, L. Zou, " Current situation and development trend of robot precise belt grinding for aero-engine blade," *Acta Aeronautica et Astronautica Sinica*, vol.40, no.3, pp.022508, 2019, doi:10.7527/S1000-6893.2018.22508.
- [16] S.Z. Zou, B. Pan, Y.L. Fu, S.X. Guo, "Improving back drivability in preoperative manual manipulability of minimally invasive surgery robot," *Industrial Robot*, vol.45, pp. 127-140, 2018, doi: 10.1108/ir-02-2017-0031.
- [17] G. J. Niu, C. C. Qu, B. Pan, Y.L. Fu, " Master-Slave control of the celiac minimally invasive surgical robot," *Robot*, vol.41, no.4, pp.551-560, 2019, doi: 10.13973/j.cnki.robot.180412.
- [18] L. Meli, C. Pacchierotti, D. Prattichizzo, "Sensory subtraction in robot-assisted surgery: fingertip skin deformation feedback to ensure safety and improve transparency in bimanual haptic interaction," *IEEE Trans. Biomedical Engineering*, vol.61, pp.1318-1327, 2014, doi: 10.1109/TBME.2014.2303052.
- [19] W. Qaisar, M. T. Riaz, A. Basit, Y. Naseem, Z. Nazir, " Disinfecting omnidirectional mobile robot with vision capabilities," *Journal of Engineering Research and Sciences*, vol.1, no.3, pp. 153-163, 2022, doi: <https://dx.doi.org/10.55708/jrs0103016>.
- [20] R. W. Brockett, "Language driven hybrid systems," *IEEE Conf. Decision and Control*, pp.4210-4214, 1994, doi: 10.1109/CDC.1994.411612.
- [21] J. N. Hua, Y. J. Cui, Q. Jia, P. Shi, H.Y. Li, "MDL-Based Control Method for Tele-robotic Systems," *Robot*, vol.35, no.5, pp.615-622, 2013, doi: 10.3724/SP.J.1218.2013.00615.
- [22] J. N. Hua, Y. J. Cui, H. Y. Li, Y. Wang, N. Xi, " Network-based Tele-robotic System with Guidance Functionality from Virtual Force," *Robot*, vol.32, no.4, pp.522-528, 2010, doi: 10.3724/SP.J.1218.2010.00522.
- [23] S. Guo, Y. H. Liang, Z. Q. Wang, H. Qu, " Dynamic Modeling and Force-feedback Control of Haptic Device with Parallel Structure Based on Virtual Simulation," *Robot*, vol.37, no.02, pp.224-230, 2015, doi: 10.13973/j.cnki.robot.2015.0224.
- [24] X. Luo, M. Li, Z. Du, W. Dong, K. Gao, D. Wu, " Modeling, planning, and control of robotic grinding on free-form surface using a force-controlled belt grinding tool, " *Proceedings of the Institution of Mechanical Engineers*, vol. 236, no.4, pp. 2009-2028, 2022, doi: 10.1177/0954406220931529.
- [25] Z. Q. Zhao, Z. H. Zhu, X. Zhou, S. F. Huang, Y. Li, "High-efficiency time-optimal trajectory planning for robots under complete dynamic constraints," *Information and Control*, vol.50, no.6, pp.701-708, 2021, doi:10.13976/j.cnki.xk.2021.0546.
- [26] Z. Liu, T. Zou, W. Sun, Y.S. Lu, "Impedance control of grinding robot based on real-time optimization genetic algorithm," *Control Theory & Applications*, vol.35, no.12, pp.1788-1795, 2018, doi: 10.7641/CTA.2018.80542.
- [27] L. Duan, Y. Huang, L. Zou, "Research on surface integrity of GH4169 Nickel-based superalloys by robotic belt grinding," *China Mechanical Engineering*, vol. 30, no.17, pp. 2044-2050, 2019, doi:10.3969/j.issn.1004-132X.2019.17.005.
- [28] J. Z. Lin, C. C. Ye, J. X. Yang, H. Zhao, H. Ding, M. Luo, " Contour error-based optimization of the end-effector pose of a 6 degree-of-freedom serial robot in milling operation, " *Robotics and Computer-Integrated Manufacturing*, vol.73, pp.102257, 2022, doi: <https://doi.org/10.1016/j.rcim.2021.102257>.
- [29] Z. Liu, T. Zou, W. Sun, Y.S. Lu, "Impedance control of grinding robot based on real-time optimization genetic algorithm," *Control theory and applications*, vol.35, pp.1788-1795, 2018, doi: 10.7641/CTA.2018.80542.
- [30] Z. Liu, R. Song, T. Zou, "End force tracking control algorithm of grinding robot based on model predictive control," *Journal of Shandong University(Engineering Science)*, vol.48, pp.42-49, 2018, doi:10.6040/j.issn.1672-3961.0.2017.569.
- [31] J. M. Ge, C. H. Deng, W. Li, C. Y. Li, X. Chen, D. P. Peng, "Research progresses of robot grinding and polishing force compliance controls," *China Mechanical Engineering*, vol.32, no.18, pp. 2217-2230, 2021, doi:10.3969/j.issn.1004-132X.2021.18.011.
- [32] Y. Mohammadi, K. Ahmadi, " Chatter in milling with robots with structural nonlinearity," *Mechanical Systems and Signal Processing*, vol.167, no. Part A, pp.108523-1-18, 2022, doi: 10.1016/j.ymsp.2021.108523.
- [33] J. Hua, H. Li, Y. Wang, N. Xi, "MDL-based control method for mobile robot with randomly varying time-delay," *IEEE Conf. Robotics and Automation*, pp.1772-1777, 2011, doi: 10.1109/ICRA.2011.5979904.
- [34] J. T. Yun, Y. Y. Liu, Q. L. Yang, H. Sang, " Research on compensation strategy for induced forces of force feedback master manipulators," *China Mechanical Engineering*, vol.28, no.10, pp.1156-1162, 2017, doi:10.3969/j.issn.1004-132X.2017.10.004.
- [35] W. Ding, H. Wang, L. Cui, S. Tian, S. Wang, "Behavior planning of flapping-wing flying robot based on cluster analysis and motion description language," *Information and Control*, vol.50, no. 01, pp. 102-112, 2021, doi: 10.13976/j.cnki.xk.2021.0211.

Copyright: This article is an open access article distributed under the terms and conditions of the Creative Commons Attribution (CC BY-SA) license (<https://creativecommons.org/licenses/by-sa/4.0/>).



WEI DING has done his bachelor's degree from Harbin University of Science and Technology in 2002. He has done his master's degree in engineering from Harbin University of Science and Technology in 2007. He has completed his PhD in Engineering from the State Key Laboratory of Robotics, Shenyang Institute of Automation, Chinese Academy of Sciences in 2012.

He has been engaged in scientific research in the field of medical robots and robot control for a long time in Shenyang Institute of Technology, and has published more than 10 papers in magazines and conferences such as "Information and Control", International Conference on Industrial Engineering and Applications and China Intelligent Robot Conference. Obtained the "Ten thousand" level talents of Liaoning Province's "Hundreds and Tens of Thousands" Talent Project.



HONGWEI WANG has done his bachelor's degree from Harbin Institute of Technology in 2013. He has done his master's degree in engineering from Harbin Institute of Technology in 2015.

He is engaged in the research of special robots in Shenyang Institute of Automation, Chinese Academy of Sciences and State Key Laboratory of Robotics. He is a member of Youth Promotion Association of Chinese Academy of Sciences. He has published more than 10 papers in journals such as "Mechanical Design and Manufacturing", "Biomimetic Intelligence and Robotics".



ZHAOMING LIU has done his bachelor's degree from Jilin University in 2012. He has done his master's degree from Jilin University in 2015. He has completed his PhD in Engineering from the University of Chinese Academy of Sciences in 2020.

Currently, he is engaged in special robot research at Shenyang Institute of Automation, Chinese Academy of Sciences, as an assistant researcher.



LONG CUI has done his bachelor's degree from Beihang University in 2003. He has completed his PhD in Engineering from Beihang University in 2009.

Currently working as a researcher at Shenyang Institute of Automation, Chinese Academy of Sciences, he has been engaged in scientific research in the field of medical robots, special robots and robot control for a long time. He has presided over and participated in more than 10 key projects of the Natural Science Foundation of China and national key research and development plans. He has published more than 20 papers in journals and conferences such as Robotics, Information and Control, and Journal of Robotics.

Fractal Research to the Production of High-strength Materials

Seoryeong Choi¹, Eunsung Jekal^{*,2}

¹Chunsang middle school, Ulsan, Republic of Korea

²Jekal's Laboratory, 471, Munsu-ro, Nam-gu, Ulsan, Republic of Korea

*Corresponding author: Eunsung Jekal, Jekal's Laboratory, 471, Munsu-ro, Nam-gu, Ulsan, Republic of Korea, Contact +82 10-3837-4733 & esjekal.jekalslab@gmail.com

ABSTRACT: SiC ceramics are excellent materials applied at high temperatures because of their lightweight, excellent high-temperature strength, and high thermal shock resistance. For better engineering properties, we made SiC with fractal lattices. Stress-strain behavior and modulus changes from room temperature to 1,250 °C were analyzed using LAMMPS S/W, a molecular dynamics program. As a result of this study, it was confirmed that the modulus of elasticity of SiC crystals changed in the range of about 475 GPa to 425 GPa as it increased from room temperature to 1,250 °C. The stress-displacement characteristics of SiC crystals, which could not be measured at a high temperature of 1,000 °C or higher, could be ensured.

KEYWORDS Fractal, SiC, LAMMPS

1. Introduction

A fractal is a geometric shape in which some small pieces are similar to the whole [1]. This characteristic is called self-similarity; in other words, a geometric structure with self-similarity is called a fractal structure. The word was first coined by Benoit Mandelbrot, and is derived from the Latin adjective fractus, meaning to be fragmented [2]–[3].

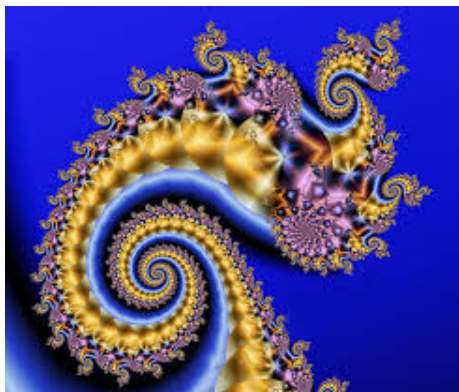


Figure 1: Example structure of fractal.

Fractal structures are found not only in natural objects but also in mathematical analysis, ecological calculations, and motion models appearing in topological space and are fundamental structures of nature [4]–[5]. You can even find rules that govern seemingly erratic and chaotic phenomena behind the scenes. The science of complexity is a science that studies the complexity of irregular nature that science has not understood so far and finds the hidden order therein. An order that can be expressed as a fractal appears in the chaos theory representing the science of complexity [6]–[7].

Fractal geometry is a branch of mathematics that studies the properties of fractals [8, 9]. This also applies to science, engineering, and computer art. Fractal structures, such as clouds, mountains, lightning, turbulence, shorelines and tree branches, are frequently found in nature. Fractals are often used for practical purposes and can be used to represent very irregular objects in the real world. Fractal techniques are used in many fields of science and technology in image compression [10]–[11]. Fractals found in nature are easy to find.

1.1. Fractal Example (Nature)

1.1.1. Lightning

Lightning discharges in the same way as a staircase over and over again. Since the route is complicated by various conditions such as humidity, atmospheric pressure, and temperature, it has a meandering shape rather than a straight line. Although it looks irregular, the overall shape and each branch form a similar structure. That is, it has a fractal structure of self-similarity [12, 13].

1.1.2. River Stream

The part and the whole of the river resemble each other. The appearance of the Nile and the Han River are similar overall, and the appearance of the river in any region has a similar shape. The appearance of the tributaries and the river as a whole is similar. Much rain creates many junctions in the mountains. Each of these becomes a small river, and the act of meeting a large stream and extending into a small stream is repeated [14, 15].

1.1.3. Tree

When a tree is divided into a large branch, various branches are formed, and several small branches are also divided from this small branch. Each tree has its own fractal dimension. The fractal shape of these trees serves to evenly distribute the transport of water and nutrients throughout the tree [16, 17].

1.1.4. Coral

As colonies grow outward through agglomeration, the material is continuously deposited on the outwardly growing surface. It has a fractal dimension in principle similar to that of a tree root [18]–[19].

1.1.5. Clouds

A very uniform fractal, about 1.35 dimensions for cumulus clouds. A cloud created by a random condensation process takes on the form of a fractal as the generated water droplets attract the surrounding water droplets [20, 21].

1.1.6. Romanesco Broccoli

When grown, Romanesco broccoli develops a thorn-like appearance, with one part of the thorn showing the same self-similarity to the whole [22, 23].

1.1.7. Lizard sole

If you zoom in on the lizard's sole, the surface of the sole has a fractal structure, which increases friction [24].

1.1.8. Bismuth

Element number 83 is self-similar in the pattern of atomic arrangement, and fractal structures can be easily found in outer space [25, 26].

1.1.9. Lung

The blood vessels in the lungs have a fractal structure and are said to be the most efficient for oxygen exchange [27, 28].

1.2. Fractal Examples (Structures)

Fractals can be easily found even in the patterns of high-strength structures.

1.2.1. Carbon nanotube

It is in the form of a tube by repeating the hexagonal shape. It has very high strength and shows self-similarity.

1.2.2. Honeycomb

The honeycomb repeats the hexagonal shape to show self-similarity, and due to its fractal structure, it is very effective in terms of space utilization, strength, and stability.

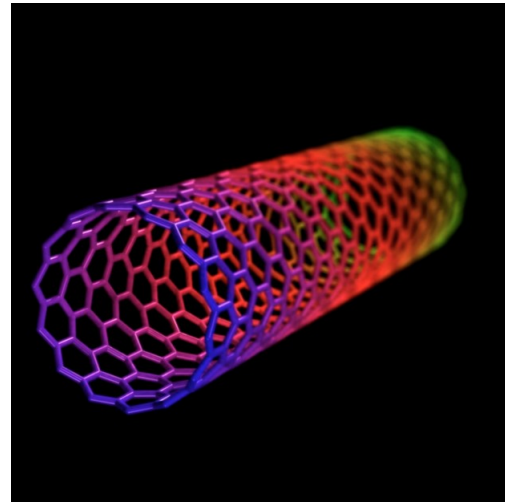


Figure 2: Illustration image of carbon nanotube.

1.3. Research Motivation

In nature, fractal structures can be easily found in high-strength structures. The common point of most structures using fractal structures is efficiency and strength. As in the previous examples, the fractal structure of a tree branch is a structure that can produce the optimal effect of transporting nutrients and water, and the fractal structure of a honeycomb is a structure that can produce the optimal effect in stability, strength, and space utilization. In other words, the structure of a fractal is the most effective and has high strength. Therefore, studying the modulus of elasticity, strength, and stress-strain characteristics when the fractal structure is applied to the structure of a new material raises the question of how effective the fractal structure will be in the new material structure study. If the strength and elasticity of the fractal structure are strong and it shows an excellent effect in stress-strain, etc., the fractal structure can play a significant role in the structure of new materials.

2. Mathematical modeling

2.1. Triangle

2.1.1. Symmetry

Since the triangle has a perfectly constant self-similarity and the number of triangles is constantly increasing based on the second largest triangle in the center, the center of gravity becomes the center of gravity of triangle ABC, and the center of gravity of this Sierpinski triangle Equal, that is, the center of gravity G is $((a+c+e)/3, (b+d+f)/3)$ when the corners are defined as A(a,b), B(c,d) and C(e,f), respectively.

2.1.2. Asymmetry

The center of gravity of the following triangle shown in fig.3 is the center of gravity G_1 of triangle $A_1B_1C_1$, the center of gravity G_2 of triangle $A_2B_2C_2$, the center of gravity G_3 of triangle $A_3B_3C_3$... The center of gravity of all the centers of gravity of each triangle up to the center of gravity G_∞ of triangle $A_\infty B_\infty C_\infty$ will be the center of gravity of the entire

triangle, and since all these centers of gravity are located in one straight line, the midpoint of the straight line that is the center of gravity of the straight line This will be the center of gravity.

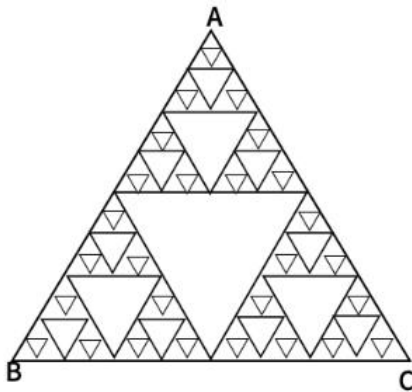


Figure 3: An equilateral fractal triangle with symmetry.

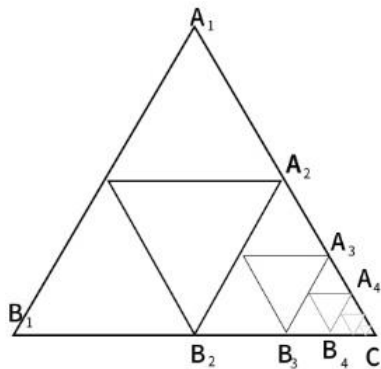


Figure 4: An equilateral fractal triangle without symmetry. In this case, smaller triangles appear only in the C direction.

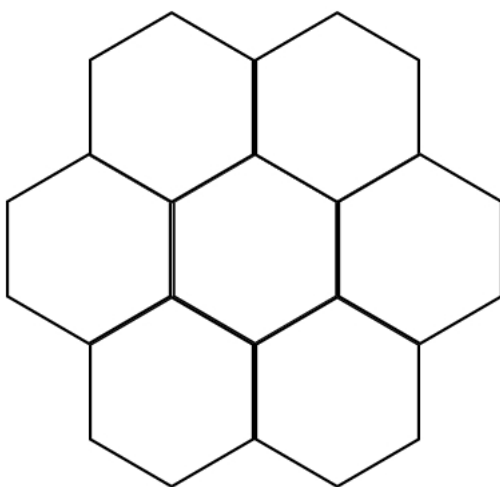


Figure 5: Symmetric honeycomb lattice with equilateral hexagon.

2.2. Hexagon

2.2.1. Symmetry

Suppose each hexagon center of gravity (G) is treated as a point, and the center of gravity of all centers of gravity is obtained. In the case, the total center of gravity of the hexagonal model is obtained. That is, the center of gravity of the hexagonal tongue at the center becomes the center of gravity of the model.

2.2.2. Asymmetry

The center of gravity of this model can also be obtained using the same method as above. First, find the centers of gravity of each hexagon, then find the centers of gravity of the adjacent hexagons, and repeat this process to find the center of gravity of each point when it comes out, this is a model of the center of gravity.

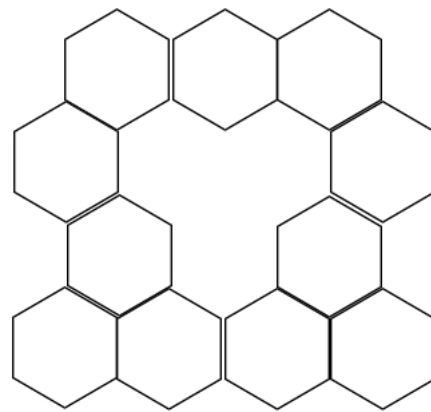


Figure 6: Fractal hexagon with broken symmetry. In this case, there is no hexagon filled in certain parts.

2.3. Deformation process when force is applied to the research model

2.3.1. Triangle

Symmetry, force downward: This is the process of change when the triangle is pressed downward. To find the center of gravity like the previous front, you just need to set the coordinates of the vertices of each angle, but the center of gravity of the triangle before applying the force to the front is located above the center of gravity after pressing. In other words, whenever you press the button, the center of gravity moves downward like each point. Point A will gradually go downwards, and the two points B and C will spread apart due to the downward force. Therefore, to find the center of gravity, first set the midpoint of B C as the origin of the coordinate plane. Then point A will be on the y-axis and each B and C will be on the x-axis. If a downward force is applied, the x-coordinate of point A will be 0, the y-coordinate will gradually decrease from the starting point, and the absolute values of the coordinates of points B and C will increase, respectively. Using the formula to find the

coordinates of the center of gravity, the x -coordinate is 0 because the sum of the x -coordinates of the point B and point C is 0, the point A is on the y -axis, so the y -coordinate is a point because the point B and C are on the x -axis We only need to care about the y -coordinate of A. The y -coordinate of point A gets smaller as the force is applied, so in conclusion, the center of gravity falls according to the amount of force applied.

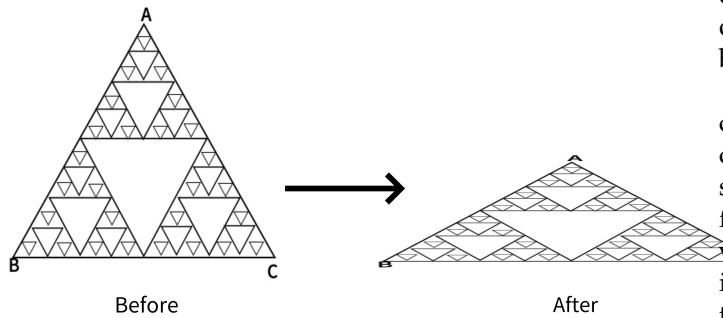


Figure 7: Downward forced symmetric fractal triangle.

Symmetry, compression by applying force from both sides: If the coordinate plane is set up the same way as before, point A is on the y -axis, and points B and C on the x -axis. This time, since it was compressed with the same force from both sides, the x -coordinate of point A remains 0. The y -coordinate increases, and since the points B and C have been pulled to the origin by the same distance, the y -coordinate remains 0, and the x -coordinate is their absolute value. This will decrease If you find the coordinates of the center of gravity with the formula for calculating the center of gravity. The x -coordinate increases due to the increase in the x -coordinate of point A, and the y -coordinate is 0. That is, the center of gravity moves upwards on the y -axis.

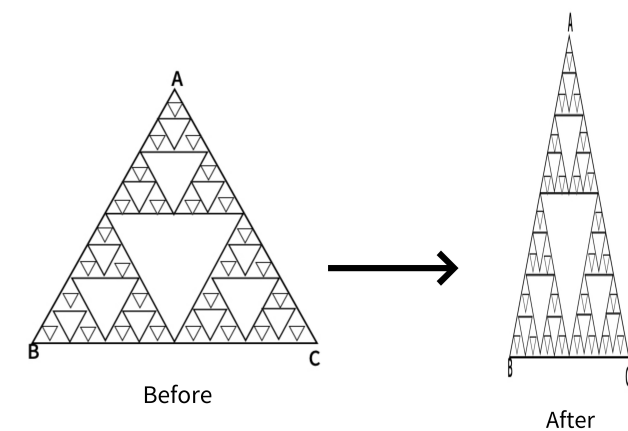


Figure 8: Both sides forced symmetric fractal triangle.

Asymmetric, press with downward force: We will show

the change in the center of gravity by finding the center of gravity of the asymmetric triangle No. 2. Let g be the center of gravity before applying the force, and let G be the center of gravity after applying the force. We will set the coordinate plane with b_2 as the origin this time. When a downward force is applied and pressed, a_1 descends downward along the y -axis, and each of the remaining b and c coordinates lengthens sideways. Now, we will explain the change in the center of gravity by finding the center of gravity. First, if the center of gravity of triangle $A_1 B_1 C$ is G_1 , the coordinates of G_1 will descend as force is applied, and the X coordinate of C will increase. This way, the center of gravity appears to be shifted diagonally in the lower right corner.

Asymmetric, press with force from both sides: If the center of gravity is changed using the method of finding the center of gravity of the asymmetric triangle No. 2, in this situation, the y coordinate of point A_1 increases because force is applied and pressed from both sides The absolute value of each x coordinate of B_1 and C is also gradually increased. Decreases $A_1 B_1 C$ if the center of gravity of the triangle is G_1 , the coordinates of G_1 rise upward as the force is applied, and point C moves to the left toward the origin. When looking at the movement of the two points, the center of gravity of the entire model shows a movement in the upper left direction.

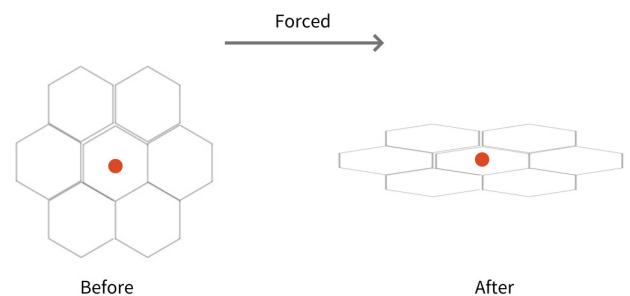


Figure 9: Downward forced symmetric fractal hexagon.

2.3.2. Hexagon

Symmetry, the downward force: Set the center of the two vertices of the following model as the origin, and set the coordinate plane so that the center of gravity (red dot) is on the y -axis. Because the model is pressed down, the overall height is lowered and spreads to the sides. Since the center of gravity of the following model coincides with the center of gravity of the regular hexagon in the center, only the change process of the center of gravity of the regular hexagon in the center needs to be examined. The center of gravity of a regular hexagon is the center of gravity of an equilateral triangle that connects the three adjacent vertices of the hexagon by one square. Therefore, to examine the change in the center of gravity of the angular shape in the center, only the change in the inner equilateral triangle is

required. Therefore, it shows the same shape as the change in the center of gravity of 1-1-1. As the force is applied and pushed down, the center of gravity goes down on the y-axis.

Symmetry, compression by applying force from both sides: Set the center of the two vertices of the following model as the origin and the coordinate plane so that the center of gravity (red point) is on the y-axis. Because it is compressed by applying force from both sides, the overall height increases and the sides are contracted. Since the center of gravity of the following model coincides with the center of gravity of the regular hexagon in the center, only the change process of the center of gravity of the regular hexagon in the center needs to be examined. The center of gravity of a regular hexagon is the center of gravity of an equilateral triangle that connects the three adjacent vertices of the hexagon by one square. Therefore, to examine the change in the center of gravity of the angular shape in the center, only the change in the inner equilateral triangle is required. This way, it shows the same shape as the 1-1-2 change in the center of gravity. As you apply force and compress it sideways, the center of gravity continues to rise upwards on the y-axis.

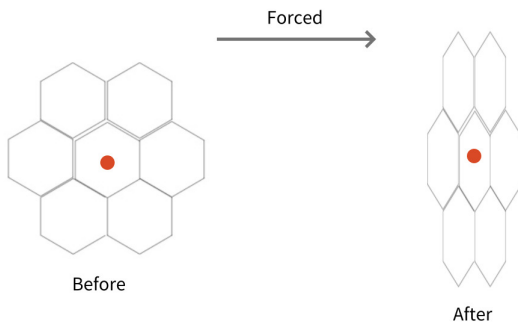


Figure 10: Side forced symmetric fractal hexagon.

3. Method

The ceramic material is relatively light, hard, and has excellent strength at a high temperature compared to other materials such as metal, and has excellent abrasion and corrosion resistance, so it is widely used as a core material for parts used at high temperatures, such as cutting tools, high-temperature parts, and gas turbine engine parts. Representative structural ceramic materials include oxide-based materials such as Al_2O_3 and ZrO_2 and non-oxide-based materials such as SiC, Si_3N_4 , B_4C , AlN, and TiC. A ceramic component material used at a high temperature requires mechanical properties such as strength, elastic modulus, stress-deformation characteristics, etc., in a temperature environment used together with thermal properties such as thermal conductivity, specific heat, thermal expansion coefficient, etc. Generally, a method of measuring the modulus of elasticity of a material includes a direct method such as a

tensile test and a 3-point or 4-point bending test [29, 30].

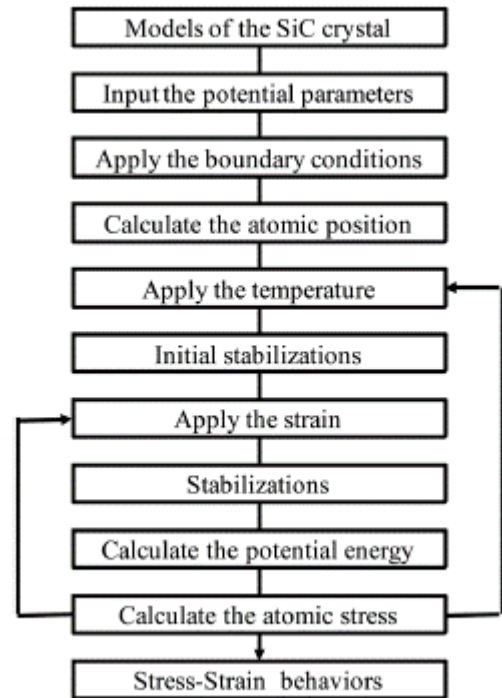


Figure 11: Strain algorithms within the LAMMPS

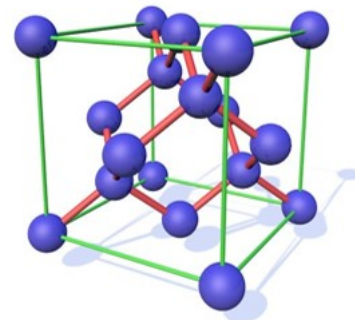


Figure 12: Unit cell structure of SiC crystal.

In addition, with the development of high-speed and large capacity of computers, computer simulation research has been actively conducted to analyze the microscopic behavior of atomic levels of materials using molecular dynamics and first principles, and research is being conducted to analyze the properties of materials, such as modulus of elasticity. Suppose it is possible to predict the mechanical properties according to the temperature of the ceramic material using this. In that case, it will significantly help the design and the development of the ceramic part material for high temperatures [31].

Using molecular dynamics, this study analyzed the stress-displacement behavior and elastic modulus of SiC fractal crystals, which are high-temperature structural materials at various temperatures. To this end, SiC crystals are modeled using Tersoff potential, and 1,2504°C from room

temperature using LAMMPS S/W, a high molecular dynamics program [32]. We tried to analyze the change in elastic modulus according to temperature by analyzing the stress-displacement characteristics up to this point

3.1. Interatomic bonding potential of SiC crystals

The unit cell structure of the SiC crystal is shown in Figure 1. Here, the Si atom is located at each corner and face center in the lattice, and the C atom is located at the center of the tetrahedron based on the Si atom. In addition, atoms inside the SiC crystal may be arranged in the form of CC-C, C-C-Si, C-Si-Si, Si-Si-Si, C-Si-C, Si-C-Si, etc., and potential energy acting between adjacent atomic arrays is required.

Tersoff developed potential energy that simulates the interatomic bonds of SiC crystals using classical interatomic potential. The Tersoff potential has been successfully used in the study of various related materials as a proposed potential to simulate bonds between elements with tetravalent covalent bonds of carbon, silicon, and germanium. Tersoff described the interaction of atoms as a potential energy function using the empirical bond-order concept. The agglomeration energy (E) of the object is described as follows in Equation (1) [33, 34].

$$E = \sum_i E_i \frac{1}{2} \sum_{i \neq j} V_{ij} \quad (1)$$

Parameter	Interactions	
	Si-Si	C-C
A , eV	1830.8	1393.6
B , eV	471.18	346.7
λ_1 , nm ⁻¹	2.4799	3.4879
λ_2 , nm ⁻¹	1.7322	2.2119
λ_3 , nm ⁻¹	0	0
n	0.78734	0.72751
c	1.0039×10^5	3.8049×10^4
d	16.217	4.384
$R^{(1)}$, nm	0.27	0.18
$R^{(2)}$, nm	0.30	0.21
β	1.1×10^{-6}	1.5724×10^{-7}
h	-0.59825	-0.57058

Figure 13: The MD simulation procedure for the elastic constant of the SiC crystal.

4. Results and discussions

Before looking at the results and the contents of the discussion, I will briefly predict the results by looking at the experimental images from Figures 4 to 8. The difference between the strength of symmetry and the strength of asymmetry resulted in the symmetric model being more powerful than the asymmetric model. Figures 4 to 8 show the deformation process of a symmetrical triangle and a symmetrical hexagonal shape among the models that modeled the SiC crystal with a fractal model. First, Figure 4 shows the deformation process at the beginning of applying force to a symmetrical triangle. When you look at the picture, you can

find that the shape of the model breaking into a diagonal shape is relatively stable and regular. However, looking at the experimental image of the LAMMPS program in Figure 5, the changes to (a) (b) (c) are quite regular and stable, but since (c) most decisions have been broken in an instant, unlike the way they have been broken. On the other hand, looking at the experimental images of the symmetrical hexagonal LAMMPS program, all (a) to (h) show relatively regular changes that are destroyed after converging to stable constant values. Therefore, it showed a regular appearance to the end rather than a triangular model. This can be predicted as the first evidence that a symmetrical hexagon is more powerful in terms of stress/change and strength than a symmetrical triangle. When looking at the graph model in Figure 7, the same results as before are derived. However, the stress change graph of Young's Modulus in Figure 8 yields slightly different results in the front tube. In (a), the symmetrical triangle is examined in (b) for the changes in the symmetrical hexagon. However, when the temperature was raised to 900K in part (a), it could be seen that it was broken after holding it a little, but in part (b), it was broken relatively faster than in (a) when it was raised to 900K. In addition, overall (a) showed superiority over (b) in all aspects.

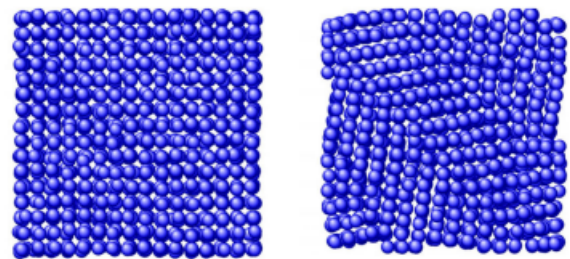


Figure 14: Deformed shapes of the SiC crystal simulated with MD at 1000°C: before and after applied 0.15 strain.

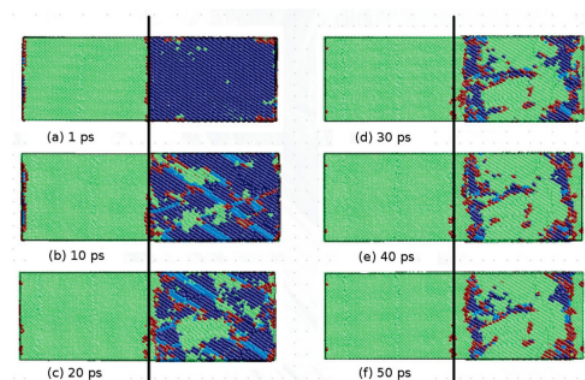


Figure 15: The process of changing a symmetrical triangle when a downward force is applied with LAMMPS.

Stress-strain properties and modulus of elasticity were analyzed while changing the temperature of SiC crystals from room temperature to 1,500°C, and the results are shown in Figure. It is shown from 4 to Fig. 8. First, when the SiC

crystal has triangular symmetry, the shape is deformed by the application of the compression displacement at 1,000°C.

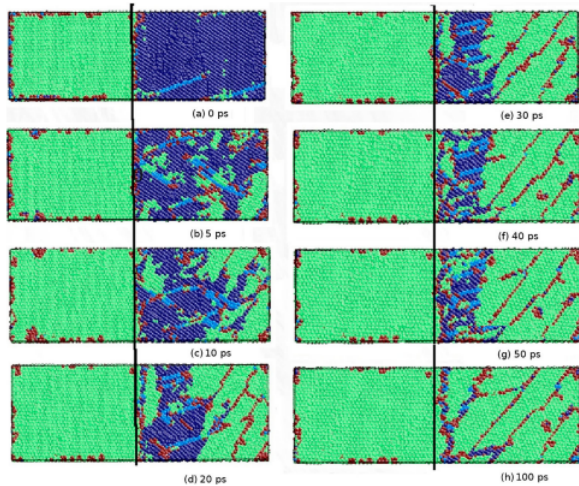


Figure 16: The process of changing a symmetrical hexagon when a downward force is applied with LAMMPS.

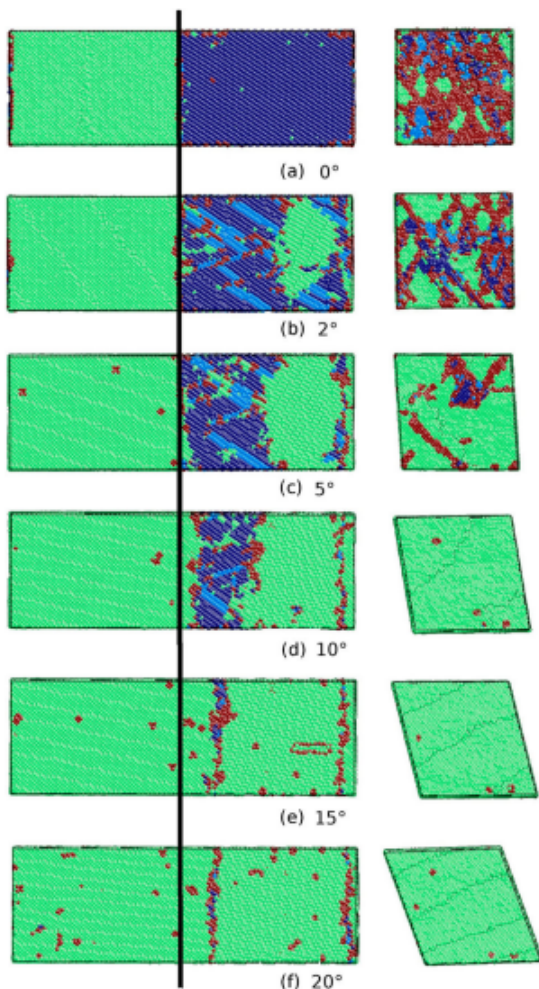


Figure 17: The process of changing a symmetrical hexagon when a shear strain force is applied with the LAMMPS.

Fig. 4(a) shows the SiC crystal thermally stabilized at

1,000°C. Fig. 4(b) shows the deformed shape by applying the compression displacement of 0.15. In particular, when high compressive stress was applied at a temperature of 1,100°C or higher, it was confirmed that some outermost specific atoms of the SiC crystal significantly deviated from the unit lattice position. This is the thermal vibration of the active atoms at high temperatures. It is believed that some outermost atoms have deviated from the unit lattice position due to the combined high displacement energy applied. Therefore, the stress-displacement characteristics of SiC crystals are calculated by calculating the average stress of the internal unit lattice with only the members, except for atoms that deviate from the unit lattice position to improve the accuracy of the analysis. The modulus of elasticity was analyzed [35, 36].

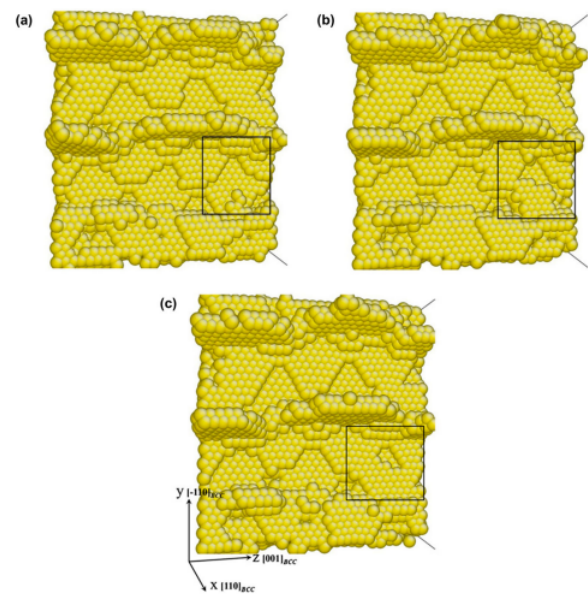


Figure 18: Lattice cracks. The black square of fig(a) shows hexagonal lattice, while black square of fig(b) represents triangle lattice. In last, fig(c) shows the liquid flow regime.

The figure uses molecular dynamics to analyze the stress-displacement characteristics of SiC crystals with triangular symmetry at 1,000°C temperature. It is shown in 5. In this case of SiC crystals, the stress increases linearly as the total energy increases as the gap between atoms approaches due to the compression displacement. Furthermore, when a compression displacement of 0.2 or more was applied, the entire stress was destroyed after converging to a certain value. In addition, even if the crystal temperature increases to 500°C, SiC crystals exhibit stress-displacement characteristics similar to room temperature. However, if the temperature of the crystal increases by more than 1,000 °C, the SiC crystal will exhibit an inflection point similar to the elastic-plastic limit of yielding stress at a displacement of about 0.1. This result is entirely different from the result that ceramics such as SiC, which are known so far, are destroyed after elastic deformation. However, it is judged that additional analysis is needed to suggest that SiC crystals may also undergo plastic deformation at high temperatures.

Changes in the modulus of elasticity of crystals with broken symmetry were also investigated using molecular dynamics from the stress-displacement characteristics of SiC with triangular symmetry. The modulus of elasticity of SiC crystals with broken symmetry is shown. It was found that it was about 475 GPa at room temperature and decreased to about 425 GPa as the temperature increased to 1,250°C.

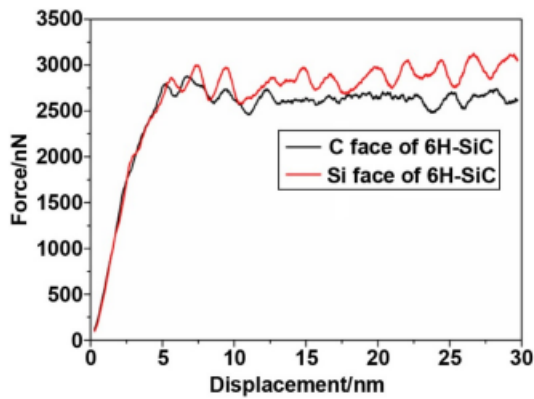


Figure 19: Deformation curve of C face of 6H-SiC and Si face of 6H-SiC.

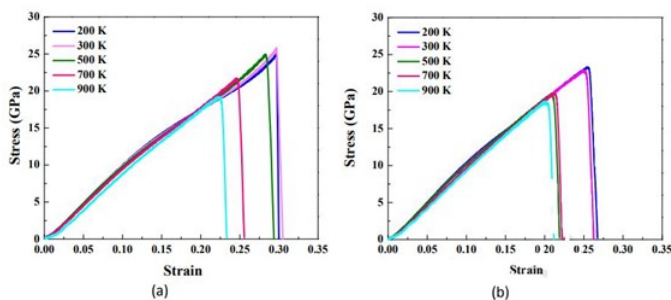


Figure 20: Young's modulus elasticity Graph for each strain.

5. Conclusion

SiC ceramics are excellent materials applied at high temperatures because of their light-weight, excellent high-temperature strength, and high thermal shock resistance. Data on stress-strain characteristics and modulus of elasticity depending on temperature are required to design a ceramic for a high temperature structure, but it is challenging to measure them. This study analyzed the elastic modulus characteristics of SiC crystals at various temperatures using molecular dynamics. To this end, SiC crystals were modeled to apply Tersoff potential between constituent atoms, and stress-strain behavior and modulus changes from room temperature to 1,250°C were analyzed using LAMMPS/W, a molecular dynamics program. As a result of this study, it was confirmed that the modulus of elasticity of SiC crystals changed in the range of about 475 GPa to 425 GPa as it increased from room temperature to 1,250 °C. The stress-displacement characteristics of SiC crystals, which could

not be measured at a high temperature of 1,000 °C or higher, could be ensured.

References

- [1] B. B. Mandelbrot, B. B. Mandelbrot, *The fractal geometry of nature*, <https://doi.org/10.1002/bbpc.19850890223>, vol. 1, WH freeman New York, 1982.
- [2] B. B. Mandelbrot, D. Passoja, A. J. Paullay, *et al.*, "Fractal character of fracture surfaces of metals, <https://doi.org/10.1038/308721a0>", *Nature*, vol. 308, no. 5961, pp. 721–722, 1984.
- [3] B. B. Mandelbrot, C. J. Evertsz, M. C. Gutzwiller, *Fractals and chaos: the Mandelbrot set and beyond*, <https://doi.org/10.1007/978-1-4757-4017-2>, vol. 3, Springer, 2004.
- [4] P. H. Coleman, L. Pietronero, "The fractal structure of the universe, [https://doi.org/10.1016/0370-1573\(92\)90112-d](https://doi.org/10.1016/0370-1573(92)90112-d)", *Physics Reports*, vol. 213, no. 6, pp. 311–389, 1992.
- [5] H. V. Meyer, T. J. Dawes, M. Serrani, W. Bai, P. Tokarczuk, J. Cai, A. de Marvao, A. Henry, R. T. Lumbers, J. Gierten, *et al.*, "Genetic and functional insights into the fractal structure of the heart, <https://doi.org/10.1038/s41586-020-2635-8>", *Nature*, vol. 584, no. 7822, pp. 589–594, 2020.
- [6] T. Higuchi, "Approach to an irregular time series on the basis of the fractal theory, [https://doi.org/10.1016/0167-2789\(88\)90081-4](https://doi.org/10.1016/0167-2789(88)90081-4)", *Physica D: Nonlinear Phenomena*, vol. 31, no. 2, pp. 277–283, 1988.
- [7] E. Fernández, H. F. Jelinek, "Use of fractal theory in neuroscience: methods, advantages, and potential problems, <https://doi.org/10.1006/meth.2001.1201>", *Methods*, vol. 24, no. 4, pp. 309–321, 2001.
- [8] K. Falconer, *Fractal geometry: mathematical foundations and applications*, DOI:10.1002/0470013850, John Wiley & Sons, 2004.
- [9] G. Captur, A. L. Karperien, A. D. Hughes, D. P. Francis, J. C. Moon, "The fractal heart—embracing mathematics in the cardiology clinic, <https://doi.org/10.1038/nrcardio.2016.161>", *Nature Reviews Cardiology*, vol. 14, no. 1, pp. 56–64, 2017.
- [10] M.-L. De Keersmaecker, P. Frankhauser, I. Thomas, "Using fractal dimensions for characterizing intra-urban diversity: The example of brussels, <https://doi.org/10.1111/j.1538-4632.2003.tb01117.x>", *Geographical analysis*, vol. 35, no. 4, pp. 310–328, 2003.
- [11] S. Bleher, C. Grebogi, E. Ott, R. Brown, "Fractal boundaries for exit in hamiltonian dynamics, <https://doi.org/10.1103/physrev.38.930>", *Physical Review A*, vol. 38, no. 2, p. 930, 1988.
- [12] J. A. Riousset, V. P. Pasko, P. R. Krehbiel, R. J. Thomas, W. Rison, "Three-dimensional fractal modeling of intracloud lightning discharge in a new mexico thunderstorm and comparison with lightning mapping observations, <https://doi.org/10.1029/2006jd007621>", *Journal of Geophysical Research: Atmospheres*, vol. 112, no. D15, 2007.
- [13] J. Valdivia, G. Milikh, K. Papadopoulos, "Red sprites: Lightning as a fractal antenna, <https://doi.org/10.1029/97gl03188>", *Geophysical Research Letters*, vol. 24, no. 24, pp. 3169–3172, 1997.
- [14] R. S. Snow, "Fractal sinuosity of stream channels, <https://doi.org/10.1007/bf00874482>", *Pure and applied geophysics*, vol. 131, no. 1, pp. 99–109, 1989.
- [15] P. La Barbera, R. Rosso, "On the fractal dimension of stream networks, <https://doi.org/10.1029/wr025i004p00735>", *Water Resources Research*, vol. 25, no. 4, pp. 735–741, 1989.
- [16] C. Puente, J. Claret, F. Sagues, J. Romeu, M. Lopez-Salvans, R. Pous, "Multiband properties of a fractal tree antenna generated by electrochemical deposition, [10.1049/el:19961579](https://doi.org/10.1049/el:19961579)", *Electronics Letters*, vol. 32, no. 25, pp. 2298–2299, 1996.
- [17] P. Perdikaris, L. Grinberg, G. E. Karniadakis, "An effective fractal-tree closure model for simulating blood flow in large arterial networks, <https://doi.org/10.1007/s10439-014-1221-3>", *Annals of biomedical engineering*, vol. 43, no. 6, pp. 1432–1442, 2015.

- [18] R. R. Bradbury, R. R. Reichelt, *et al.*, "Fractal dimension of a coral reef at ecological scales, doi:10.3354/meps010169", *Marine Ecology Progress Series*-pages: 10: 169-171, 1983.
- [19] B. Martin-Garin, B. Lathuilière, E. P. Verrecchia, J. Geister, "Use of fractal dimensions to quantify coral shape, https://doi.org/10.1007/s00338-007-0256-4", *Coral Reefs*, vol. 26, no. 3, pp. 541-550, 2007.
- [20] R. F. Cahalan, J. H. Joseph, "Fractal statistics of cloud fields, https://doi.org/10.1175/1520-0493(1989)117<0261:fsocf>2.0.co;2", *Monthly weather review*, vol. 117, no. 2, pp. 261-272, 1989.
- [21] N. Sánchez, E. J. Alfaro, E. Pérez, "On the properties of fractal cloud complexes, 10.1086/500351", *The Astrophysical Journal*, vol. 641, no. 1, p. 347, 2006.
- [22] S.-H. Kim, "Fractal dimensions of a green broccoli and a white cauliflower, doi: 10.1093/cercor/6.6.830", *arXiv preprint cond-mat/0411597*, 2004.
- [23] M. Peleg, G. V. Barbosa, "Fractals and foods, https://doi.org/10.1080/10408399309527617", *Critical Reviews in Food Science & Nutrition*, vol. 33, no. 2, pp. 149-165, 1993.
- [24] J. González, A. Gamundi, R. Rial, M. C. Nicolau, L. de Vera, E. Pereda, "Nonlinear, fractal, and spectral analysis of the eeg of lizard, *galloia galloti*, doi: 10.1152/ajpregu.1999.277.1.r86", *American Journal of Physiology-Regulatory, Integrative and Comparative Physiology*, vol. 277, no. 1, pp. R86-R93, 1999.
- [25] F. Chen, K. Wang, B. Shi, H. Hu, "Dendrite and fractal patterns formed on the surface of bismuth-ion-implanted linbo3, doi:10.1088/0953-8984/13/26/304", *Journal of Physics: Condensed Matter*, vol. 13, no. 26, p. 5893, 2001.
- [26] A. S. Priya, D. Geetha, Ş. Tãlu, "Advanced micromorphology study of the mn-doped bismuth ferrite thin films, https://doi.org/10.1016/j.matlet.2020.128615", *Materials Letters*, vol. 281, p. 128615, 2020.
- [27] F. E. Lennon, G. C. Cianci, N. A. Cipriani, T. A. Hensing, H. J. Zhang, C.-T. Chen, S. D. Murgu, E. E. Vokes, M. W. Vannier, R. Salgia, "Lung cancer—a fractal viewpoint, doi: 10.1038/nrclinonc.2015.108", *Nature reviews Clinical oncology*, vol. 12, no. 11, pp. 664-675, 2015.
- [28] T. Nelson, B. West, A. Goldberger, "The fractal lung: universal and species-related scaling patterns, doi: 10.1007/bf01951755", *Experientia*, vol. 46, no. 3, pp. 251-254, 1990.
- [29] Y.-T. Zuo, H.-J. Liu, "Fractal approach to mechanical and electrical properties of graphene/sic composites, 10.22190/fume201212003z", *Facta Universitatis. Series: Mechanical Engineering*, vol. 19, no. 2, pp. 271-284, 2021.
- [30] C. Atzeni, G. Pia, U. Sanna, "Fractal modelling of medium-high porosity sic ceramics, https://doi.org/10.1016/j.jeurceramsoc.2008.03.039", *Journal of the European Ceramic Society*, vol. 28, no. 14, pp. 2809-2814, 2008.
- [31] B. Li, Z. Chen, E. Ren, "A fractal analysis for the microstructures of β -sic films, https://doi.org/10.3139/146.111802", *International Journal of Materials Research*, vol. 110, no. 8, pp. 746-756, 2019.
- [32] M. T. Humbert, Y. Zhang, E. J. Maginn, "Pylat: Python lammmps analysis tools, doi:10.1021/acs.jcim.9b00066", *Journal of chemical information and modeling*, vol. 59, no. 4, pp. 1301-1305, 2019.
- [33] P. G. Mezey, "Potential energy hypersurfaces, https://doi.org/10.1016/b978-044452227-6/50015-6", 1987.
- [34] E. N. Lorenz, "Available potential energy and the maintenance of the general circulation, https://doi.org/10.1111/j.2153-3490.1955.tb01148.x", *Tellus*, vol. 7, no. 2, pp. 157-167, 1955.
- [35] S. Ito, M. Hashimoto, B. Wadgaonkar, N. Svizero, R. M. Carvalho, C. Yiu, F. A. Rueggeberg, S. Foulger, T. Saito, Y. Nishitani, *et al.*, "Effects of resin hydrophilicity on water sorption and changes in modulus of elasticity, doi: 10.1016/j.biomaterials.2005.04.052", *Biomaterials*, vol. 26, no. 33, pp. 6449-6459, 2005.
- [36] A. Pauw, *Static modulus of elasticity of concrete as affected by density*, https://doi.org/10.3390/ma14247578, University of Missouri, 1960.

Copyright: This article is an open access article distributed under the terms and conditions of the Creative Commons Attribution (CC BY-SA) license (<https://creativecommons.org/licenses/by-sa/4.0/>).



Seoryeong Choi is a student in Chunsang middle school. His recent research interests are heading to Physics and applied mathematics.



Eunsung Jekal is a representative of Jekal's laboratory where magnetism researches are studied.

IoT Based Smart Physiotherapy System: A Review

Adil Ali Saleem¹, Kainat Zafar¹, Muhammad Amjad Raza¹, Zahid Kareem¹, Mui-zzud-din¹, Hafeez Ur Rehman Siddiqui^{*1}, Sandra Dudley²

¹ Institute of Computer Science, Khwaja Fareed University of Engineering and Information Technology, Rahim Yar Khan, 64200, Pakistan

² School of Engineering, London South Bank University, 103 Borough Road, London SE1 0AA, UK

*Corresponding author: Hafeez Ur Rehman Siddiqui, KFUEIT, Rahim Yar Khan Pakistan, +923090997554 & siddiqov@gmail.com

ABSTRACT: During recent years, the increase in the ageing population, the ubiquity of chronic diseases in the world, and the development in technologies have resulted in high demand for efficient healthcare systems. Physical anomalies mostly caused by injury, disease, and ageing lead to limit the regular ability of people to move and function. Primary health care providers often refer patients to conservative regular exercises as the first stage of the remedial process. The exercises operated under trained supervision are effective, but it is not feasible to supervise each patient under the growing number of such cases. Smart Physiotherapy exercise is one of the most beneficial and need of the time. The proper and systematic execution of recommended exercises is required for effective home-based physiotherapy. This study aims at exploring recent investigations performed by researchers in this discipline and subsequently, provide a ground for new researchers to improve or bring innovation in the approach. Electronic databases were searched between 2015 and 2020 in addition the reference lists of the articles that meet the criteria were also searched. The outcome of this study indicates that there is no prolific application that automatically monitors and guides the patients in performing the right and systematic exercises advised by the physiotherapist.

KEYWORDS: IoT, Machine Learning, Smart Physiotherapy, Sensors, Remote Health Monitoring

1. Introduction

The effectuation of an Internet of things (IoT) healthcare system is a potential challenge for acquiring coverage for a more significant proportion of people in various locations at reduced prices [1]. In recent years there has been an increased ageing population, and the pervasiveness of chronic diseases in the world has resulted in high demand for efficient healthcare systems [2]. IoT is a smart approach to make systems sensible, remotely manageable, and reliable in many ways. IoT is comprehended by many organizations and is one of the most significant areas of future innovation. IoT is a system of physical objects, gadgets, cars, infrastructures, and other things integrated into a network of hardware, software, and sensors that can gather and interchange data [3].

With the increased development in communication technology, electronics miniaturization with low cost and high processing power made the IoT possible to bring the science fiction world into reality. IoT will arrive at 50 billion units by 2020 [4]. IoT is gaining wide acceptance

and rapid penetration in various domains of work [5]. This ranges from agriculture to smart grid, smart homes to smart parking. The health sector is a catching domain of IoT, proving remote health monitoring [3]. One of the key roles of IoT in the health sector is to develop applications for remote monitoring [1]. Remotely health monitoring, a key integral feature of IoT in the health sector, could be efficiently used in assisting physiotherapy-related activities to be performed precisely and effectively [1].

Researchers have investigated and envisaged IoT as a virtual physiotherapist that has the potential for the systematic execution of prescribed exercises that eventually leads to a speedy recovery and prevents from permanent joints disorders [1], [6], [7].

Physical exercise is the only way to enjoy a healthy and physically active life. Many of the physical and subsequent issues that individuals encounter may be solved without the need for drugs with the help of physiotherapy. Physiotherapy can help patients regain and maintain mobility and functioning. It does that with

several approaches such as massage, exercise, counseling, and the provision of mobility and functioning aids. Healthcare professionals frequently recommend regular exercise to patients suffering from fatigue caused by accident, sickness, or ageing that restricts their normal ability to walk and perform regular tasks, these orthodox doctrines to addressing physical problems of patients are deemed not fully efficacious.

The proper and systematic execution of recommended exercise is required for effective home-based physiotherapy [2]. Physiotherapy is often not only used to repair functionality, but also to avoid motor problems [2]. To recuperate the specified treatment plan, the exercise must be performed regularly and correctly [2].

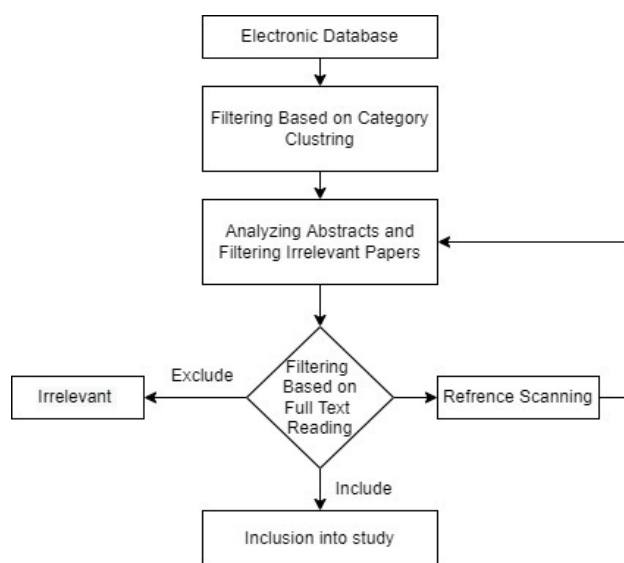


Figure 1: Study Flow Diagram

This study is aimed at analyzing different research about physiotherapy assistant smartphone applications that help out patients during the execution of prescribed exercises and explore which research/methodology is more useful for patients and capable to assist in the execution of correct physiotherapy activities as well as psychological support to the patient remotely. Different electronic databases were used to search different IoT-based physiotherapy assistant articles. IoT-based physiotherapy system coupled with machine learning, “Smart IoT-based physiotherapy assistant” and “Remote IoT-based physiotherapy system with machine learning” were the terms used to search related articles. There were numerous physiotherapy assistant systems, but in our case, only solutions based on IoT and IoT coupled with machine learning were considered. The rest document is structured as A literature review on the work of investigators is described in section 2. Section 3 and section 4 comprise of Discussion Analysis and conclusion respectively. Flow diagram of the study is presented in Figure 1.

2. Literature Review

In a conventional physiotherapy approach, there is no proper system to monitor and assist the physical exercise of the patient outside the clinic. The evaluation of the physical exercise of the patient is done at the clinic [7]. Thus, it entirely relies on the availability of physiotherapists. The evaluation of prescribed exercise requires more effort, more care, more expenses, and more time from the physiotherapist [8]. This approach leads to a waste of resources, money, and time which creates a lack of interest in patients about the execution of the exercise. Furthermore, the physiotherapist is bound to monitor patient exercise on site. The traditional system also suffers from a lack of communication that sometimes leads to the absence of response or feedback to the patient regarding their exercise. Several variations from the ideal movement may arise in these cases: unconscious introduction of offset motions or postures, inadequate movement range, incorrect muscle activation time, or even biomechanical imbalance.

Home-based physiotherapy exercise helps patients to stimulate muscle activity by allowing them to perform the recommended workout at home [2]. The patient has to train and impart proper education for the benefit of physiotherapy and allow him/her continuous faithfulness to the program [9]. Exercise should be performed correctly and effectively, but patients are often unsure about the right approach without recalling the whole program as advised by the clinic [10]. Such challenges can be overcome by a smart physiotherapy system that has remained a target research area for researchers. Several researchers have proposed smart physiotherapy systems using IoT.

The accuracy of the Microsoft Kinect skeleton joint tracking system is evaluated by using the Vicon Bonita system is presented in [6]. The Microsoft Kinect system uses the camera and two IDS at a specific distance to check the angle of movement of specific joints and three-dimensional coordinates of different body parts. The Vicon Bonita system is an array of eight infrared cameras positioned around the test subject. Infrared light is emitted by 68 LEDs positioned around the lens, that emitted light is reflected by markers affixed to the body of the subject. Vicon Nexus software was used to collect data from cameras and calculate marker placements. The IR light reflection from tags placed on selected body parts was recorded to form a spatial triangular shape that helps to build 3D shape. Vicon Bonita system was used for data collection and analysis. An angle comparison computed with both Vicon and Kinect system is performed and found that the minimum deviation is 2.7° and the maximum deviation is 14.2° at the hip with an angle of

135°. The evaluation shows that the Microsoft Kinect system provides accurate joint position during exercise.

In [11], the author provide the Kinect-based physiotherapy system to execute the prescribed exercises at home. It uses two Infrared Depth Sensors (IDS), one RGB camera, Microsoft Kinect System, and a tablet. To cover all joints, two IDS are used. It uses the Microsoft Kinect skeleton joints tracking system to check the accuracy of exercise, patient's movements were tracked by an infrared camera, to reflect pictorial form on the tablet screen RGB camera was used and an acceleration sensor was to check the body motion. Microsoft Kinect library is used to collect data from all the sensors, camera, and stored into the database for future analysis by the physiotherapist. The Kinect software provides information to the user about the exercise to be executed and keeps track of the exercise execution frequency or number of steps patient performed.

In [12], a system based on smart connected devices, such as a smart walker, and a force platform that employs a variety of sensing technologies, including piezoresistive force sensors and microwave radars was presented. In smart walkers, the Fexiforce sensor and the FMCW 24GHz microwave radar are employed. The Fexiforce sensor monitors pressure and user balance when using the walker. Gait was measured using an FMCW 24GHz microwave radar array. The gathered data is transmitted through Bluetooth. To produce a force platform, load cells are put beneath an acrylic plate. During a complex game, the system evaluates the ground response force caused by a subject's applied force. The data from both devices is kept on a shared client-server architecture. Two people were chosen for the experiments, and two mint walks for gait training over a distance of 20m were done. The development of the obtained signals associated with lower limb mobility was supplied by microwave radar. Subjects used Therasoup to capture things on the force platform. Participants utilized both their left and right hands. The force values from the platform can be utilized to track the evolution of patient stability over the course of several training sessions.

The proposed method by [13] enables paralyzed persons to move freely and safely while lowering the cost of therapist services. To control the wheelchair's movement, a voice recognition system was combined with an Arduino interfaced joystick to create a smart wheelchair. Furthermore, the device may detect impediments automatically by employing an ultrasonic sensor. Power wheelchairs include both control systems and therapy alternatives for disabled people that have only lower limb, upper limb, or mixed lower limb and upper limb impairments. A mobile application to control the movement of a wheelchair, with speech recognition

was developed to take commands from a microphone and match them with predefined voices. An ultrasonic sensor is used to identify obstructions. For therapy, an auto pulley system and vibration pads are used. The proposed device lacks the power to carry more than 93kg of weight, has only rudimentary therapies for the upper limb, only an auto pulley that can't handle more than 10kg of weight, and only a vibration pad for the lower limb.

In [14], m-Therapy, a multimodal therapeutic framework that collects data using various environmental and gesture-tracking sensors was proposed. The gathered data is compressed and sent to a server using the m-Therapy framework. The framework employs a therapeutic paradigm to help a patient complete therapy activities at home. The proposed system can identify rotational and angular motions of thirty-five joints. The system can identify whether any of the preset high-level gestures are performed. Data from therapy sessions include text, video, gesture, motion, and audio data. After the completion of the therapy session, data is uploaded to the server. The server is responsible to utilize a big data analytics engine to drive structural data gathered from therapy session data using various gesture recognition techniques. This system was evaluated using usability testing and system testing, and the findings were good.

The work investigated by [15] proposed a system to monitor, guide, and remote treatment of the patient. The system comprises of the medical dynamometer, range of motion encoder, force sensor, torque sensor, encoder input board, SQL database, main Controller (Computer system), internet, DiagnoConn a doctor and patient Module, professional interface, and user interface. Four distinct exercises, including isometric, isotonic, passive, and resistive, were performed using a robot. The robot can flex, ulnar, radial, extend, and deviate for the wrist, supination, and pronation for the forearm. The robotic manipulators exercise according to the medical criteria. Three patient categories were treated in the DiagnoConn application: new patients, continuous therapy patients, and patients whose therapeutics have been completed, and all of the information are stored in an SQL database. The doctors are logged in to system with their username and password. Firstly, they assess a patient's physical characteristics and then the doctor evaluates these data and allocates date/time, kind of workout, level of difficulty, motion range, and strength of the workout and stored it in an SQL table. The patient executes the exercise at the specified place and parameters for the next session were determined by a specialist based on the result of the previous session. A survey comprised of seven questions was conducted from 26 people. According to the survey results, the highest satisfaction rates for speed and availability at all times were 92% and 93%. The reliability

criterion had the lowest satisfaction percentage, at 75%. The total satisfaction percentage for performance is 88 percent, which is sufficient for user satisfaction.

The physical telerehabilitation system (PTS) is proposed by [16] to support patients and physiotherapists over the internet. It uses camera, microphone, and motion sensors to collect data produced during exercise. Twenty-five therapists and twelve physiotherapists responsible for the rehabilitation of ninety elder patients collaborated to design PTS. This system provides the facility of audio, video, drawing, and messaging communication channels to the users. The evaluation of this system is performed by the interview of 15 elderly people more than 65 years old and 10 other stakeholders. The outcome of the interviews highlighted issues related to the need for reliable services, sure access to the system, and data protection. Aside from that, all stakeholders recognize the tool's tremendous potential.

In [17], the system which is used to evaluate the swimming method of different swimmers at the same position is proposed. This system integrates a single, wearable sensor device in a pair of identical, redundant IMU six-DoF sensors, and a 3-D accelerometer and gyroscope. The initial experiments employ two redundant 6-DoF IMU sensors due to the measurement reliability of the waterproof sensor device prototype. The motion signals from both sensors were of the same quality. A virtual link is established between the patient and the physiotherapist in order to give feedback about swimming to the concerned.

In [18], an IoT based Smart walker system is presented which is composed of IMU, Load cells, a Force Sensor, a Doppler Sensor, an RFID Reader, a Cloud System, an Atmega2560 microcontroller, a computer system, wireless, Bluetooth 4.0, an internet, software module and augmented with two interfaces Professional interface for physiotherapist and user Interface for patients. The RFID Reader recognizes the patient's ID and initiates a physiotherapy smart walker session. The sensors sense data about elevation, weight, and movement and send it to the gateway (laptop) via Bluetooth. Subsequently, the data is sent to the cloud and made visible to the physiotherapist remotely. During a physiotherapy session, two ultrasonic sensors are utilized to extract the patient's walker's elevation on each side. This measurement is taken so that the physiotherapist may see if the patient is lifting the walker more on one side than the other, which indicates that one arm is weaker than the other. Data is transferred to the cloud using Wi-Fi. At the user end, a mobile app is used for two purposes. The first one is to provide an alternative path to get data from the sensor via Bluetooth and send it to the cloud when the internet is accessible. The second purpose

is to access historical data and feedback from physiotherapists. At the physiotherapist's end, a website, as well as the mobile app, is developed to access cloud data to monitor or get updates. A group of five healthy males of age group ranging from 24 to 30 years with an average weight between 65-80Kg participated in the experiment. The test was evaluated by dictating a participant to simulate as an abnormal right-side tilt walking and the other is asked to walk the natural way and normal way. The analysis of data showed a clear difference between them.

In [19], the author offers a home monitoring system to assist older people with self-rehabilitation. This system employs an ambient sensor, a Bio Signal Sensor, and three wearable IMUs on dominating ankle, on his/her chest, and dominating wrist, with the sensors' y-axis. Through the Data Fusion layer, the data received from the sensors is converted into a single model. Each wearable sensor captures data in three dimensions, velocity, and acceleration, namely direction, at a sampling rate of 10 Hz. Through the system's recording, specialists may also assess the patient's development and leave opinions. The five specially developed rehabilitative exercises are as follows:

- Knee's flexion extension while sitting.
- Lifting and lowering one's arm.
- Rotation of the trunk while seated.
- Standard backward leg extension.
- A light "squat"

Each patient's personal "golden standard" that is validated by a medical expert is stored at the first-time workout is done in the clinic under the guidance of a competent trainer. Previously stored benchmarked patterns were used to aid patient performance and measure effectiveness of self-managed rehabilitation process.

A set of smart gloves for upper-limb rehabilitation that can be used to naturally interact with therapeutic serious games is presented by [20]. Patients with motor disabilities can utilize these games to do highly engaging workouts based on diverse VR settings. The system is comprised of a series of software tools that assist in data collecting and processing, as well as a set of highly interactive therapeutic games to be used in hand and finger rehabilitation session exercises. Throughout a rehabilitation session, the physiotherapist can use the information acquired to evaluate the patient's performance during various physical tasks.

In [21], Smart Pants, a home rehabilitation method after the stroke that uses IMU, Pressure Sensor, Force Sensor, and wireless communication to send data to the mobile devices was presented. It uses IMU along with an

accelerometer, magnetometer, and gyroscope. Pressure sensors are resistors that alter resistance according to the scale they are pushed. It comprises 4 IMU nodes, two of which are located on the thighs and shins each. Furthermore, the nodes attached to the shins are coupled to the two pressure sensors implanted within a footwear insole. Finally, the data from all the sensors were collected by mobile device that collected data is used to provide real-time audio or video feedback to the subject about the performance of the workout. Performance of the proposed system is assessed by five exercises (lower limbs Abduction, Extension, Sit-to-Stand, Gait and Bipedal Bridge). Several ML models were evaluated, that includes C4.5 Random Tree (RT) and J48, Random Forest (RF), LibSVM, Naive Bayes (NB) Sequential Minimal Optimization (SMO), Logistic Regression (LR) and Multilayer Perceptron. K-fold cross-validation with 10 folds is performed to validate the system. Results obtained from the dataset with less features were the same as the results obtained from complete dataset. A dataset with small data set was preferred due to faster calculation and immediate feedback. The experiment showed that the Random Forest outperformed and showed more Precision, Recall, and F-Measure results (99.3%) compared to the Multilayer Perceptron (97.9%) result.

In [2], a system that consists of an Electromyography sensor and inertial sensor unit (Accelerometer, Gyroscope, and Magnetometer Sensor) to monitor the human body motion and muscular activation was proposed. Two body area networks were deployed with an electromyography sensor and two inertial units on the subject's body for maximum retrieval of the relevant information. Three women and four males aged about 27 years old took part in the study and completed three activities labeled with three classes: correctly, deviation 1, and deviation 2. Two sets of features were considered which were extracted by Body Area Network (BAN) and BAN + inertial unit. Four machine learning (ML) models that include K-Nearest-Neighbors (KNN), Random Forest (RF), Decision Tree (DT), and Support Vector Machine (SVM) were used for classification. DT and KNN outperformed other ML models with an accuracy between 95% to 100% on all three exercises.

ePhysio, a platform for physiotherapy with sensors and remote monitoring of a rehabilitation system for musculoskeletal exhaustion is proposed in [7]. The proposed system comprises of Inertial Measurement Unit (IMU), textile Sensor, accelerometer, gyroscope, magnetometer, cloud system, rehabilitation hub, computer system, Wireless communication technology (Bluetooth 4.0), and ePhysio module. Inertial sensors can be attached to the forearm, the sternum, and the scapula.

The ePhysio stimulates and encourages patient activity. This system creates a virtual link between the therapist and the patient. The physiotherapeutic specialist may provide the patient with information on training protocol quality, therefore offering users an actual comment on the effectiveness of the workout. The sensors send data to the rehabilitation hub using wireless Bluetooth and store enriched data (sensor data with Metadata) at the cloud system by using the wired connection. The metadata contains information such as the patient's identity, workout type, execution time, and so on. From the cloud, the physiotherapist can visualize patient data and adds comments about the patient exercise. The enriched data stored at cloud system can be then used for future analysis and to train machine learning models for continuous prediction and evaluation. Accelerometer, gyroscope, and magnetometer were utilized to integrate arm abduction and horizontal flexion angles with scapular movement to extract the hand position during traditional shoulder rehabilitation activities and assess the difference in arm trajectory between the real and expected arm. The patient's context information can eventually be displayed, for example, as a report to specialists on a patient's performance over time.

In [22], a series of games for physiotherapy using a Kinect natural user interface and a set of Unity3D VR games was presented. A smartphone application was developed to allow physiotherapists that connect to physical therapy serious games via a remote server to access patient electronic health records, game remote configuration, and data presentation. Using a Kinect sensor, the device records the patient's motions. Thirty-three people were chosen to take part in virtual reality games. The Kinect sensor is utilized to calculate the hand's ability to perform arm movements as well as the elbow and wrist angles. Some workout game sessions and angle values were kept in the database. The right hand outperforms the left hand in terms of amplitudes of reached angles throughout the intensive gaming session, according to the findings. There were no significant differences between male and female gaming sessions when the data for game sessions were compared. Using a smartphone app, therapists can visualize data and provide training plans.

Remote Monitoring of Stroke Patients Physical Rehabilitation Using IoT and Virtual Reality is presented by [23]. The goal is to create smart gloves and a headband for physical rehabilitation monitoring. Merging Virtual Reality (VR) serious games with a Wearable Sensor Network to boost patient involvement during physical therapy and analyze their progress. Gloves and headgear with flexion sensors to record angular flexion, Force Sensors (FlexiForce A201) to record the force of each

finger, gyroscope for angular motion, accelerometer, and magnetometer for movements. For exercise, virtual reality-based 3D games are utilized. The Arduino nano communicates with the sensors and the mobile app through Bluetooth. In addition, data is transferred to a web server for remote access. Five sessions are performed by two participants in which they grab the virtual objects. Volunteers that grabbed a substantial number of objects has stronger muscles. The results reveal that men volunteers have stronger macular abilities than female volunteers since they grabbed a greater number of objects and have more scores.

In [24] a low-cost elbow exoskeleton linked to a Context-Aware architecture that enables the patient to practice rehabilitative tasks interactively through a virtual reality system was presented. The data from the exoskeleton sensor is transferred to the local context monitoring system, which is focused on patient monitoring and follow-up. The data is then sent to the cloud, where it may be accessed by medical remote monitoring, exercise monitoring, and e-health care services, as well as saved in historical data where an exercise and medical log is kept. The results of sensors can be used by physical therapists to modify the exercise. During the experiment, the number of average collisions identified is larger in the initial sessions than in the last. The results of the reference patient demonstrate that, although not have an elbow injury, the difficulty of the exercise causes him to make some errors while performing the exercises with both actual and simulated weight.

Virtual Reality-based homecare VirtualPT on a personal computer for the physiotherapist to assist elders in regaining full physical function is proposed by [25]. Important health metrics are continually monitored and tracked while performing home-based suggested physiotherapy activities by integrating immersive Virtual Reality with the wearable VirtualPT Sensor kit. The MAX30100 Pulse Oximeter sensor and temperature sensor are used to measure pulses and body temperature, respectively. Body deviations are computed using the k-nearest neighbor and decision tree techniques. A regression algorithm forecasts the patient's future situation. The system determines whether or not the patient is physically fit to continue exercising. The Brainwave Starter Kit was used to examine the patient's mental condition, and based on the results, exercises were prescribed. The Microsoft Kinect sensor is used to evaluate a patient's skeletal movements in conjunction with the movement of the VR assistance, which involves calculating angle deviations of active joints. The Microsoft Kinect sensor is used to analyze the acceleration and rotation of bodily components. Using MPU9250 IMU

sensors and the Dynamic Time Warping algorithm, determine the rate of the exercise. For each exercise, the CNN model is trained. The technology compares the patient's workout acceleration data with the trained model to detect the movement. If the user's medical condition changes, the system tells the user and makes the necessary adjustments, such as reducing the exercise count or speed. The system reschedules the exercise based on previous progress saved in the system. The data is displayed to the user via a virtual reality dashboard. The supervised assessment in the clinical setting, according to the physiotherapists and based on the responses, made participants feel safe in their surroundings. 90% of those who utilized VirtualPT at home were dependable.

3. Discussion and Analysis

The IoT based smart physiotherapy system presented in [2] doesn't provide real time monitoring to be supervised by physiotherapist remotely and thus it lacks a real time communication/feedback between patient and physiotherapist. The subjects participated were also not covering a wide age group. Furthermore, the participant numbers were too low to deduce performance on the base of generalization i.e., 4 men and 3 women of the selected age group (27-28 years old) were used. It covers four exercises, Isometric scapular retraction, Strengthening, Prone scapular retraction, and Forward lunge. Deploying four ML models (DT, SVM, KNN, and RF) makes it inappropriate for real-time applications.

The [6] provides the system which evaluates the accuracy of Microsoft Kinect System. The tag placement on different body part doesn't help to exercise in a natural way. The scope of the investigation is confined to the comparison of Microsoft Kinect to how precisely it can track joint movements. The system neither provides to classify the types of exercise nor real-time monitoring involved in it. It also does not provide any virtual communication link between the user and physiotherapist to communicate.

The IoT-based smart physiotherapy system investigated in [7] provides real-time monitoring, where physiotherapists send his/her feedback. No, automatic exercise evaluation capability exists and thus physiotherapist presence is necessary to assist and evaluate the exercise in real-time. Furthermore, this data may be examined and processed to discover statistical features such as abnormalities, recurring errors, and so on. The [11] provides the Kinect-based physiotherapy system to execute the prescribed exercise at home. It does not provide any real-time feedback from the system about prescribed exercise. It does not use any machine learning tool to automate the system and hence evaluation of

patient exercise is not performed in an automatic manner and hence requires physiotherapist presence for assisting and evaluation. The patient feels uncertainty due to sensors attached to patient body using tags.

The IoT-based Smart Walker Physical Rehabilitation System provided by [18] monitors the patient's movement during rehabilitation sessions and the physiotherapist sends his/her feedback. No automatics exercise evaluation capability exists and thus the physiotherapist's presence is necessary to assist and evaluate the exercise in real-time. Every patient cannot purchase a smart walker and cannot afford expenses of regular physiotherapist services. The specifically designed walker serves as an obstacle in natural movements and makes the patient uncomfortable. Furthermore, this data may be examined and processed to discover statistical features such as abnormalities, recurring errors, and so on.

DiagnoConn (the Mobile Application for Robotic Rehabilitation) presented by [15] does not provide real time monitoring to be supervised by physiotherapists remotely and subsequently a lack of real time communication/feedback between patient and physiotherapist. The subject' participants move his/her body parts according to the movement of robotics if any issue creates in system, then it can create more problems for the patients. It includes four types of exercises: passive, isometric, isotonic, and resistive. It does not use any machine learning tool to automate the system and hence no automatic evaluation of patient exercise is performed. Further, the system is costly and probably not beneficial to all patients.

Like [18], The system designed by [21] does not provide smart monitoring and there is no real time communication/feedback between patient and physiotherapist.

The system presented in [19] requires presence of the physiotherapist to assist and evaluate the exercise in real time. This system also does not provide two-way communication between the physiotherapist and the patient; only physiotherapist can monitor the patient and comments on exercises. Sensors attached to the body also make the patient uncomfortable and serve as an obstacle in natural movements. It monitors only 5 exercises and experiments done on 2 persons. The patient exercise is compared with golden standards which show from 10 repetitions' count and 9 are correctly predicted. Also, a machine learning algorithm can be introduced to evaluate the exercise types and assists the patients to a possible extent. This leads to lessening the physiotherapist intervention for minor assistance and subsequently the physiotherapist will be available to more serious patients.

The Patient Telerehabilitation system (PTS) presented in [16] does not provide real time monitoring to be supervised by physiotherapists remotely and subsequently. Only physiotherapist can monitor the patient data from cloud and audio video connection is also established. Real time monitoring is not done and not uses any Machine learning tool to automate the system. Because machine learning algorithm are not used there is not any prediction of system and no evaluation of patient exercise performed automatically. Patient feels uncertainty due to sensors attached to patient body using tags. It provides costly setup which all patients cannot bear. In this research proposed system cannot automatically work.

m-Therapy, a multisensory framework that is presented by [14] does not provide real time monitoring to be supervised by physiotherapist remotely and subsequently. Internet connectivity is required to performed exercise sessions. It does not use any machine learning tool to automate the system. Further, the system is costly and probably not beneficial to all patients.

In [17], a system to evaluate rehabilitation based on swimming is proposed. The wearable inertial sensor devices are used in this study to monitor and evaluate the key parameters of rehabilitation activities. The system tracks the swimming movements and uploads on cloud. The physiotherapist then monitors the movement and guides the patient accordingly thus physiotherapist's presence is necessary all the time to monitor patient exercise in real time. User Interface and Professional Interface are designed to login into system. No automatic monitoring of swimming exercises is performed, and there is no two-way communication channel between the patient and physiotherapist in real time.

VR games along with different wearable sensors by [20, 22-25] were used to develop a smart physiotherapy assistance system. In [20, 23], the author developed a glove for arm rehabilitation. In [20], the author does not describe the sensors used in the system. Both of these systems can be used only for upper limb rehabilitation. System developed by [19] used two healthy volunteers to assess the system. Testing of the system in [20] is not presented in the paper. A low-cost exoskeleton linked to VR system is presented by [24]. The results of the physiotherapy session are stored on cloud which can be further used by physiotherapist to modify the exercises accordingly. The result of assessment of system shows that exercises were difficult even for a healthy person.

Kinect interface with VR games was used to aid physiotherapy sessions at home by [22]. Only hand rehabilitation is focused in [22] and system was evaluated by thirty-three healthy volunteers. [12] used FMCW

microwave radar and Flexiforce sensor. Two people assessed the system by doing multiple exercises. There is no monitoring and modifying system for exercise for physiotherapist according to the results of the physiotherapy sessions. A smart wheelchair coupled with pulleys to therapy lower and upper limbs was presented by [13]. A mobile application can be used to control the wheelchair along with speech commands. The device proposed by [13] cannot carry more than 93 kg of weight and pulley cannot manage weight of more than 10 Kg.

The systems presented by [12, 13, 20, 22-24] do not use and ML algorithm and there is a lack of two-way

communication between the physiotherapist and the patient except [24]. These systems are not beneficial for all because they can only be used for the rehabilitation of specific body part. [25] presented VirtualPT measures body temperature and other vital signs during physiotherapy session. ML models were trained that automates the system. The system is costly and not beneficial for all patients. System is evaluated only on older patients.

The following table summarizes the reviewed investigations and presents a comparison among the investigations.

Table 1: Comparison Table

Reference	Technologies used	Machine Learning Models	Pros	Cons
[2]	Electromyography sensor and inertial sensor unit (Accelerometer, Gyroscope and Magnetometer Sensor). Computer System and Module coding Body Area Network (BAN)	DT, KNN, SVM and RF	Forwarding step to Automatically Monitor the exercise Apply Machine Learning Model Train Model on data set Evaluation Parameters used to check Accuracy Guide in research point of view in future	Size of dataset is very small List of sensors required to use this system Tags used to bind sensor with body For Limited exercises No communication channel b/w patient and physiotherapist Model train on specific age group Not more efficient due to small dataset
[6]	Microsoft kinect skeleton system, Vicon Bonita system and 8 infrared cameras	No Machine Learning Model used	Evaluate the accuracy of Microsoft Kinect skeleton system by using 8 IR Cameras	Only evaluate the accuracy of skeleton system no benefit to patient. Large set up and software required. No patient assistance
[7]	Inertial Measurement Unit (IMU), Textile Sensor, accelerometer, gyroscope, and magnetometer, Cloud System, Rehabilitation Hub, Computer system, Wireless (Bluetooth 4.0), Internet and ePhysio Module Professional Interface, User Interface	No Machine Learning Model used	Provide three use cases (Outdoor and indoor group therapy, or single user) Create virtual link b/w patient and physiotherapist Provides immediate feedback.	A complete system required to monitor exercise, Unidirectional communication channel. No automatic evaluation of exercise, wired connection between Hub and Computer
[11]	Microsoft Kinect skeleton system, Two Infrared Depth Sensors (IDS), Acceleration Sensor, RGB camera and Tablet Kinect code library	No Machine Learning Model used	Track the patient movements and reflect the motions on the tablet screen User log and administrative log available Physiotherapist can monitor patient exercise at clinic Built in module of Microsoft used count no of time exercise performed	Two IR Sensors and Camera required Computer system required Internet access required Microsoft Kinect system required No proper communication channel available
[12]	Fexiforce sensor and the FMCW 24GHz microwave radar	No Machine Learning Model was used	System is used for lower limb rehabilitation.	No automatically monitor patient exercise, no two-way communication channel b/w patient, System can be used only for lower limb rehabilitation
[13]	Arduino interfaced joystick to create a smart wheelchair	No Machine Learning Model was used	Smart wheelchair with lower and upper limb rehabilitation.	No automatically monitor patient exercise, no two-way communication channel b/w patient

				System can be used only for lower and upper limb rehabilitation, can only lift weight up to 93 Kg
[15]	Medical dynamometer, Range of motion encoder, force sensor, torque sensor, Encoder Input board, SQL database, Main Controller (Computer system), Internet, DiagnoComm a doctor and patient Module, Professional Interface and User Interface	No Machine Learning Model was used	Automatic remote treatment of patient. User interface and professional interface created to do and monitor exercise. Good step to automate and recover physical disorders	Work on four exercises, each patient body parts have different movement style, it can create more issues for some patients. More movement can apply from patient capacity, system programmed on standard movements not train on each subject, Internet connection required to send data.
[16]	Camera, microphone, Drawing Tool, motion sensors, User Interface (Client and Doctor) and Patient Telerehabilitation system	No Machine Learning Model was used	Good step to automate the system, Real time feedback to patient through Audio, Video Channel and Messaging, Online Checkup of patients, patient no need to visit clinic	No automatically monitor patient exercise, Test the system only on 15 elderly people, Inter Connection required, Physiotherapist is bound to monitor patient exercise
[17]	A redundant 6-DoF IMU sensor that includes 3-D gyroscope and accelerometer	No Machine Learning Model was used	Track the Swimming movements and upload on cloud to monitor by physiotherapist and guide to patient about his session Physiotherapist can monitor patient swimming at clinic. User Interface and Professional Interface designed to login on system.	No automatically monitor swimming exercise, No two-way communication channel b/w patient and physiotherapist, Physiotherapist is bound to monitor swimming
[19]	Environmental sensor, Bio Signal Sensor, 3 wearable Inertial Measurement Unit (IMU), dominating ankle and wrist, with the y-axis of the sensors	No Machine Learning Model was used	Collected data can be used in future for further prediction, Check the accuracy of system by golden standards, use 10 Hz carrier frequencies, Immediate feedback about the workout is provided by physiotherapist.	No automatically monitor patient exercise, Test the system on 2 men and 5 exercises, List of sensors required to use this system Tags used to bind sensor with body For Limited exercises, No two-way communication channel b/w patient and physiotherapist Physiotherapist is bound to monitor patient exercise
[20]	Not Presented in paper	No Machine Learning Model was used	Developed a glove for arm rehabilitation, VR games were used for physiotherapy session, physiotherapist can view the results of the exercise session,	No automatically monitor patient exercise, no two-way communication channel b/w patient, no information about sensors used, only for arm rehabilitation
[21]	Inertial Measurement Unit (IMU), Pressure Sensor, Force Sensor, wireless communication (Blue tooth)	MLP, LibSVM, SMO, J48, RF, NB, LR and C4.5 RT	Good step to automate the system, Audio, and video feedback to patient	Lake of in written communication, Not automatic working, A large list of ML Models used , Test only on five exercises, Internet connection required to send data , Physiotherapist required to monitor the patient exercise
[22]	Kinect natural user interface and a set of Unity3D VR games.	No Machine Learning Model was used	Kinect interface was used along with VR games for rehabilitation. Thirty-three healthy subjects assessed the system, Therapist can view the results of the session using a mobile application.	No automatically monitor patient exercise, No two-way communication channel b/w patient. System can be used only for lower limb rehabilitation
[23]	FlexiForce A201, Gyroscope, accelerometer, and magnetometer	No Machine Learning Model was used	Developed a glove for arm rehabilitation, VR games were used for physiotherapy session, System was tested by grabbing different subjects in VR games by healthy subjects,	No automatically monitor patient exercise, No two-way communication channel b/w patient, only for arm rehabilitation

[24]	Exoskeleton sensor	No Machine Learning Model was used	Exoskeleton linked with VR games is used for elbow rehabilitation, Therapist can view results and modify the exercise.	No automatically monitor patient exercise and exercises were difficult even for healthy persons, only for elbow rehabilitation
[25]	Kinect sensor, MAX30100 Pulse Oximeter sensor and temperature sensor	KNN, CNN and DT	VirtualPT that measures body temperature and other vital signs during physiotherapy session. ML models were trained that automates the system. The system is costly and not beneficial for all patients	System is costly and only assessed over older patients.

4. Conclusion

In recent years, there has been an increased need for effective healthcare systems in response to the world's ageing population, the rise in the incidence of chronic diseases, and the proliferation of new medical technologies. Some persons are unable to move and function normally due to a physical abnormality, most of which are the result of accident, illness, or old age. Numerous methods have been developed by researchers to help and remotely monitor these individuals. This study reviewed the strategies adopted by numerous scholars, together with the analysis and application of technology, to take on these crucial issues. The purpose is to provide a concise summary of current approaches and tools to aid future researchers in their pursuit of a global solution. The rapid development of compactness and robustness of processors, sensors, and coupling with machine learning has increased the potential of smart and single global solutions conceivable for future researchers to address issues related to remote physiotherapy assistance systems.

Conflict of Interest

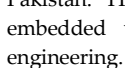
The authors declare no conflict of interest.

References

- [1]. L. J. Ramírez López, A. Rodriguez Garcia, and G. Puerta Aponte, "Internet of things in healthcare monitoring to enhance acquisition performance of respiratory disorder sensors," *International Journal of Distributed Sensor Networks*, vol. 15, no. 5, p. 1550147719847127, 2019, doi: <https://doi.org/10.1177/1550147719847127>.
- [2]. A. Pereira, D. Folgado, R. Cotrim, and I. Sousa, "Physiotherapy Exercises Evaluation using a Combined Approach based on sEMG and Wearable Inertial Sensors," 2019, pp. 73-82, doi: 10.5220/0007391300730082.
- [3]. C. Stergiou, K. E. Psannis, B.-G. Kim, and B. Gupta, "Secure integration of IoT and cloud computing," *Future Generation Computer Systems*, vol. 78, pp. 964-975, 2018, doi: [doi:10.1016/j.future.2016.11.031](https://doi.org/10.1016/j.future.2016.11.031).
- [4]. M. A. Al-Garadi, A. Mohamed, A. K. Al-Ali, X. Du, I. Ali, and M. Guizani, "A survey of machine and deep learning methods for internet of things (IoT) security," *IEEE Communications Surveys & Tutorials*, vol. 22, no. 3, pp. 1646-1685, 2020, doi: 10.1109/COMST.2020.2988293.
- [5]. I. Lee and K. Lee, "The Internet of Things (IoT): Applications, investments, and challenges for enterprises," *Business Horizons*, vol. 58, no. 4, pp. 431-440, 2015, doi: doi.org/10.1016/j.bushor.2015.03.008.
- [6]. S. Phommahavong, D. Haas, J. Yu, S. Krüger-Ziolek, K. Möller, and J. Kretschmer, "Evaluating the microsoft kinect skeleton joint tracking as a tool for home-based physiotherapy," *Current Directions in Biomedical Engineering*, vol. 1, no. 1, pp. 184-187, 2015, doi: 10.1515/cdbme-2015-0046.
- [7]. C. Vallati, A. Viridis, M. Gesi, N. Carbonaro, and A. Tognetti, "ePhysio: a wearables-enabled platform for the remote management of musculoskeletal diseases," *Sensors*, vol. 19, no. 1, p. 2, 2019, doi: 10.3390/s19010002.
- [8]. W. Wei, Y. Lu, E. Rhoden, and S. Dey, "User performance evaluation and real-time guidance in cloud-based physical therapy monitoring and guidance system," *Multimedia Tools and Applications*, vol. 78, no. 7, pp. 9051-9081, 2019, doi: 10.1007/s11042-017-5278-5.
- [9]. S. F. Bassett, "The assessment of patient adherence to physiotherapy rehabilitation," *New Zealand journal of physiotherapy*, vol. 31, no. 2, pp. 60-66, 2003.
- [10]. J. Smith, J. Lewis, and D. Prichard, "Physiotherapy exercise programmes: are instructional exercise sheets effective?," *Physiotherapy theory and practice*, vol. 21, no. 2, pp. 93-102, 2005, doi: [doi:10.1258/jtt.2009.0810](https://doi.org/10.1258/jtt.2009.0810).
- [11]. D. Haas, S. Phommahavong, J. Yu, S. Krüger-Ziolek, K. Möller, and J. Kretschmer, "Kinect based physiotherapy system for home use," *Current Directions in Biomedical Engineering*, vol. 1, no. 1, pp. 180-183, 2015, doi: 10.1515/cdbme-2015-0045.
- [12]. O. Postolache and P. S. Girão, "Physiotherapy smart connected devices for S-health," 2016: IEEE, pp. 1-6, doi: 10.21307/ijssis-2019-131.
- [13]. M. M. Rahman, S. Chakraborty, A. Paul, A. M. Jobayer, and M. A. Hossain, "Wheel therapy chair: A smart system for disabled person with therapy facility," 2017: IEEE, pp. 630-635, doi: 10.1109/ICSCAN53069.2021.9526427.
- [14]. M. A. Rahman and M. S. Hossain, "m-Therapy: A multisensor framework for in-home therapy management: A social therapy of things perspective," *IEEE Internet of Things Journal*, vol. 5, no. 4, pp. 2548-2556, 2017, doi: 10.1109/JIOT.2017.2776150.
- [15]. M. E. Aktan and E. Akdoğan, "Design and development of a mobile application for a robotic rehabilitation process: Diagnoconn," 2017: IEEE, pp. 1-5, doi: 10.3906/elk-2007-24.
- [16]. M. Caporuscio, D. Weyns, J. Andersson, C. Axelsson, and G. Petersson, "Iot-enabled physical telerehabilitation platform," 2017: IEEE, pp. 112-119, doi: 10.1109/ICSAW.2017.43.
- [17]. A. Kos and A. Umek, "Wearable sensor devices for prevention and rehabilitation in healthcare: Swimming exercise with real-time therapist feedback," *IEEE internet of things journal*, vol. 6, no. 2, pp. 1331-1341, 2018, doi: 10.1109/JIOT.2018.2850664.

- [18]. C. Nave and O. Postolache, "Smart walker based IoT physical rehabilitation system," 2018: IEEE, pp. 1-6, doi: 10.1109/ISSI.2018.8538210.
- [19]. A. Candelieri, W. Zhang, E. Messina, and F. Archetti, "Automated rehabilitation exercises assessment in wearable sensor data streams," 2018: IEEE, pp. 5302-5304, doi: 10.1109/BigData.2018.8621958.
- [20]. R. Alexandre and O. Postolache, "Wearable and IoT technologies application for physical rehabilitation," 2018: IEEE, pp. 1-6, doi: 10.1109/ISSI.2018.8538058.
- [21]. I. Bisio, C. Garibotto, F. Lavagetto, and A. Sciarbone, "When eHealth meets IoT: A smart wireless system for post-stroke home rehabilitation," *IEEE Wireless Communications*, vol. 26, no. 6, pp. 24-29, 2019, doi: 10.1109/MWC.001.1900125.
- [22]. O. Postolache *et al.*, "Tailored virtual reality for smart physiotherapy," 2019: IEEE, pp. 1-6, doi: 10.1109/ATEE.2019.8724903.
- [23]. O. Postolache, D. J. Hemanth, R. Alexandre, D. Gupta, O. Geman, and A. Khanna, "Remote monitoring of physical rehabilitation of stroke patients using IoT and virtual reality," *IEEE Journal on Selected Areas in Communications*, vol. 39, no. 2, pp. 562-573, 2020, doi: 10.1109/JSAC.2020.3020600.
- [24]. D. H. de la Iglesia, A. S. Mendes, G. V. González, D. M. Jiménez-Bravo, and J. F. de Paz Santana, "Connected elbow exoskeleton system for rehabilitation training based on virtual reality and context-aware," *Sensors*, vol. 20, no. 3, p. 858, 2020, doi: doi.org/10.3390/s20030858.
- [25]. T. A. Heiyanthuduwa, K. W. N. U. Amarapala, K. D. V. B. Gunathilaka, K. S. Ravindu, J. Wickramaratne, and D. Kasthurirathna, "VirtualPT: Virtual reality based home care physiotherapy rehabilitation for elderly," 2020, vol. 1: IEEE, pp. 311-316, doi: 10.1109/ICAC51239.2020.9357281.

Copyright: This article is an open access article distributed under the terms and conditions of the Creative Commons Attribution (CC BY-SA) license (<https://creativecommons.org/licenses/by-sa/4.0/>).



Adil Ali Saleem is PhD research scholar at institute of Computer Science, Khwaja Fareed university of engineering and information and technology (KFUEIT), Rahim Yar Khan, Pakistan. He received his MS in Computer Science degree in 2021 from KFUEIT, Rahim Yar Khan, Pakistan. He received his BS in Computer Science degree in 2016 from university of Lahore, Lahore, Pakistan. His research interests include IoT based smart system embedded with machine learning, Text mining and Biomedical engineering.

Kainat Zafar received her BS degree in software engineering from Bahria University, Islamabad, Pakistan in 2016. She went to United states for her higher studies and graduated from New Jersey Institute of Technology with a M.S degree in Computer Science. She is currently pursuing her PhD in Computer Science from KFUEIT, RYK, Pakistan. Her research interests include Biomedical engineering applications, image processing, artificial intelligence, machine learning and software project management.



Muhammad Amjad Raza was born in Liaquatpur, Pakistan, in 1992. He received BS in Information Technology degree from The Islamia University Bahawalpur, Pakistan, in 2017, the MS in Computer Science degree from Khwaja Fareed University of engineering and information technology (KFUEIT), Rahim Yar Khan, Pakistan, in 2021. He has been

working as a Visiting Lecturer with the KFUEIT, Rahim Yar Khan, since

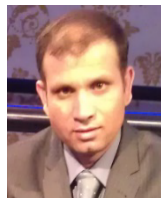
February 2022. He is currently an Active Researcher in the field of the Internet of Things and data science.



Zahid Kareem was born in Rahim Yar Khan, Pakistan, in 1995. He received BS in Computer Science degree from The Superior College Lahore, Pakistan, in 2019. Currently he is doing MS in Computer Science degree from Khwaja Fareed University of engineering and information technology (KFUEIT), Rahim Yar Khan, Pakistan. He is currently an Active Researcher in the field of the Internet of Things and Machine Learning.



MUI-ZZUD-DIN was born in Multan, Pakistan, in 1980. He received the B.Sc. and M.I.T. degrees in computer science and the M.S. (C.S.) degree from Bahauddin Zakariya University, Multan, in 2001, 2005, and 2014, respectively. From 2007 to 2017, he was a lecturer with different educational institutes. Since February 2017, he has been working as a Lecturer with the Department of Computer Science, Khwaja Fareed University of Engineering and Information Technology, Rahim Yar Khan. He has almost ten years of teaching experience. His current research interests include image processing, the IoTs, cognitive radio networks, and data science.





Hafeez-Ur-Rehman Siddiqui (S'15) received his PhD and MSc in Electronic Engineering from London South Bank University in April 2016. He received the BSc. Degree in Mathematics from Islamia University Bahawalpur (IUB). His research interests include Biomedical and Energy Engineering applications, data recognition, image processing, system embedded programming IoT based smart system incorporation with machine learning. Dr. Hafeez-Ur-Rehman is an IEEE IoT journal reviewer.



Sandra Dudley (M'11) was born in Carlow, Ireland. She received the B.Sc. (Hons.) and Ph.D. Degrees in Physics from the University of Essex, Essex, U.K., in 1998 and 2004, respectively. She spent two years working as a Postdoctoral Researcher at Essex University on a British Telecom project resulting in world record broadband-system power consumption for last mile access. In August 2009, she joined the School of Engineering, London South Bank University, London, U.K., as a Lecturer and become a Principal lecturer in March 2014. Her research interests are in physical layer system design, automated health technologies, data recognition, optical-wireless systems, and solution finding for the broadband urban-rural divide. Dr. Dudley is an IET and IEEE journal reviewer.

The Current Trends of Deep Learning in Autonomous Vehicles: A Review

Raymond Ning Huang ¹ , Jing Ren ^{*2} , Hossam A. Gabbar ³

¹Department of Mechanical Engineering, University of Toronto, Toronto, M5S 1A4, Canada

²Department of Electrical and Computer Engineering, Ontario Tech University, Oshawa, L1H 7K4, Canada

³Department of Energy and Nuclear Engineering, Ontario Tech University, Oshawa, L1H 7K4, Canada

*Corresponding author: Jing Ren, 2000 Simcoe Street N. Oshawa, ON, Canada, jing.ren@uoit.ca

ABSTRACT: Autonomous vehicles are the future of road traffic. In addition to improving safety and efficiency from reduced errors compared to conventional vehicles, autonomous vehicles can also be implemented in applications that may be inconvenient or dangerous to a human driver. To realize this vision, seven essential technologies need to be evolved and refined including path planning, computer vision, sensor fusion, data security, fault diagnosis, control, and lastly, communication and networking. The contributions and the novelty of this paper are: 1) provide a comprehensive review of the recent advances in using deep learning for autonomous vehicle research, 2) offer insights into several important aspects of this emerging area, and 3) identify five directions for future research. To the best of our knowledge, there is no previous work that provides similar reviews for autonomous vehicle design.

KEYWORDS: Deep learning, Autonomous Vehicles, Control

1. Introduction

Autonomous vehicles are the future of road traffic. As intelligent agents equipped with sensing technology including GPS, Inertial Navigation Systems (INS), Lidar, and Cameras combined with advanced control systems, autonomous vehicles have important applications in the future. In addition to improving safety and efficiency from reduced errors compared to conventional vehicles, autonomous vehicles can also be implemented in applications that may prove to be difficult or unsafe for a human driver.

However, before they can be safely commercially introduced, several essential technologies necessary for the design and operation of autonomous vehicles must be developed and refined. The function of an autonomous vehicle can be simplified to be a vehicle that can plan and follow a safe and efficient path from given starting points to endpoints with some control constraints. To achieve this goal, it is important to have strong understanding of human visual system and plan the substitution with an effective visual sensor system with robust data analytics. Beyond simple visual data, other sensory data such as location and inertial data can be integrated to improve safety and performance in control and path planning. In

effect, the use of more data can improve system safety and performance. A common strategy deployed to increase the amount of data AVs has access to is facilitating vehicle-to-vehicle (V2V) communication, allowing vehicles to have access to data from more sensors and more accurate state information of surrounding vehicles. Beyond cellular V2V communication, it is also important to consider the issue of bandwidth efficiency and the application of unmanned autonomous vehicles (UAVs) and other technologies to facilitate communication. However, as communication increases and deep learning is increasingly used more in AVs, it is essential to ensure user data is secure and the vehicles are resistant to any malicious attacks. Because autonomous vehicles require accurate sensory and system information, it is especially relevant to detect and diagnose faults. In this paper, we will consider seven key technologies needed for autonomous vehicles: path planning, computer vision, sensor fusion, data security, fault diagnosis, control, and lastly, communication and networking.

While conventional methods have been tried for these technologies, deep learning is arguably the most promising method. This is due to deep learning's ability to accurately approximate complex nonlinear relationships using multi-layer transformations. The difference is

especially highlighted in imaging tasks such as object recognition and image classification. The key types of deep neural networks are Convolutional Neural Network (CNN), Deep Autoencoder (DAE), Deep Belief Network (DBN) and Deep Reinforcement Learning (DRL). DBNs and DAEs can conduct unsupervised pre-training on the weights, which can ease the difficulty of the subsequent supervised training of the deep networks. However, a fundamental problem in DBNs and DAEs is that there are too many weights to train when the inputs are raw signals or their time-frequency representations.

In contrast, CNN can avoid these issues by using strategies like local receptive field and weight sharing to reduce computational complexity during training. However, CNN has a relevant disadvantage which is its tendency to fall into a local minimum in training. The last key network, Deep Reinforcement Learning (DRL), can achieve exceptional results using a Q-learning or policy gradient algorithm to gain the best rewards for the chosen actions.

Our paper is an extension of “Applying Deep Learning to Autonomous Vehicles: A Survey” [1]. We will review the headway in deep learning algorithms to review these seven essential fields. Some relevant reviews have been published in recent years [2], where some new functions are discussed. The main contributions of our paper are:

1. New data security, and communication and networking sections.
2. Reviewed most recent papers for path planning, computer vision, sensor fusion, fault diagnosis, and control.
3. Identified five directions for future research

2. Deep Learning for Path Planning

In an ordinary environment, path planning aims to guide a vehicle on a collision-free paths for where both static and dynamic obstacles need to be avoided. This method can either have a model-based or model-free design and include local or global planning and optimization for some criteria. Models usually aim to find the shortest time or shortest path method. In the following section, we will review recent literature on path planning for autonomous vehicles and the three primary deep learning tools applied., i.e. DRL, CNN, and Long Short-Term Memory (LSTM).

CNN is commonly used for classification tasks due to its ability to extract features from images. While image classification problems are different from path planning tasks, CNN can be used when generating control signals from sensor data from sources such as cameras and lidars. In [3], a high-level control framework was created for the steering of autonomous angles. The authors mapped input camera data directly to a steering angle to implicitly solve

path planning tasks. More commonly, CNN is applied to extract features to be applied in a path planning subtask. In one study, an unmanned aerial vehicle (UAV) was tasked with generating a path through 26 gates in an indoor 3-D environment. In this task, CNN was employed to detect the center of a gate to enable the guidance of the vehicle without collision in real time [4]. CNN can also be applied to tasks of higher difficulty beyond simple 2-D and 3-D single vehicle path planning tasks. In [5], the authors applied CNN in a path planning task of guiding multiple UAVs in a 3-D environment using 2-D CNNs.

LSTM is another type of network used to process image data. As a recurrent neural network, it is often used for sequential image data. In [6], the authors use a model where a LSTM network is applied to extract hidden features to aid in accurately planning sequential moves of AVs. In further works, LSTM has also been successful applied for path planning in an environment with vulnerable road users which includes smaller vehicles such as bicycles and motorcycles as well as pedestrians. In another study, the authors use a model-free planning approach with a deep stacked LSTM network to assess pedestrians’ intentions and plan a vehicle’s motion accordingly [7].

The last primary deep learning tool is deep reinforcement learning which does not rely on labelled data sets and can achieve extraordinary result. In the recent past, DRL has been commonly used in path planning applications for various types unmanned vehicles in diverse environments. The first application involves navigation for road vehicles in an environment with mixed autonomous and traditional vehicles. In this application, DRL is used to generate a shareable driving policy which doesn’t need to consider facts such as system dynamics compared with traditional control methods [8]. DRL has frequently been applied to path planning problems in environments with cluttered obstacles and rough terrain. With an application for robots employed for urban search and rescue missions, the authors in [9] proposed a path planning method using DRL with the input of depth images, elevation maps, and orientation to generate navigation actions. In [10], the authors apply DRL to address the issues of path planning in large complex environments where simultaneous localization and mapping (SLAM) and other conventional methods are less effective and have reduced accuracy due to computational constraints. Thus, DRL is used to directly map sensor input data to output control system directives. While conventional control strategies for aerial vehicles are somewhat mature, there is still reliance on human intervention. Deep learning methods are promising approaches for the control of UAVs. The first of these methods involves using a deterministic policy gradient method in path planning for multiple aerial vehicles. This

model can achieve real-time performance in a dynamic environment due to its parameter requirements of only the locations of threat areas, targets, and other UAVs [11]. With applications in search and rescue missions as well as aerial inspections for oil and gas fields, the authors in [12] propose a path planning strategy of UAVs based on a Nokia Snake game strategy. This control policy can be applied to plan more complex paths than comparable previous DRL methods. In [13], path planning for drones using a DQN method which combines deep learning with time-difference learning. The authors used a drone equipped with ultrasonic sensors in a 3D simulation environment. In [14], a similar path planning problem using the DQN method was used to conduct local path planning of unmanned surface vehicles equipped with 360-degree lidar in a 3D simulation environment.

In recent years, mobile edge computing, where computations are done locally at an edge node of a network, has been developed. In [15], a UAV-mounted mobile edge computing system is developed to dynamically take and compute tasks from mobile terminal users. With terminal users starting at random locations with random travel paths, the authors apply DDQN to optimize path plans with time-varying targets. In [16], the authors innovate by applying a multi-agent system to the mobile edge computing network path planning task. Using energy consumption, distance, and computational intensity of each task as parameters, the proposed algorithm is a form of a multi-agent DDPG utilizing a framework of centralized training and decentralized execution. An alternative approach to this problem is shown in [17], where a multi-agent DQL-based algorithm is used. In this study, each UAV is trained with an independent DQN and autonomously executes its actions, only receiving state information from each UAV. In [18], the authors use a mobile edge computing network to tackle the problem of traffic. This study claims that one major issue in traffic and higher fuel consumption in an environment with autonomous vehicles can be solved by having cars travel in a platoon model by reducing changes in speeds and increasing aerodynamic flow. A path can be planned using Q-Learning to optimize speed and fuel consumption.

3. Deep Learning for Computer Vision

Machine learning has always been crucial for environmental perception and computer vision, and their applications such as autonomous vehicles. Deep learning methods have improved on their understanding of sensor data and to some extent, are able to accomplish perception, localization, and mapping. Sensors are divided into two categories: passive sensors such as cameras and active sensors such as lidar, radar, and sonar. Between these two categories, research works on environmental perception generally focus on cameras due to its lower cost and mass

availability. Cameras are further divided into two common types, the first of which is a monocular camera with the ability to extract precise information from images in the form of pixel intensities. To the arrangement of pixel densities can be used to identify properties such as texture and shape. However, monocular cameras have inadequate accuracy in estimating the size and position of an object because of the limited depth data available in a single image. Thus, a stereo camera system is often used to improve depth estimation. Beyond monocular and stereo cameras, there exists other more specialized cameras, such as Time-of-flight cameras, which can accurately estimate depth from the delay between transmitting and receiving infrared range pulses [19]. An integral part of object detection is distance estimation. While conventional methods have been applicable to only a singular type of camera, the authors in [20] have designed a depth perception model that can be generalized to a variety of camera with varying camera geometries.

Weather and light conditions can negatively influence the accuracy of camera sensors, especially at night or in snowy and rainy weather, where calculations such as depth perception become more complex. In [21], the authors designed a method to address detecting vehicles at night with a monocular camera. This was accomplished using support-vector machines to detect headlight and taillights. While this is an improvement, cameras are still not reliable when used as the only sensor, and lidar still provides the most accurate measurement during nighttime. Object detection and identification is necessary for the safe operation of autonomous vehicles, and it is essential to balance the costs of lidar and the reliability of a camera.

To avoid accidents, it is crucial for autonomous ground vehicles to detect domain of the path it takes and any objects along it. Thus, the first step in detecting vehicles, pedestrians, and other obstacles on the road. In [22], the study conducted proposed a road detection model using a CNN network with residual learning and pyramid pooling techniques using monocular vision data. In [23], a method incorporating CNN is proposed to detect various types of speed bumps and solve the problem of the dynamic appearance of speed bumps. Potholes present another problem and the authors in [24] tackle this problem by automatically developing a strategy to detect potholes using information from stereo cameras.

In the operation of vehicles, accidents most commonly occur at road intersections. Therefore, it is critical to obtain information from sensors or connected technologies of nearby road agent positions at intersections. In [25], the authors conducted a study about the effectiveness of various deep neural networks on autonomous vehicles learning road vehicle information from aerial

photographs. This can have applications in a smart city where connected technologies enable the sharing of aerial photography data between road agents. Later in this review, we will discuss using wireless connections between vehicles to share various data that may have applications for road intersection safety.

Beyond detecting obstacles and nearby road agents at intersections, it is also crucial to be able to detect and interpret traffic control signals. Traffic Light Recognition (TLR) techniques are comprised of two steps: detecting traffic signals and estimating the state of the signal. Some key challenges are addressing false positives and computational complexity while under dynamic lighting conditions. One proposed TLR method uses a multi-channel high dynamic range (HDR) camera to capture images with multiple exposure values where deep neural networks are used to estimate traffic light signals. In this study, the network detects traffic lights from bright frame data and classifies the signal using dark frame data [26]. In another study, a TLR method with using a video dataset input with six color spaces was proposed. The authors applied three different networks based on region-based deep learning network models with the best result attained with pairing of RGB color space with a R-CNN model [27].

In object detection and identification, key targets for autonomous vehicle systems to reliably detect are passengers and pedestrians. In one approach, the authors of [28] combined RGB-D stereo vision and thermal cameras. In this study, the authors compared Histogram of Oriented Gradient (HOG) and Convolutional Channel Features (CCF) methods with the results indicating CCF superior to HOG for pedestrian detection. In [29], a vision-based system using monocular camera data was developed to predict passenger movement and to detect other objects on the road. This study used a party affinity fields model to estimate the pose of pedestrians in combination with AI to aid in estimating results for risk assessment. In emergency situations, it can be important for autonomous vehicles to detect nearby vehicle passengers to make more informed decisions. This issue is addressed in [30], which proposes a CNN-based method for detecting nearby cars and passengers within those cars using monocular cameras.

With respect to traffic and road rules, CV-based deep learning techniques can also be applied to detecting vehicle road violations. In [31], YoloV3, a real-time object-detection algorithm for detection and tracking integrates a license plate recognition system with LPRNet and MTCNN. Using this, they can track traffic violations and impolite pedestrians.

With eco-friendliness and fuel costs taking greater importance, research has expanded more on optimizing driving patterns to reduce fuel consumption. Applying

CNN and computer vision, the authors [32] propose an object detection method that increases the fuel efficiency of hybrid vehicles. In a test, they achieved 96.5% fuel economy of the global optimum with dynamic programming, increasing fuel efficiency by up to 8.8% over an existing method. In [33], the authors propose a different approach to reduce fuel consumption. They proposed a DQN-based car-following strategy and a learning-based energy management strategy to achieve a low fuel consumption while maintaining a safe real-time distance. In [34], they tackled fuel efficiency for fuel cell vehicles using a spatiotemporal-vision-based deep neural network. This method improved the accuracy of predicted speed, especially when the traffic was dense.

4. Deep Learning for Sensor Fusion

Autonomous vehicles are typically equipped with multiple sensors such as Global Positioning System (GPS), Inertia Measurement Unit (IMU), cameras, radar, ultrasound, as well as light detection and ranging (Lidar). While each sensor provides key data, they each have their limitations. However, by combining the strengths of each sensor, together, they can provide autonomous vehicles with superior information to render decisions for control, path planning, and fault management.

Traditionally, sensor data was fused using the Kalman filter algorithm. However, deep learning has become an increasingly more popular method of combining sensor data due to its effectiveness and relative simplicity. One key application in sensor fusion is overcoming the shortfall of cameras. While cameras are used to capture important data such as object size and shape, it lacks the ability to accurately measure key values such as distance and velocity, that sensors like radars and lidars can compensate for. In [35], the authors explore the application of a CNN network in the fusion of camera raw pixels and lidar depth values to generate a feature vector. This study employed a novel temporal-history based attention mechanism which proved to be resilient to errors in sensor signals. To address the lack of clarity in camera data in severe weather conditions and at night, the authors in [36] conducted a study fusing camera and radar data with a model based on RetinaNet. In [37], the authors propose a vehicle detection model based on the fusion of lidar and camera data. In this model, possible vehicle locations are obtained from lidar point cloud data and a CNN network is used to refine and detect vehicle locations. Beyond detecting vehicles, lidar camera fusion was applied in [38] for high accuracy road detection even in difficult road conditions such as in extreme weather. In sensor fusion and deep learning for segmentation tasks, the quality of training data plays a vital role in these studies' success. In [39], a new collaborative method of collective multi-sensor training data and automatically generating accurate labels is proposed.

In [40], the authors propose a deep convolutional network for vehicle detection with three modalities: color image, lidar reflectance map, and lidar depth map. This model is able to produce a more accurate prediction using joint learning because joint learning generates more data for safely operating vehicles compared to learning environmental data and driving policy independently. In [41], the authors propose a dual-modal DNN to create an improved detection model in severe environmental conditions such as rain, snow, and night-time where features can be blurry. This network fuses color and infrared images and achieves improved performance for low-observable targets. In [42], the authors proposed an Integrated Multimodality Fusion Deep Neural Network, which processed each modality independently before being processed together in further networks, which creates modularity and increased flexibility, thus providing a greater ability for generalization.

In [43], a cooperative perception system was proposed to expand the scope of vehicle perception and eliminate blind spots by integrating data from multiple vehicle sources using both graphic and semantic alignment. In [44], the authors introduce a cooperative visual-free sensor fusion technique combining vehicle detector, remote microwave sensors, and toll collection data to predict fine-grain flow traffic. In [45], the authors presented a model integrating various smartphone sensor data to detect real time vehicle maneuvers. This system uses GPS, gyroscope, accelerometer, and magnetometer to detect turns and other movements to be communicated to enhance safety. In [46], a smartphone sensor-based method is proposed to detect human activity recognition. In [47], the authors propose Gated Recurrent Fusion Units (GRFU) which have gating mechanisms similar to those in LSTM to create a new joint learning mechanism, which proved to have an improved error rate. In [48], a novel end-to-end driving DNN is proposed. This proposed network that incorporates scene understanding, which understands spatial, functional, and semantic relationships and uses lidar and camera.

5. Deep Learning for Data Security

With the rapid development of deep learning, increasing amounts of user data are required to train and models. In some systems, the privacy of user data can be a concern. In addition, it is also essential for systems to accurately detect attacks with intentions to corrupt the model. Current data security methods will be discussed for centralized and federated learning models. Model training requires a large number of data samples. In addition to the information required to train the models, these models also inadvertently include auxiliary that malicious actors can use to infer information about the individuals such as location and trajectory. In [49], the

authors use a GAN to generate privacy-preserving data that still retain its usefulness in training.

In recent times, federated learning has been introduced, where a model is downloaded and trained locally with private data before being uploaded, and model aggregation occurs. It became popular due to offloading some computational power to individual devices, and privacy concerns as users don't have to share their private data [50] [51]. In federated learning, two problems being tackled are detecting bad actors that maliciously upload faulty data to distort the accuracy of the model and preserving privacy before model aggregation. In [52], the authors use a blockchain method for UAVs, which replaces the central curator to combine the learned parameters in the model. In addition, they also use a local differential privacy algorithm to mask personal data. In [53], the authors propose a different method to tackle this problem. They introduce a privacy-preserving model aggregation scheme named FedLoc by using homomorphic encryption and a bounded Laplace mechanism. In [54], the authors introduced CLONE, a collaborative edge learning framework using federated learning techniques. This can be applied to a multitask tracking problem or in EV battery fault detection. In [55], the authors tackle the problem of sharing data for model training for data collected by independent companies/vehicles by using federated learning. A blockchain structure can also be used to enhance privacy. In [56], a hybrid blockchain architecture is proposed to be used in federated learning for vehicular applications. In [57], the authors also use blockchain to facilitate communication in a mobile edge computing application, however, with the innovation of applying a hybrid model intrusion detection system to the data. Their proposed framework has shown reduced false alarm rate and a high accuracy of 99%.

In addition to data-privacy, it is also essential to detect and prevent malicious attacks. These attacks can corrupt the model during training or operation by providing malicious input. One example of an attack using adversarial GPS trajectories against crowdsourced navigation systems is Cybil attacks. In [58], a Bayesian deep learning method was used to identify Sybil attacks. In [59], the authors discuss the development of poisoning and evasion attacks and review recent methods used to address them. The methods used against poisoning attacks include ensemble learning methods to increase resistance against variance and comparing classifiers for each training data set. Adversarial training is the main method used against evasion attacks which works by introducing both legalized and adversarial samples to train the model on detecting adversarial samples. In [60], the authors proposed a multi-strength adversarial

training technique which combines adversarial training examples with different adversarial strengths.

6. Deep Learning for Data Security

As the field of autonomous vehicles develops, these vehicles require more sensors and actuators and become increasingly reliant on them. However, the proliferation of sensors and actuators in vehicles which heavily rely on their accuracy also increases the occurrence of a vehicle fault. To ensure the safe operation of autonomous vehicles, fault detection methods need to be able to be more reliable. Conventional fault detection methods can be classified into three categories: model based, signal based and knowledge based. In recent years, DNN-based fault detection has become popularized as it can achieve faster and more accurate results. In addition, deep learning can accurately map complex patterns and signals to accurately assess the health condition of the components, leading to its prospects of becoming a promising research field. In recent years, CNN, DAE and DBN have all been applied in fault diagnosis tasks.

Planetary gearboxes are commonly used in mechanical systems such as transmission systems present in ICE and some electric vehicles. Using a deep residual network with vibration signals as input, the authors in [61] created a model integrating the network with domain knowledge to identify faults and the condition of planetary gearboxes. An alternate approach is taken to detect faults in a planetary gearbox in [62] where a model is formed with transfer learning combined with a deep autoencoder with wavelet activation functions. The resulting model is effective under variable conditions such as changing speed and location.

In-vehicle gateways are modules that connect to and receives data from various sensors in a vehicle. Several studies have been conducted to utilize this information for fault diagnosis. In [63], the authors combined a LSTM network with an in-vehicle gateway to diagnose faults based on fault data by using comparisons with previous sensor data. In [64], an IoT Gateway combined with deep learning is used to diagnose the faults of the sensors. This self-diagnosis information can be used for self-repairing. The inputs of the deep learning network are sensor signals, and the outputs are the condition of parts, of which the driver will be informed through diagnostic results. One innovation of the work is that data collected by a gateway are from different protocols such as CAN, FlexRay, and MOST.

Deep learning can be used to detect faults in many components of the vehicle. In [65], electrical signals are analyzed to detect the fault in the spacecraft's electronic load system. A deep autoencoder-based clustering system and a CNN-based classification method is used to process

high-dimensional signal data to detect and classify faults. In [66] a combined CNN and LSTM model is used to detect the pre-ignition of engine control signals using in-vehicle data. In [67], the training data are generated from the UAV system model. One dimensional signal is then extended to time-frequency domains using wavelet transform. Then, deep learning is performed on the image data to find different sensor or actuator faults.

Electric vehicles have microgrids that encompasses energy storage systems, electric motor, motor drive and protective components. With complete reliance on microgrids, detecting faults in the micro-grid of an electric vehicle is crucial to the safety of the vehicle. In [68], a CNN-based method was studied to detects false battery data in battery energy storage systems, with application to those in electric vehicles. In [69], the authors used a CNN-based model to solve the fault classification problem for micro-grids. This method uses voltage and other measures from inverters, converter, capacitors to create a fault detection method to reinforce traditional methods. It is especially important to reliably detect faults in unmanned autonomous vehicles due to the higher cost of failure. In [70], the authors presented a strategy for diagnosing faults in actuators of multi-rotor UAVs based on a hybrid LSTM-CNN model. One common constraint in UAVs is the challenge of running complicated fault detection methods in real-time, which have size, weight, and power consumption constraints. To tackle this problem, [71] proposes an LSTM-based fault detection model acceleration engine. In [72], the authors use LSTM to estimate the estimated wheel angle and an improved sequential probability ratio test to detect a fault in vehicle wheel angle signals.

In the future, connected and automated vehicles communicating in real-time are expected to improve road safety. In [73], the problem of anomalous sensor readings is tackled with a CNN-based sensor anomaly detection and identification method. In [74], the authors address detecting malicious actors in connected and automated vehicles during cruise control. Using a multi-agent DRL method, they can cooperatively and accurately detect attackers.

7. Deep Learning for Control Algorithms

Autonomous vehicle control models consist of two parts: perception planning and control paradigm. Traditionally, control systems methods relied on mathematical models including optimal control, robust control, PID control, and adaptive control. While conventional models are more easily interpreted and have a theoretical foundation, they performance worse for more complex data or larger data sets. In comparison, deep learning control approaches are model-free, data-driven which indicates its applicability to both discrete

and continuous systems. Due to these differences, deep learning can't be directly applied in conventional models. Instead, contemporary deep learning solutions for autonomous driving employs end-to-end controllers to improve or provide state estimation.

Recently, deep learning has been the chosen method for the state estimation of different controllers [75] and enhancing state estimation quality [76]. In control systems, the dynamic model that identifies the uncertainties and hidden states form the foundation. However, the conventional system identification method does not easily identify model parameters. Helicopters require complex control systems due to having complex interactions with external forces and internal controls. In [77], the authors propose a deep convolutional neural network-based dynamic identifier for a controller. This scheme can accurately identify the helicopter's dynamic behavior, maintain stability even in untrained maneuvers. In [75], the authors present a flight control method for autonomous helicopters. A deep learning network is used as the identifier for an adaptive control scheme. The complete model includes a first principle-based dynamic model and a CNN based model for modelling hidden states and uncertainties where all parameters and weights are trained with real flight data. In [76], a deep learning network with the drop out technique is used to improve the performance of the attitude state estimation by the Kalman filter. This network is trained to model the measurement noises, which in turn is used to filter out the noise and enhance the quality of the Kalman filter. Deep learning is used to compensate for delays and measurement noises. The information extracted by a modular deep recurrent neural network is combined with sensory readings before being fed into the Kalman filter for state prediction and update. This deep learning network can detect the hidden states, which are normally difficult to be measured by sensors. In [78], a CNN and LSTM-based observer is presented. First, LSTM processes videos and adds a temporal dimension to the cost map. Then a particle filter is used for state estimation. Lastly, the cost map generated by the deep learning network is combined with readings from IMU and wheel speed encoders to predicate and update the states for model predictive control.

Deep learning can also replace conventional discrete controllers such as PID controllers and instead use a deep learning model to generate output control actions which can be either discrete or continuous [79]. Another application combines the learning with the conventional controller to form a hierarchical or better control system. Oceans and other large bodies of water have complex environments and as a result, existing autonomous underwater vehicles relying on conventional controllers have imposed paths and pre-planned tasks. In [80], the

authors present a model based on deep interactive reinforcement learning to facilitate path following. This model uses a dual reward method by which the network can learn from both human and environmental feedback simultaneously. In [81], the authors investigated a low-level DRL-based control strategy for underwater vehicles. A deep reinforcement learning network is introduced with sensory signals serving as the sole input of the network without prior knowledge of vehicle dynamics. In [82], a deep learning tracking control algorithm is applied to improve the accuracy and adaptability of driving trajectory tracking. In [83], the deep learning network is used to analyze the environment to predict lateral and longitudinal control. In this network, two separate models are used for vehicle speed and steering, where the inputs are road images, and the outputs are the speed and steering. In [84], the authors propose to use a CNN network as an end-to-end controller for driving, while two other CNN-based deep networks generate both the feature map and error map to help the controller better understand the scene. An attention model is used to identify the regions that affect the output most. In [85], the authors have explored the use of reinforcement learning for high-level decision-making in the context of a robotic game. In this hierarchy structure, the high-level DL is combined with low-level controllers to deliver a better control performance. The design of the controller with multiple levels can accommodate the challenges in the game, such as action delay. In [86], DRL was applied in intelligent control with a self-organizing control system based on DDPG. Using simulations, the reference signal self-organizing control system was able to stabilize an inverted pendulum using a rotor. Autonomous vehicle control systems often have trouble with hard to predict actions such as cut-in maneuvers. In [87], a control strategy is developed using a two-part training strategy of experience screening followed by policy learning to increase performance in uncertain scenarios.

Deep learning can also be applied to larger-scale control algorithms such as wide-range traffic control and power grids. Inefficient traffic control results in more stop-and-go traffic, increasing wait times and fuel consumption. In [88], RL is applied to adaptive traffic signal control. This is achieved by using multi-agent RL that distributes global control to each local agent with a new decentralized multi-agent RL algorithm that has improved observability and reduced the learning difficulty of each agent. In [89], the authors present a more centralized method of traffic control. Using information about vehicles near a particular intersection, including speed and location as input, they train a model that controls the duration of traffic signal timings to reduce vehicle wait times and trip lengths.

In the electrical grid, conventional control systems are not well optimized and do not adapt to changes well. Although with high difficulty and complexity, AI has been applied in power grid control, which will be an important research front for future autonomous vehicles. A novel two-timescale voltage control system is presented in [90]. Using a feed-forward DQN with physics driven optimization, a two-timescale approach was able to minimize voltage deviations and optimize power flow. [91] developed a DRL based autonomous voltage control for power grid operations. They proposed to use both DQN and DDPG to create autonomous voltage control strategies to better adapt to unknown system changes.

8. Deep Learning for Communication and Networking

Autonomous vehicles can play an important role in communication and networking. In communications, there is often an inefficient use of allocated bandwidth. In [92], a deep learning-based channel and carrier frequency offset equalization technique is proposed to improve bandwidth efficiency. In emergencies, it is common for base stations and power sources to be destroyed, restricting access to communication networks when needed. As UAVs evolved, they have been purposed to assist in emergency communication networks as a base station. A fundamental problem being solved is the optimization of resources, while UAVs are both limited by their coverage area and energy consumption. In [93], the authors propose a novel DRL method to optimize energy consumption. In [94], the authors approach this problem with a DRL based on Q-Learning and CNN to optimize macro base power allocation and UAV service selection. Recently, vehicular ad hoc networks have been used in autonomous vehicles for vehicles to improve safety and comfort [95]. However, vehicles often have a restrictive communication range. To address this issue, communication between vehicles and other types of devices is used. In [96], a deep learning-based algorithm is proposed for transmission mode selection and resource allocation for cellular vehicle-to-everything communication. In [97], the authors propose using UAVs as relays in these networks. Using DISCOUNT, a DRL framework, an organized and intelligent group of UAVs are optimized to increase connectivity and minimize energy consumption. A common issue in cellular-connected UAVs is interference between each relay. In [98], the authors propose a deep learning algorithm based on echo state network architecture to create an interference-aware path planning strategy.

Beyond UAVs, which have range and power constraints, satellites have merit as a solution to improve vehicle-to-vehicle communication on the ground, especially in depopulated areas. However, satellites have

limited computing and communication resources. To tackle this issue, the authors in [99] used deep learning with the Lagrange multiplier method to improve joint task offloading and resource allocation. Maritime communications are often bottlenecked by the immense data volumes required. In [100], the authors propose a transmission scheduling strategy based using a deep-Q network. This strategy optimizes the network routing.

9. Discussion

Autonomous vehicles will significantly impact the future of the automobile industry. Fully autonomous vehicles can improve safety and travel comfort as smooth and consistent driving will reduce congestion. They have various benefits and advantages as follows:

- **More independent mobility.** Better access for people who cannot drive, including the elderly and young people.
- **Facilitating car sharing and ride sharing.** An increase in car-sharing opportunities will reduce the need to own a car and associated costs.
- **More efficient vehicle traffic.** Reduces congestion and roadway costs due to more consistent behavior on the road.
- **Fewer cars on the road.** Reduce drivers' stress and increase productivity. While traveling, motorists can rest, play, and work.
- **Greater safety.** Several opinions say that autonomous vehicles will eliminate 95% of all human error. Thus, autonomous vehicles reduce crash risks and high-risk driving since they are not impacted by human emotions or bias while driving.

Because deep learning is able to learn or discover very complex high-dimensional nonlinear patterns or relationships from a large amount of training samples, deep learning has been successfully applied in seven research areas in autonomous vehicles. However, we still need to further investigate new techniques to overcome some limitations associated with most deep learning algorithms, including easily getting trapped in a local minimum, slow convergence during training especially for deep reinforcement learning, requiring a large set of training samples or overfitting for small training datasets.

- **Future directions.** We still need to overcome serious major challenges before fully autonomous vehicles are ready for public use. In the near future, autonomous vehicles may be limited to some specific scenarios, such as narrower situations and clearer weather.
- **Employ deep learning to develop new sensor fusion techniques for autonomous cars with different certain road conditions.** Current techniques mainly focus on narrower good road conditions. They cannot handle more complicated road conditions such as

changing road conditions, night conditions, unlit roads at night, unmarked roads, even unpaved roads, unexpected conditions such as animals suddenly crossing roads, or combinations of the above situations. These complicated conditions require novel sensor fusion algorithms and probably require to develop new perception devices. Deep learning is more suitable for these very complex scenarios than conventional methods. We need to investigate novel deep learning-based fusion techniques for more complicated road conditions.

- **Developing new sensor devices and novel algorithms for challenging bad weather conditions.** Current sensing techniques work relatively well with clearer weather. However, like our eyes, vehicle sensors do not work as well in bad weather conditions such as rain, fog, snow, and ice, which not only reduce the visibility but also cause dangerous road conditions. Many autonomous cars employ Lidar technology using lasers. However, snow and ice absorb laser light rather than reflecting it, making these vehicles blind in inclement weather conditions and making it difficult for Lidar to accurately identify obstacles. Therefore, these bad conditions make autonomous cars harder to navigate and cause potential safety issues for other drivers and pedestrians alike. They also make conventional processing algorithms more challenging to obtain accurate perception from low quality sensor data in bad weather conditions. We need to develop novel intelligent sensors to obtain accurate perception and corresponding processing techniques for these bad weather conditions. Deep learning techniques have the potential to deal with these more challenging scenarios.
- **Investigate novel deep reinforcement learning techniques to achieve multiple objectives in the design of autonomous vehicles.** The design of fully autonomous vehicles often involves multiple, even conflicting, objectives or criteria. For example, car connectivity using vehicle-to-vehicle communication (V2V) communications with surrounding vehicles makes many tasks, such as merging easier, but securing the communication system could be extremely difficult. Thus, it also increases cybersecurity risks since there are more ways to get into them and disrupt what they're doing as vehicles get more connected. Therefore, we need to investigate new techniques and strategies in order balance the benefits of using V2V communications and cybersecurity risks. We believe DRL is one suitable technique to make the optimal decision for these complicated situations.
- **Early fault diagnosis and prognosis of autonomous vehicles.** Since the occurrence of faults increases due

to the significant increase of sensors and components in autonomous vehicles, early fault diagnosis and prognosis are more important and more challenging to ensure the vehicle safety. We need to investigate new real-time early fault diagnosis methods for more complicated scenarios considering not only the components and sensors associated with the vehicle itself but also the faults or disruption of V2V communications and the reliability of some global information from networking infrastructure such as real-time road conditions. Early fault diagnosis under relatively normal driving conditions is especially important to discover potential issues at an earlier stage, provide early warning or alert, and take actions such as timely checkup and maintenance to prevent getting stuck in the middle of remote roads or even catastrophic accidents. Since many faults at early stage often involve small or subtle changes, it is more difficult to accurately detect these small anomalies, especially under normal driving operations due to the lack of special expensive instruments in car dealers. However, this is a very important research topic for vehicle safety and timely maintenance.

- **Developing novel low-cost techniques to make autonomous vehicles more approachable and affordable.** Autonomous cars are currently very costly, which makes investing in them difficult for most people. Even current techniques can achieve the required performance criteria under good road and weather conditions, we still need to investigate novel effective and efficient algorithms for more complicated scenarios where they require more advanced sensors and more computation power. However, it is a time-critical mission for autonomous vehicles with rapid response time. We believe deep learning will play an important role in developing novel intelligent technologies for environment perception, planning and navigation on challenging roads while keeping low cost.

10. Conclusion

In this article, we reviewed recent developments in the area of deep learning applications in autonomous vehicles. These seven active research areas are control, computer vision, sensor fusion, path planning, fault diagnosis, communication and networking, and data security. Several types of deep neural networks were reviewed and compared, in which deep learning were successfully applied to various design and operation aspects of autonomous vehicles. Deep learning has taken a significant role in the development of technologies for autonomous vehicles. It will continue to play an important role in the future development and refinement of these technologies.

Table 1: Path Planning Solutions

Research paper	Application(s)	Deep learning method	Network	Comments
[3]	Unmanned Vehicles	ReLU	CNN	Camera map steering angle
[4]	Unmanned Aerial Vehicles	-	CNN	Real-Time
[5]	Unmanned Vehicles	Imitation Learning	CNN	3D
[6]	Unmanned Vehicles	LSTM	LSTM	Feature Extraction
[7]	Unmanned Vehicles	LSTM	LSTM	Pedestrian Detection
[8]	Unmanned Vehicles	DRL	DDQN	Mixed environment with manual vehicles
[9]	Unmanned Vehicles	DRL	DDPG	Unknown Environment
[10]	Unmanned Vehicles	DRL	DQN	3D, Autonomous, Real-Time
[11]	Unmanned Vehicles	DRL	MADDPG	Multi-Agent, Dynamic
[12]	Unmanned Aerial Vehicles	DRL	A3C Model	
[13]	Unmanned Aerial Vehicles	DRL	DQN	Ultrasonic Sensor, 3D , Obstacle Avoidance
[14]	Unmanned Surface Vehicles	DRL	DQN	High Degrees of Freedom
[15]	Unmanned Aerial Vehicles	DRL	DQN	Mobile-Edge Computing
[16]	Multi-UAV (mobile communications system)	DRL	DDPG	Multi-Agent, 3D, Real-Time, Mobile-Edge Computing
[17]	Multi-UAV (wireless communications system)	DRL	DQN	Mobile Edge Computing
[18]	Multi-Vehicle optimization	DRL	DQN	Mobile-Edge computing

Table 2: Fault Diagnosis Solution Comparisons

Research paper	Application(s)	Deep learning method	Network	Comments
[61]	Fault Detection Gearbox	CNN	DRN	Vibratory Signals
[62]	Fault Detection Gearbox	Autoencoder		Vibratory Signals
[63]	Part-Diagnosis UAV	CNN	CNN, LSTM	In Vehicle,
[64]	Fault Detection UAV	-	NN	Vehicle Data, Sensors
[65]	Spacecraft Electronic Systems	CNN	CNN	High Dimensional Electric Data
[66]	Fault Detection Parts and Pre-Ignition	CNN	CNN, LSTM	Vehicle Data
[67]	Fault Detection and Identification UAV	LQR	DNN	CIFTA Graphs
[68]	False Battery Data Detection	CNN	CNN	Battery Health Sensor, Charging Sensor
[69]	Fault Detection UEV Microgrid	CNN	DNN, CNN	Converter, Inverter Data
[70]	Fault Detection UAV	CNN	CNN, LSTM	Actuator, Flight Data
[71]	Fault Detection UAV	-	LSTM	Real-Time
[72]	Fault Detection Signal	-	LSTM	Wheel Angle Data
[73]	Fault Detection UAV Sensor	CNN	CNN	Connected Vehicles, Real-Time
[74]	Attack Detection UAV	MDP, Gradient Descent	DRL	Connected Vehicles, Multi-Agent

Acknowledgment

We acknowledge the financial support of the Natural Sciences and Engineering Research Council of Canada (NSERC).

References

[1] J. Ren, H. Gaber and S. S. Al Jabar, "Applying Deep Learning to Autonomous Vehicles: A Survey," 2021 4th International Conference on Artificial Intelligence and Big Data (ICAIBD), 2021, pp. 247-252, doi: 10.1109/ICAIBD51990.2021.9458968.

[2] C. Hodges, S. An, H. Rahmani, & M. Bennamoun. Deep Learning for Driverless Vehicles. In V. Balas, S. Roy, D. Sharma, & P. Samui

(Eds.), *Handbook of Deep Learning Applications* pp. 83-99. (Smart Innovation, Systems and Technologies; Vol. 136). Springer, 2019

[3] V. Rausch et al, "Learning a Deep Neural Net Policy for End-to-End Control of Autonomous Vehicles" *American Control Conference*, Seattle, May 2017.

[4] S. Jung et al, "Perception, Guidance, and Navigation for Indoor Autonomous Drone Racing Using Deep Learning" *IEEE Robotics and Automation Letters*, 2018.

[5] K. Wu et al, "TDPP-Net: Achieving Three-Dimensional Path Planning via a Deep Neural Network Architecture" *Neurocomputing*, vol. 357, pp. 151-162, 2019.

[6] Z. Bai et al, "Deep Learning Based Motion Planning for Autonomous Vehicle Using Spatiotemporal LSTM Network" *Chinese Automation Congress*, 2018.

- [7] K. Saleh, M. Hossny and S. Nahavandi, "Intent Prediction of Pedestrians via Motion Trajectories using Stacked Recurrent Neural Networks" *IEEE Transaction on Intelligent Vehicles*, vol. 3, no. 4, 2018.
- [8] K. Makantasis et al, "Deep Reinforcement -Learning-Based Driving Policy for Autonomous Road Vehicles" *IET Intelligent Transport Systems*, 2020.
- [9] K. Zhang et al, "Robot Navigation of Environments with Unknown Rough Terrain Using Deep Reinforcement Learning" *Proc. IEE Int. Symp. Sat. Secur. Rescue Robot.*, 2018.
- [10] C. Wang et al, "Autonomous Navigation of UAVs in Large-Scale Complex Environment: A Deep Reinforcement Learning Approach" *IEEE Transactions on Vehicle Technology*, 2019.
- [11] H. Qie et al, "Joint Optimization of Multi-UAV Target Assignment and Path Planning Based on Multi-Agent Reinforcement Learning," *IEEE Access*, vol. 7, 2019.
- [12] C. Wu et al, "UAV Autonomous Target Search Based on Deep Reinforcement Learning in Complex Disaster Scene," *IEEE Access*, vol. 7, 2019.
- [13] G. -T. Tu and J. -G. Juang, "Path Planning and Obstacle Avoidance Based on Reinforcement Learning for UAV Application," 2021 International Conference on System Science and Engineering (ICSSE), 2021, pp. 352-355, doi: 10.1109/ICSSE52999.2021.9537945.
- [14] H. Zhai, W. Wang, W. Zhang and Q. Li, "Path Planning Algorithms for USVs via Deep Reinforcement Learning," 2021 China Automation Congress (CAC), 2021, pp. 4281-4286, doi: 10.1109/CAC53003.2021.9728038.
- [15] Q. Liu, L. Shi, L. Sun, J. Li, M. Ding and F. Shu, "Path Planning for UAV-Mounted Mobile Edge Computing With Deep Reinforcement Learning," in *IEEE Transactions on Vehicular Technology*, vol. 69, no. 5, pp. 5723-5728, May 2020, doi: 10.1109/TVT.2020.2982508.
- [16] L. Wang, K. Wang, C. Pan, W. Xu, N. Aslam and L. Hanzo, "Multi-Agent Deep Reinforcement Learning-Based Trajectory Planning for Multi-UAV Assisted Mobile Edge Computing," in *IEEE Transactions on Cognitive Communications and Networking*, vol. 7, no. 1, pp. 73-84, March 2021, doi: 10.1109/TCCN.2020.3027695.
- [17] J. Tang, J. Song, J. Ou, J. Luo, X. Zhang and K. -K. Wong, "Minimum Throughput Maximization for Multi-UAV Enabled WPCN: A Deep Reinforcement Learning Method," in *IEEE Access*, vol. 8, pp. 9124-9132, 2020, doi: 10.1109/ACCESS.2020.2964042.
- [18] C. Chen, J. Jiang, N. Lv and S. Li, "An Intelligent Path Planning Scheme of Autonomous Vehicles Platoon Using Deep Reinforcement Learning on Network Edge," in *IEEE Access*, vol. 8, pp. 99059-99069, 2020, doi: 10.1109/ACCESS.2020.2998015.
- [19] E. Arnold, O.Y. Al-Jarrah, M. Dianati, S. Fallah, D. Oxtoby, and A. Mouzakitis. "A Survey on 3D Object Detection Methods for Autonomous Driving Applications," *IEEE Trans. Intell. Transp. Syst.*, vol. 20, no. 10, Oct. 2019.
- [20] V. Ravi Kumar et al., "SVDistNet: Self-Supervised Near-Field Distance Estimation on Surround View Fisheye Cameras," in *IEEE Transactions on Intelligent Transportation Systems*, vol. 23, no. 8, pp. 10252-10261, Aug. 2022, doi: 10.1109/TITS.2021.3088950.
- [21] N. Kosaka and G. Ohashi, "Vision-based night-time vehicle detection using CenSurE and SVM," *IEEE Trans. Intell. Transp. Syst.*, vol. 16, no. 5, pp. 2599-2608, 2015.
- [22] D. A. Yudina, A. Skrynnik, A. Krishtopika, I. Belkina, and A. I. Panova, "Object Detection with Deep Neural Networks for Reinforcement Learning in the Task of Autonomous Vehicles Path Planning at the Intersection," *Optical Memory and Neural Networks (Information Optics)*, vol. 28, no. 4, p 283-295, 2019.
- [23] J. Wang, and L. Zhou "Traffic Light Recognition With High Dynamic Range Imaging and Deep Learning," *IEEE Trans. Intell. Transp. Syst.*, vol. 20, no. 4, Apr. 2019.
- [24] H. Kim, J. H. Park, and H. Y. Jung, "An Efficient Color Space for Deep-Learning Based Traffic Light Recognition," *Journal of Advanced Transportation*, Dec. 2018.
- [25] Z. Chen, and X. Huang, "Pedestrian Detection for Autonomous Vehicle Using Multi-Spectral Cameras," *IEEE Transactions on Intelligent Vehicles*, vol. 4, No. 2, Jun. 2019.
- [26] A. Amanatiadis, E. Karakasis, L. Bampis, S. Ploumpis, and A. Gasteratos, "ViPED: On-road vehicle passenger detection for autonomous vehicles," *Robotics and Autonomous Systems*, Dec. 2018.
- [27] Y. Li et al, "A Deep Learning-Based Hybrid Framework for Object Detection and Recognition in Autonomous Driving," in *IEEE Access*, vol. 8, pp. 194228-194239, 2020, doi: 10.1109/ACCESS.2020.3033289.
- [28] X. Liu, and Z. Deng, "Segmentation of Drivable Road Using Deep Fully Convolutional Residual Network with Pyramid Pooling," *Cognitive Computation*, Nov. 2017.
- [29] D. K. Dewangan and S. P. Sahu, "Deep Learning-Based Speed Bump Detection Model for Intelligent Vehicle System Using Raspberry Pi," in *IEEE Sensors Journal*, vol. 21, no. 3, pp. 3570-3578, 1 Feb.1, 2021, doi: 10.1109/JSEN.2020.3027097.
- [30] A. Dhiman and R. Klette, "Pothole Detection Using Computer Vision and Learning," in *IEEE Transactions on Intelligent Transportation Systems*, vol. 21, no. 8, pp. 3536-3550, Aug. 2020, doi: 10.1109/TITS.2019.2931297.
- [31] R. Xu, Y. Chen, X. Chen and S. Chen, "Deep learning based vehicle violation detection system," 2021 6th International Conference on Intelligent Computing and Signal Processing (ICSP), 2021, pp. 796-799, doi: 10.1109/ICSP51882.2021.9408935.
- [32] Y. Wang, H. Tan, Y. Wu and J. Peng, "Hybrid Electric Vehicle Energy Management With Computer Vision and Deep Reinforcement Learning," in *IEEE Transactions on Industrial Informatics*, vol. 17, no. 6, pp. 3857-3868, June 2021, doi: 10.1109/TII.2020.3015748.
- [33] X. Tang, J. Chen, K. Yang, M. Toyoda, T. Liu and X. Hu, "Visual Detection and Deep Reinforcement Learning-Based Car Following and Energy Management for Hybrid Electric Vehicles," in *IEEE Transactions on Transportation Electrification*, vol. 8, no. 2, pp. 2501-2515, June 2022, doi: 10.1109/TTE.2022.3141780.
- [34] Y. Zhang et al., "Improved Short-Term Speed Prediction Using Spatiotemporal-Vision-Based Deep Neural Network for Intelligent Fuel Cell Vehicles," in *IEEE Transactions on Industrial Informatics*, vol. 17, no. 9, pp. 6004-6013, Sept. 2021, doi: 10.1109/TII.2020.3033980.
- [35] H. Unlu et al, "Sliding-Window Temporal Attention Based Deep Learning System for Robust Sensor Modality Fusion for UGV Navigation," *IEEE Robotics and Automation Letters*, vol. 4, no. 4, 2019.
- [36] F. Nobis et al, "A Deep Learning-Based Radar and Camera Sensor Fusion Architectur for Object Detection," *Sensor Data Fusion: Trends, Solutions, Applications*, 2019.
- [37] X. Du et al, "Car Detection for Autonomous Vehicle: LIDAR and Vision Fusion Approach through Deep Learning Framework," *International Conference on Intelligent Robots and Systems*, 2017.
- [38] C. Luca et al, "Lidar-Camera Fusion for Road Detection Using Fully Convolutional Neural Networks," *Robotics and Autonomous Systems*, vol. 111, 2019.
- [39] H. Liu and D. M. Blough, "MultiVTrain: Collaborative Multi-View Active Learning for Segmentation in Connected Vehicles," 2021 IEEE 18th International Conference on Mobile Ad Hoc and Smart Systems (MASS), 2021, pp. 428-436, doi: 10.1109/MASS52906.2021.00060.
- [40] A. Alireza et al, "Multimodal Vehicle Detection: Fusing 3D-LIDAR and Color Camera Data," *Pattern Recognition Letters*, vol. 115, 2018.
- [41] K. Geng et al, "Low-Observable Targets Detection for Autonomous Vehicles Based on Dual-Modal Sensor Fusion with Deep Learning Approach," *Proceedings of the Institution of Mechanical Engineers, Part D: Journal of Automobile Engineering*, 2019.
- [42] J. Nie, J. Yan, H. Yin, L. Ren and Q. Meng, "A Multimodality Fusion Deep Neural Network and Safety Test Strategy for Intelligent Vehicles," in *IEEE Transactions on Intelligent Vehicles*, vol. 6, no. 2, pp. 310-322, June 2021, doi: 10.1109/TIV.2020.3027319.
- [43] Z. Xiao et al, "Multimedia Fusion at Semantic Level in Vehicle Cooperative Perception," *IEEE International Conference on Multimedia & Expo Workshops*, 2018.
- [44] P. Wang, W. Hao and Y. Jin, "Fine-Grained Traffic Flow Prediction of Various Vehicle Types via Fusion of Multisource Data and Deep

- Learning Approaches," in *IEEE Transactions on Intelligent Transportation Systems*, vol. 22, no. 11, pp. 6921-6930, Nov. 2021, doi: 10.1109/TITS.2020.2997412.
- [45] P. Li, M. Abdel-Aty, Q. Cai and Z. Islam, "A Deep Learning Approach to Detect Real-Time Vehicle Maneuvers Based on Smartphone Sensors," in *IEEE Transactions on Intelligent Transportation Systems*, vol. 23, no. 4, pp. 3148-3157, April 2022, doi: 10.1109/TITS.2020.3032055.
- [46] Z. Chen, C. Jiang, S. Xiang, J. Ding, M. Wu and X. Li, "Smartphone Sensor-Based Human Activity Recognition Using Feature Fusion and Maximum Full a Posteriori," in *IEEE Transactions on Instrumentation and Measurement*, vol. 69, no. 7, pp. 3992-4001, July 2020, doi: 10.1109/TIM.2019.2945467.
- [47] A. Narayanan, A. Siravuru and B. Dariush, "Gated Recurrent Fusion to Learn Driving Behavior from Temporal Multimodal Data," *IEEE Robotics and Automation Letters*, vol. 5, no. 2, 2020.
- [48] Z. Huang, C. Lv, Y. Xing and J. Wu, "Multi-Modal Sensor Fusion-Based Deep Neural Network for End-to-End Autonomous Driving With Scene Understanding," in *IEEE Sensors Journal*, vol. 21, no. 10, pp. 11781-11790, 15 May 2021, doi: 10.1109/JSEN.2020.3003121.
- [49] Z. Xiong, Z. Cai, Q. Han, A. Alrawaiis and W. Li, "ADGAN: Protect Your Location Privacy in Camera Data of Auto-Driving Vehicles," in *IEEE Transactions on Industrial Informatics*, vol. 17, no. 9, pp. 6200-6210, Sept. 2021, doi: 10.1109/TII.2020.3032352.
- [50] M. Yang, Y. He and J. Qiao, "Federated Learning-Based Privacy-Preserving and Security: Survey," 2021 Computing, Communications and IoT Applications (ComComAp), 2021, pp. 312-317, doi: 10.1109/ComComAp53641.2021.9653016.
- [51] M. A. Ferrag, O. Friha, L. Maglaras, H. Janicke and L. Shu, "Federated Deep Learning for Cyber Security in the Internet of Things: Concepts, Applications, and Experimental Analysis," in *IEEE Access*, vol. 9, pp. 138509-138542, 2021, doi: 10.1109/ACCESS.2021.3118642.
- [52] Y. Wang, Z. Su, N. Zhang and A. Benslimane, "Learning in the Air: Secure Federated Learning for UAV-Assisted Crowdsensing," in *IEEE Transactions on Network Science and Engineering*, vol. 8, no. 2, pp. 1055-1069, 1 April-June 2021, doi: 10.1109/TNSE.2020.3014385.
- [53] Q. Kong et al., "Privacy-Preserving Aggregation for Federated Learning-Based Navigation in Vehicular Fog," in *IEEE Transactions on Industrial Informatics*, vol. 17, no. 12, pp. 8453-8463, Dec. 2021, doi: 10.1109/TII.2021.3075683.
- [54] S. Lu, Y. Yao and W. Shi, "CLONE: Collaborative Learning on the Edges," in *IEEE Internet of Things Journal*, vol. 8, no. 13, pp. 10222-10236, 1 July 2021, doi: 10.1109/JIOT.2020.3030278.
- [55] W. Y. B. Lim et al., "Towards Federated Learning in UAV-Enabled Internet of Vehicles: A Multi-Dimensional Contract-Matching Approach," in *IEEE Transactions on Intelligent Transportation Systems*, vol. 22, no. 8, pp. 5140-5154, Aug. 2021, doi: 10.1109/TITS.2021.3056341.
- [56] Y. Lu, X. Huang, K. Zhang, S. Maharjan and Y. Zhang, "Blockchain Empowered Asynchronous Federated Learning for Secure Data Sharing in Internet of Vehicles," in *IEEE Transactions on Vehicular Technology*, vol. 69, no. 4, pp. 4298-4311, April 2020, doi: 10.1109/TVT.2020.2973651.
- [57] P. Kumar, R. Kumar, G. P. Gupta and R. Tripathi, "BDEdge: Blockchain and Deep-Learning for Secure Edge-Envisioned Green CAVs," in *IEEE Transactions on Green Communications and Networking*, vol. 6, no. 3, pp. 1330-1339, Sept. 2022, doi: 10.1109/TGCN.2022.3165692.
- [58] J. J. Q. Yu, "Sybil Attack Identification for Crowdsourced Navigation: A Self-Supervised Deep Learning Approach," in *IEEE Transactions on Intelligent Transportation Systems*, vol. 22, no. 7, pp. 4622-4634, July 2021, doi: 10.1109/TITS.2020.3036085.
- [59] W. Jiang, H. Li, S. Liu, X. Luo and R. Lu, "Poisoning and Evasion Attacks Against Deep Learning Algorithms in Autonomous Vehicles," in *IEEE Transactions on Vehicular Technology*, vol. 69, no. 4, pp. 4439-4449, April 2020, doi: 10.1109/TVT.2020.2977378.
- [60] C. Song et al., "MAT: A Multi-strength Adversarial Training Method to Mitigate Adversarial Attacks," 2018 IEEE Computer Society Annual Symposium on VLSI (ISVLSI), 2018, pp. 476-481, doi: 10.1109/ISVLSI.2018.00092.
- [61] M. Zhao et al., "Deep Residual Networks with Dynamically Weighted Wavelet Coefficients for Fault Diagnosis of Planetary Gearboxes," *IEEE Transactions on Industrial Electronics*, vol. 65, no. 5, 2018.
- [62] Z. He et al., "Improved Deep Transfer Auto-encoder for Fault Diagnosis of Gearbox under Variable Working Conditions with Small Training Samples," *IEEE Access*, vol. 7, 2019.
- [63] K. Kim et al., "A Deep Learning Part-Diagnosis Platform (DLPP) Based on an in-Vehicle on-Board Gateway for an Autonomous Vehicle," *KSII Transactions on Internet and Information Systems*, vol. 13, no. 8, 2019.
- [64] Y. Jeong et al., "An Integrated Self-Diagnosis System for an Autonomous Vehicle Based on an IoT Gateway and Deep Learning," *Applied Science*, 2018.
- [65] Y. Liu et al., "MRD-Nets: Multi-Scale Residual Networks w. Dilated Convolutions for Classification and Clustering Analysis of Spacecraft Electrical Signal," *IEEE Access*, vol. 7, 2019.
- [66] P. Wolf et al., "Pre-ignition Detection Using Deep Neural Networks: A Step Towards Data-Driven Automotive Diagnostics," *International Conference on Intelligent Transportation Systems*, 2018.
- [67] M. Olyael et al., "Fault Detection and Identification on UAV System with CITFA Algorithm Based on Deep Learning," *Iranian Conference on Electrical Engineering*, 2018.
- [68] H. -J. Lee, K. -T. Kim, J. -H. Park, G. Bere, J. J. Ochoa and T. Kim, "Convolutional Neural Network-Based False Battery Data Detection and Classification for Battery Energy Storage Systems," in *IEEE Transactions on Energy Conversion*, vol. 36, no. 4, pp. 3108-3117, Dec. 2021, doi: 10.1109/TEC.2021.3061493.
- [69] H. Moinul et al., "Deep Learning Based Micro-Grid Fault Detection and Classification in Future Smart Vehicle," *IEEE Transportation and Electrification Conference and Expo*, 2018.
- [70] J. Fu et al., "A Hybrid CNN-LSTM Model Based Actuator Fault Diagnosis for Six-Rotor UAVs," *Chinese Control and Decision Conference*, 2019.
- [71] B. Wang, X. Peng, M. Jiang and D. Liu, "Real-Time Fault Detection for UAV Based on Model Acceleration Engine," in *IEEE Transactions on Instrumentation and Measurement*, vol. 69, no. 12, pp. 9505-9516, Dec. 2020, doi: 10.1109/TIM.2020.3001659.
- [72] S. Zou, W. Zhao, C. Wang and F. Chen, "Fault Detection Strategy of Vehicle Wheel Angle Signal via Long Short-Term Memory Network and Improved Sequential Probability Ratio Test," in *IEEE Sensors Journal*, vol. 21, no. 15, pp. 17290-17299, 1 Aug. 1, 2021, doi: 10.1109/JSEN.2021.3079118.
- [73] F. van Wyk, Y. Wang, A. Khojandi and N. Masoud, "Real-Time Sensor Anomaly Detection and Identification in Automated Vehicles," in *IEEE Transactions on Intelligent Transportation Systems*, vol. 21, no. 3, pp. 1264-1276, March 2020, doi: 10.1109/TITS.2019.2906038.
- [74] G. Raja, K. Kottursamy, K. Dev, R. Narayanan, A. Raja and K. B. V. Karthik, "Blockchain-Integrated Multiagent Deep Reinforcement Learning for Securing Cooperative Adaptive Cruise Control," in *IEEE Transactions on Intelligent Transportation Systems*, vol. 23, no. 7, pp. 9630-9639, July 2022, doi: 10.1109/TITS.2022.3168486.
- [75] B. G. Maciel-Pearson et al., "Multi-Task Regression-Based Learning for Autonomous Unmanned Aerial Vehicle Flight Control within Unstructured Outdoor Environment," *IEEE Robotics and Automation Letters*, vol. 4, no. 4, 2019.
- [76] M. K. Al-Sharman et al., "Deep-Learning-Based Neural Network Training for State Estimation Enhancement: Application to Attitude Estimation," *IEEE Transactions on Instrumentation and Measurement*, vol. 69, issue 1, 2020.
- [77] Y. Kang et al., "Deep Convolutional Identifier for Dynamic Modeling and Adaptive Control of Unmanned Helicopter," *IEEE Transactions on Neural Networks and Learning Systems*, vol. 30, no. 2, 2019.

- [78] Y. Li et al, "Compensating Delays and Noises in Motion Control of Autonomous Electric Vehicles by Using Deep Learning and Unscented Kalman Predictor," *IEEE Transactions on Systems, Man and Cybernetics*, 2018.
- [79] P. Drews et al, "Vision-Based High-Speed Driving with a Deep Dynamic Observer," *IEEE Robotics and Automation Letters*, vol. 4, no. 2, 2019.
- [80] Q. Zhang et al, "Deep Interactive Reinforcement Learning for Path Following of Autonomous Underwater Vehicle," *IEEE Access*, 2020.
- [81] I. Carlucho et al, "Adaptive Low-Level Control of Autonomous Underwater Vehicles Using Deep Reinforcement Learning," *Robotics and Autonomous Systems*, 2018.
- [82] Y. Shang and W. Qiao, "Intelligent driving trajectory tracking control algorithm based on deep learning," 2021 IEEE 4th International Conference on Automation, Electronics and Electrical Engineering (AUTEEE), 2021, pp. 618-621, doi: 10.1109/AUTEEE52864.2021.9668724.
- [83] S. Sharma, G. Tewolde and J. Kwon, "Lateral and Longitudinal Motion Control of Autonomous Vehicles Using Deep Learning," *IEEE International Conference on Electro Information Technology*, 2019.
- [84] S. Yang et al, "Scene Understanding in Deep Learning-based End-to-End Controllers for Autonomous Vehicles," *IEEE Transaction on Systems, Man, and Cybernetics*, vol. 49, no. 1, 2019.
- [85] J. Zhu et al, "Hierarchical Decision and Control for Continuous Multitarget Problem: Policy Evaluation with Action Delay," *IEEE Transactions on Neural Networks and Learning Systems*, vol. 30, no. 2, 2019.
- [86] Q. Chen, W. Zhao, L. Li, C. Wang and F. Chen, "ES-DQN: A Learning Method for Vehicle Intelligent Speed Control Strategy Under Uncertain Cut-In Scenario," in *IEEE Transactions on Vehicular Technology*, vol. 71, no. 3, pp. 2472-2484, March 2022, doi: 10.1109/TVT.2022.3143840.
- [87] H. Iwasaki and A. Okuyama, "Development of a Reference Signal Self-Organizing Control System Based on Deep Reinforcement Learning," 2021 IEEE International Conference on Mechatronics (ICM), 2021, pp. 1-5, doi: 10.1109/ICM46511.2021.9385676.
- [88] T. Chu, J. Wang, L. Codecà and Z. Li, "Multi-Agent Deep Reinforcement Learning for Large-Scale Traffic Signal Control," in *IEEE Transactions on Intelligent Transportation Systems*, vol. 21, no. 3, pp. 1086-1095, March 2020, doi: 10.1109/TITS.2019.2901791.
- [89] A. Boukerche, D. Zhong and P. Sun, "FECO: An Efficient Deep Reinforcement Learning-Based Fuel-Economic Traffic Signal Control Scheme," in *IEEE Transactions on Sustainable Computing*, vol. 7, no. 1, pp. 144-156, 1 Jan.-March 2022, doi: 10.1109/TSUSC.2021.3138926.
- [90] Q. Yang, G. Wang, A. Sadeghi, G. B. Giannakis and J. Sun, "Two-Timescale Voltage Control in Distribution Grids Using Deep Reinforcement Learning," in *IEEE Transactions on Smart Grid*, vol. 11, no. 3, pp. 2313-2323, May 2020, doi: 10.1109/TSG.2019.2951769.
- [91] J. Duan et al., "Deep-Reinforcement-Learning-Based Autonomous Voltage Control for Power Grid Operations," in *IEEE Transactions on Power Systems*, vol. 35, no. 1, pp. 814-817, Jan. 2020, doi: 10.1109/TPWRS.2019.2941134.
- [92] S. Kumari, K. K. Srinivas and P. Kumar, "Channel and Carrier Frequency Offset Equalization for OFDM Based UAV Communications Using Deep Learning," in *IEEE Communications Letters*, vol. 25, no. 3, pp. 850-853, March 2021, doi: 10.1109/LCOMM.2020.3036493.
- [93] C. H. Liu, Z. Chen, J. Tang, J. Xu and C. Piao, "Energy-Efficient UAV Control for Effective and Fair Communication Coverage: A Deep Reinforcement Learning Approach," in *IEEE Journal on Selected Areas in Communications*, vol. 36, no. 9, pp. 2059-2070, Sept. 2018, doi: 10.1109/JSAC.2018.2864373.
- [94] C. Wang, D. Deng, L. Xu and W. Wang, "Resource Scheduling Based on Deep Reinforcement Learning in UAV Assisted Emergency Communication Networks," in *IEEE Transactions on Communications*, vol. 70, no. 6, pp. 3834-3848, June 2022, doi: 10.1109/TCOMM.2022.3170458.
- [95] M. Fadda, M. Murrioni and V. Popescu, "Interference Issues for VANET Communications in the TVWS in Urban Environments," in *IEEE Transactions on Vehicular Technology*, vol. 65, no. 7, pp. 4952-4958, July 2016, doi: 10.1109/TVT.2015.2453633.
- [96] X. Zhang, M. Peng, S. Yan and Y. Sun, "Deep-Reinforcement-Learning-Based Mode Selection and Resource Allocation for Cellular V2X Communications," in *IEEE Internet of Things Journal*, vol. 7, no. 7, pp. 6380-6391, July 2020, doi: 10.1109/JIOT.2019.2962715.
- [97] O. S. Oubbati, M. Atiquzzaman, A. Baz, H. Alhakami and J. Ben-Othman, "Dispatch of UAVs for Urban Vehicular Networks: A Deep Reinforcement Learning Approach," in *IEEE Transactions on Vehicular Technology*, vol. 70, no. 12, pp. 13174-13189, Dec. 2021, doi: 10.1109/TVT.2021.3119070.
- [98] U. Challita, W. Saad and C. Bettstetter, "Interference Management for Cellular-Connected UAVs: A Deep Reinforcement Learning Approach," in *IEEE Transactions on Wireless Communications*, vol. 18, no. 4, pp. 2125-2140, April 2019, doi: 10.1109/TWC.2019.2900035.
- [99] G. Cui, Y. Long, L. Xu and W. Wang, "Joint Offloading and Resource Allocation for Satellite Assisted Vehicle-to-Vehicle Communication," in *IEEE Systems Journal*, vol. 15, no. 3, pp. 3958-3969, Sept. 2021, doi: 10.1109/JSYST.2020.3017710.
- [100] T. Yang, J. Li, H. Feng, N. Cheng and W. Guan, "A Novel Transmission Scheduling Based on Deep Reinforcement Learning in Software-Defined Maritime Communication Networks," in *IEEE Transactions on Cognitive Communications and Networking*, vol. 5, no. 4, pp. 1155-1166, Dec. 2019, doi: 10.1109/TCCN.2019.2939813.

Copyright: This article is an open access article distributed under the terms and conditions of the Creative Commons Attribution (CC BY-SA) license (<https://creativecommons.org/licenses/by-sa/4.0/>).

RAYMOND NING HUANG is currently pursuing a bachelor's degree in Mechanical Engineering at the University of Toronto. His research interests include deep learning and robotics.

JING REN has done her bachelor's degree from Shandong University in 1993. She has done her master's degree from Western University in 2003. She has completed her PhD degree in Robotics from Western University in 2005. Dr. Ren is an associate professor in the Faculty of Engineering and Applied Science at Ontario Tech University. Her research interests include deep learning, image processing and robotics. She is a recipient of University Faculty Award in 2006.

HOSSAM A. GABBAR obtained his B.Sc. degree in 1988 with first class of honor from the Faculty of Engineering, Alexandria University (Egypt). In 2001, he obtained his Ph.D. degree from Okayama University (Japan). Dr. Gabbar is a full Professor in the Faculty of Energy Systems and Nuclear Science, and cross appointed in the Faculty of Engineering and Applied Science, at Ontario Tech University (UOIT), where he has established the Energy Safety and Control Lab (ESCL), Smart Energy Systems Lab, and Advanced Plasma Engineering Lab. He is the recipient of the Senior Research Excellence Award for 2016, UOIT. He is recognized among the top 2% of worldwide scientists with high citation in the area of energy. He is a Distinguished Lecturer of IEEE NPSS. He is leading national and international research in the areas of smart energy grids, energy safety and control systems, and waste to energy using advanced plasma technologies. From 2001 till 2004, he joined Tokyo Institute of Technology (Japan), as a research associate. From 2004 till 2008, he joined Okayama University (Japan) as an Associate Professor, in the Division of Industrial Innovation Sciences. From 2007 till 2008, he was a Visiting Professor at the University of Toronto. He also worked as process control, safety, and automation specialist in energy and oil & gas industries. Dr. Gabbar has more than 230 publications, including patents, books / chapters, journal and conference papers.

Received: 15 August, 2022, Revised: 10 October 2022, Accepted: 18 October, 2022, Online: 31 October, 2022

DOI: <https://dx.doi.org/10.55708/js0110009>

Fast Labeled Spanning Tree in Binary Irregular Graph Pyramids

Majid Banaeyan^{*,1} , Walter G. Kropatsch¹ ¹Pattern Recognition and Image Processing Group, Institute of Visual Computing and Human-Centered Technology, TU Wien, Vienna, Austria

*Corresponding author: Majid Banaeyan, 1040 Wien, Favoritenstr. 9/5, E193-03, Vienna, Austria, +43 (1) 58801 - 18667 & majid@prip.tuwien.ac.at

ABSTRACT: Irregular Pyramids are powerful hierarchical structures in pattern recognition and image processing. They have high potential of parallel processing that makes them useful in processing of a huge amount of digital data generated every day. This paper presents a fast method for constructing an irregular pyramid over a binary image where the size of the images is more than 2000 in each of 2/3 dimensions. Selecting the contraction kernels (CKs) as the main task in constructing the pyramid is investigated. It is shown that the proposed fast labeled spanning tree (FLST) computes the equivalent contraction kernels (ECKs) in only two steps. To this purpose, first, edges of the corresponding neighborhood graph of the binary input image are classified. Second, by using a total order an efficient function is defined to select the CKs. By defining the redundant edges, further edge classification is performed to partition all the edges in each level of the pyramid. Finally, two important applications are presented: connected component labeling (CCL) and distance transform (DT) with lower parallel complexity $O(\log(\delta))$ where the δ is the diameter of the largest connected component in the image.

KEYWORDS Spanning Tree, Irregular Pyramid, Total Order, Parallel Processing

1. Introduction

Pyramids are important structures in pattern recognition and image processing. They were invented [1] as ordered collection of images at multiple resolutions that are able to process high resolution data at lower resolution and propagating the local information into global and abstracted information at higher levels [2]. In [3], the authors states that the pyramid is a general model for human problem solving where a massively parallel processing must be accomplished in order to recognizing a complex scene (like a busy street) in the blink of an eye [4, 5].

Motivated by a biological point of view, this paper introduces a fast method to construct the pyramidal structure of a given 2D binary image in a fully parallel scheme. Using the built pyramid, fundamental operations in analysing the binary images can be performed with lower complexity: Connected Component Labeling (CCL) and Distance Transform (DT). In particular, the current research is an extension of the previous work [6] that computes connected components (CCs) with the help of the pyramid. Propagating the labels in [6] is performed in linear time, hence the parallel complexity at the worst case is $O(\delta)$ where δ is the diameter of the largest CC in the image. In contrast, this paper mathematically proves that the parallel complexity is decreased to $O(\log(\delta))$.

The paper is organized as follows. Sec. 1 gives a short overview of the theoretical background of image pyramids, graph pyramids and different graph representations. The classification of edges is defined in Sec. 2. Selecting the contraction kernels as the main step in constructing the irregular pyramid is completely described in Sec. 3. To this

aim, the concept of *redundant* edges is covered by detail. The proposed fast labeled spanning tree (FLST) is defined in Sec. 4. Two main applications are presented in Sec. 5. The last section, provides a conclusion and considerations for future research.

1.1. Image Pyramids

Image Pyramids consist of a series of successively reduced images produced from a high resolution base image [2]. Generally, two types of the pyramids, namely regular and irregular pyramids exist. In regular pyramids [7] the resolution is decreased in regular steps and therefore the size of the pyramid is fixed. On the contrary, in irregular pyramids [8, 9] the size of the pyramid is not fixed and it is adapted to the image data. In addition, unlike the regular ones, the irregular pyramids are shift- and rotation-invariant which make them useful to use in a variety of tasks, in particular image segmentation [10, 11].

It should be noticed that the irregular image pyramid is interpreted as the irregular graph pyramid when its pixels and the neighborhood relations between adjacent pixels correspond to the vertices and the edges of the graph, respectively.

1.2. Irregular Graph Pyramids

Irregular pyramids are a stack of successively reduced graphs where each graph is constructed from the graph below by selecting a specific subset of vertices and edges. For generation of irregular pyramids, two basic operations on graphs are needed: edge contraction and edge removal. The former contracts an edge connecting two vertices, and

the two vertices are joined into one. All edges that were incident to the joined vertices will be incident to the resulting vertex after the operation. The latter removes an edge from the graph, without changing the number of vertices or affecting the incidence relationships of other edges.

In each level of the pyramid, the vertices/edges which disappear in a level above are called *non-surviving* vertices/edges. Those vertices/edges which appear in the upper level are called *surviving* vertices/edges. Consider $G = (V, E)$ as the neighborhood graph of an image P where V corresponds to the vertex set and E corresponds to the edge set. The vertex $v \in V$ associates with the pixels in image P and the edge $e \in E$ connects the corresponding adjacent vertices. Let the gray-value of vertex $g(v) = g(p)$ where $p \in P$ is a pixel in the image corresponding to vertex v . Consider *contrast*(e) as an attribute of an edge $e(u, v)$ where $u, v \in V$ and *contrast*(e) = $|g(u) - g(v)|$ in the base level. Since we are working with binary images only, the vertices have either of the two values 0 and 1. Similarly the contrast of an edge is either 0 or 1.

Definition 1 (Contraction Kernel (CK)). *A CK is a tree consisting of a surviving vertex as its root and some non-surviving neighbors with the constraint that every non-survivor can be part of only one CK.*

An edge of a CK is denoted by the directed edge and points towards the survivor.

In this paper, the 4-connectivity between pixels of the input image is assumed. The reason is that the 8-connectivity would not be a plane graph [12]. A *plane* graph is a graph embedded in the plane such that its edges intersect only at their endpoints [13]. In a plane graph there are connected spaces between edges and vertices and every such connected area of the plane is called a *face*. The *degree* of the face is the number of edges bounding the face. In addition a face bounded by a cycle is called an *empty face*. In a non-empty face, traversing the boundary would require to visit vertices or edges twice [12].

An empty face consisting only one edge is called an empty *self-loop*. Consider an empty face of degree 2: it contains two edges that have the same endpoints. These parallel edges are called *multiple* edges. The multiple edges mean edges between the same endpoints, i.e. for example edges $e_{u_1, v_1} \neq e_{u_2, v_2} \neq e_{u_3, v_3}$ where $u_1 = u_2 = u_3$ and $v_1 = v_2 = v_3$.

1.3. Graph Representation

Graphs as a versatile representative tool are common in the representation of the irregular pyramid. There are different graph representations such as a *simple* graph, a *dual* graph and a *combinatorial* map.

A simple graph [14] $G = (V, E)$ consists of a set of vertices V and of edges E without *self-loops* and *multiple* edges between pairs of vertices. The relationships between different regions can be represented by the *region adjacency graph* (RAG). Although plane simple graphs are a common model for the RAG they cannot distinguish between different topological configurations, namely inclusion and multiple adjacency relationships (*multi-boundaries*) of regions [14].

A dual graph model encodes multiple boundaries between regions in a non-simple graph. The problem with

dual graphs [9] is that they cannot unambiguously represent a region enclosed in another one on a local level [14]. Therefore, in this paper the combinatorial map (CM), as a planar embedding of a RAG, is used. It not only solves the mentioned problems but also provides an efficient structure to preserve topological relations between regions while it can be extended to higher dimensions (nD).

1.4. Combinatorial Pyramid

A combinatorial pyramid [15] is a hierarchy of successively reduced combinatorial maps. A combinatorial map (CM) is similar to a graph but explicitly stores the orientation of edges around each vertex. The 2D combinatorial map (G) is defined by a triple $G = (D, \alpha, \sigma)$ where the D is a finite set of darts [14]. A dart is defined as a half edge and it is the fundamental element in the CM's structure. The α is an *involution* on the set D and it provides a one-to-one mapping between consecutive darts forming the same edge such that $\alpha(\alpha(d)) = d$. The σ is a *permutation* on the set D and encodes consecutive darts around the same vertex while turning counterclockwise [16]. Note that the clockwise orientation is denoted by σ^{-1} .

Fig. 1a shows a set adjacent darts with their σ and α encoding. Note that the edge e between two vertices u and v is denoted by $e = (d, \alpha(d))$. The $u, v \in V$ and the $e \in E$ where the V and E are the set of vertices and edges of the graph $G = (V, E)$, respectively.

The removal and the contraction operations in the combinatorial pyramid is defined as follows:

Definition 2 (Removal operation). *The removal operation removes one edge, $G \setminus \{e\}$, while it modifies the adjacent darts such that:*

$$\sigma(\sigma^{-1}(d)) = \sigma(d), \quad \sigma(\sigma^{-1}(\alpha(d))) = \sigma(\alpha(d)) \quad (1)$$

Definition 3 (Contraction operation). *The contraction operation removes one edge, $G / \{e\}$, and collapses its two endpoints and modifies the adjacent darts such that:*

$$\sigma(\sigma^{-1}(d)) = \sigma(\alpha(d)), \quad \sigma(\sigma^{-1}(\alpha(d))) = \sigma(d) \quad (2)$$

Fig. 1b and Fig. 1c illustrate the removal and contraction operations in the combinatorial map. Note that the contraction operation does not disconnect the graph, and thus preserves connectivity [8].

2. Edge Classification in a Binary Image Graph

Let neighborhood graph $G = (V, E)$ be the undirected connected plane graph consisting of a finite set of vertices V and a finite set of edges E . In the neighborhood graph of the binary input image, each connected component (CC) consists of a set of vertices with the same gray value, 0 or 1. In the paper, black pixels (vertices) are shown by 0 while white pixels (vertices) are shown by 1. In this regard, we partition the edges of the neighborhood graph into two categories: edges connecting two vertices of the same CC, intra-CC and edges connecting vertices of different CCs, inter-CCs as follows:

Definition 4. *Intra-CC edge: an edge $e = (u, v) \in E$ within a CC is *intra-CC* iff $g(u) = g(v)$.*

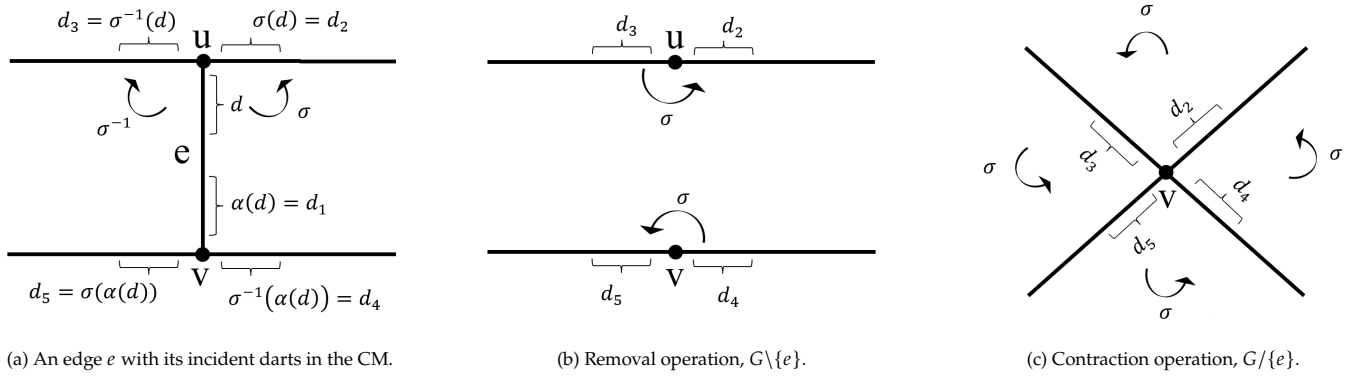


Figure 1: Two main operations in irregular graph pyramids. (a) Before applying an operation. (b), (c) after applying the operations.

Definition 5. *Inter-CC edge:* an edge $e = (u, v) \in E$ between two CCs is *inter-CC* iff $g(u) \neq g(v)$.

The contrast of an intra-CC edge is equal to zero, $c(\text{intra-CC}) = 0$. Therefore, we denote the intra-CC edge by $e_0 \in E_0$. The contrast of an inter-CCs edge is one, $c(\text{inter-CCs}) = 1$. Therefore, the inter-CCs edge is denoted by $e_1 \in E_1$. All edges in the neighborhood graph are partitioned into E_0 and E_1 edges:

$$E = E_0 \cup E_1 \quad (3)$$

3. Selecting the CKs using a Total Order

Selecting the CKs plays the main role in constructing the irregular pyramid. The height of the built pyramid and the complexity of the construction depends on how the CKs are selected. In order to achieve an efficient and a unique selection of the CKs a **total order** is defined over the vertices [17]. Consider G as the neighborhood graph of an binary input image with M by N vertices. Let $(1, 1)$ be the coordinate of the vertex at the upper-left corner and (M, N) at the lower-right corner. Let r and c denote the row and the column in the grid structure of G , respectively. The vertices of G receive a unique index as follows:

$$\text{Idx} : [1, M] \times [1, N] \mapsto [1, M \cdot N] \subset \mathbb{N} \quad (4)$$

$$\text{Idx}(r, c) = (c - 1) \cdot M + r \quad (5)$$

We use the properties of the total order [18] in selecting the CKs. First, every two elements of a total ordered set (indices of vertices) are comparable. Second, each subset of the total ordered set (a set of vertices) has exactly one minimum and one maximum.

In the binary neighborhood graph G a CC consists of only intra-CC (E_0) edges. In constructing the irregular pyramid this CC is shown by only one single vertex at the top of the pyramid. Therefore, all the CKs are selected only from the intra-CC edges. From the vertex point of view, a vertex that is not incident to an intra-CC edge is an *isolated* vertex. This vertex is surrounded by only inter-CC edges.

Let v be a non-isolated vertex, i.e, it is the endpoint of at least one intra-CC edge. The *upper* neighborhood \mathcal{N} is defined as follows :

$$\mathcal{N}(v) = \{w \in V | (v, w) \in E_0, \text{Idx}(w) > \text{Idx}(v)\} \quad (6)$$

The cardinality of the set $|\mathcal{N}(v)|$ indicates the number of intra-CC edges incident to v having greater vertex than v . Therefore, the cardinality of the non-isolated vertex is $|\mathcal{N}(v) \geq 1|$.

In order to determine the CKs in the graph $G = (V, E)$, the *selecting contraction kernel* **SCK(.)** function is defined as follows:

$$\text{SCK} : [1, M \cdot N] \mapsto [1, M \cdot N] \quad (7)$$

$$\text{SCK}(\text{Idx}(v)) = \max\{\text{Idx}(w) | w \in \mathcal{N}(v)\} \text{ if } |\mathcal{N}(v)| \geq 1 \quad (8)$$

$$\text{SCK}(\text{Idx}(v)) = \text{Idx}(v) \text{ if } |\mathcal{N}(v)| = 0 \quad (9)$$

The output of the SCK function partitions the vertices into two categories: surviving vertices and non-surviving vertices as follows:

Definition 6. [*Surviving vertex*] A vertex $v \in V$ in a binary neighborhood graph $G = (V, E)$, is a *surviving vertex* iff $\text{SCK}(\text{Idx}(v)) = \text{Idx}(v)$.

Proposition 1. *An isolated vertex survives always.*

Proof. Assume v is an isolated vertex. Since there is no intra-CC edge incident to the isolated vertex, it leads to $|\mathcal{N}(v)| = 0$. Based on the (9), $\text{SCK}(\text{Idx}(v)) = \text{Idx}(v)$ and therefore employing the Def. 6 v is the surviving vertex. \square

Definition 7 (Non-surviving vertex). A vertex $v \in V$ in a binary neighborhood graph $G = (V, E)$, is a *non-surviving vertex* iff $\text{SCK}(\text{Idx}(v)) \neq \text{Idx}(v)$.

Proposition 2. *For a non-surviving vertex v at the base level, $|\mathcal{N}(v)| \in \{1, 2\}$.*

Proof. Based on (5) a non-surviving vertex may be incident to maximum two vertices with greater indices (right or down vertices) at the base level. In addition, the non-surviving vertex must be incident to at least one vertex, namely its right or its down vertex. The former states $|\mathcal{N}(v)| = 2$ while the latter states $|\mathcal{N}(v)| = 1$. \square

¹All total orders are permutations of each other.

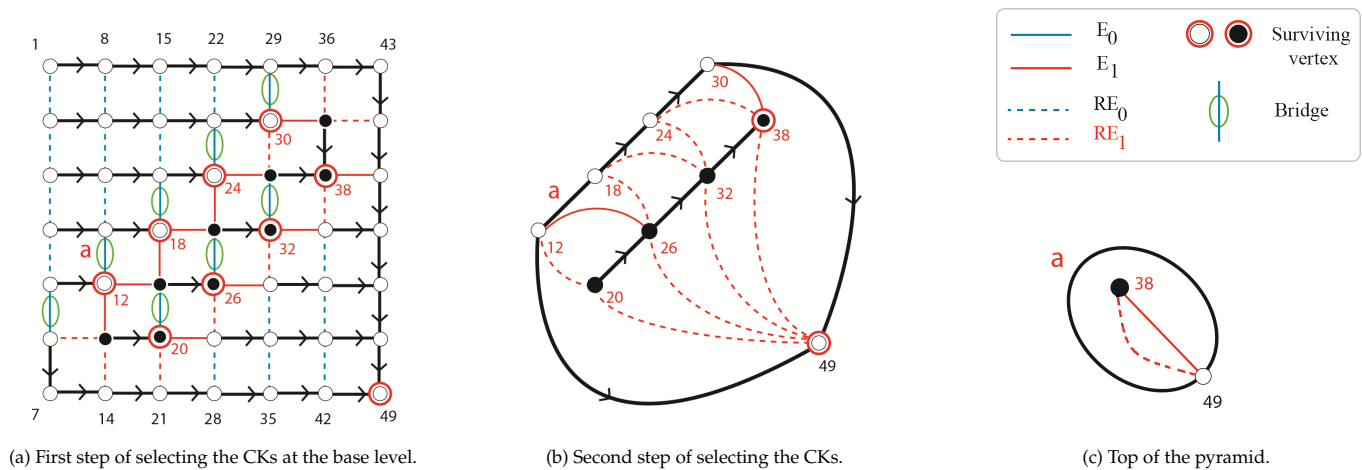


Figure 2: Two steps of selecting the CKs. The edge a shows the inclusion relationship between CCs.

In a CK there is one surviving vertex (the root of the CK) while the remaining vertices are non-surviving vertices. Each non-surviving vertex connects to the surviving root by a unique monotonically Idx -increasing path of oriented edges. In a graph with n vertices there are $n!$ different total order¹. Each selected total order has its own properties. Selecting an efficient total order effects on selecting the CKs where the number of CKs determines the height of the pyramid. Pyramids with logarithmic height reduce the parallel computational complexity of fundamental operations such as connected component labeling [19, 17] and distance transform [20]. Therefore, a proper selection of the total order must result in constructing the pyramid with logarithmic height. In Sec. 4.1 it is proved that the proposed total order leads to this logarithmic height.

In contrast to the common methods of constructing the pyramid [2, 8], using the proposed total order has the advantage that the vertices are partitioned in every level of the pyramid. In other words, the vertices are either the non-surviving or the surviving vertices. Next sections show how this partitioning reduces the number of steps in selecting the CKs into only two steps.

3.1. First Step of Selecting the CKs

Selecting the CKs at the base level of the pyramid is the first step of the selection. To this aim, the SCK function is performed over each vertex of the neighborhood graph of the base level. As the result, each CK has one surviving vertex and all the other vertices of the CK do not survive. In Fig. 2-a the surviving vertices at the base level are denoted by a red circle around each vertex while all the other vertices do not survive.

At the base level of the pyramid, all faces in the grid structure are bounded by four edges containing two horizontal and two vertical edges.

Proposition 3. A horizontal intra-CC edge in a face of degree 4 at the base level of the pyramid always belongs to a CK.

Proof. Assume a horizontal intra-CC edge $e = (u, v)$ at the base level does not belong to a CK. Let u and v locate at the left and the right side of the edge e , respectively. Since

u is the endpoint of e , thus u is not an isolated vertex ($|\mathcal{N}(u)| > 1$) and based on (5), $Idx(u) < Idx(v)$. Due to Pro. 2 if $|\mathcal{N}(u)| = 1$ then v is the only vertex of $\mathcal{N}(u)$ that is incident to u and thus v is selected as the survivor. In case $|\mathcal{N}(u)| = 2$, there are two right and down vertices in the $\mathcal{N}(u)$ where based on (5) the right vertex is selected as surviving vertex. \square

3.2. Redundant Edges

Graphs as a versatile representative tool may have many unnecessary (*redundant*) edges [17]. Through the construction of the pyramid, contracting edges results in a smaller induced graph at the upper level. The resulting graph may consist of empty self-loops or double-edges. At this point, the edge removal simplifies the graph and removes these redundant edges.

Definition 8 (Redundant Edges). In a hierarchical structure, those edges that are not needed to fully reconstruct the hierarchy are considered as *redundant edges*.

Generally, the definition of the redundant edges depends on the applications and to what extend the reconstruction needs to be performed. For example, in [6, 17, 19], the authors defined the concept of the redundant edges in a binary graph pyramid in order to do the connected component labeling task where the fully reconstruction is performed. They showed that the redundant edges can be detected (predicted) before performing the contraction of edges. In this paper, we use the same concept for defining the redundant intra-CC and redundant inter-CC edges.

Definition 9 (Redundant Intra-CC edge (RE_0)). In an empty face consisting of only intra-CC edges, the non-oriented edge incident to the vertex with lowest Idx is a redundant intra-CC edge.

The definition above states that a redundant intra-CC edge (RE_0) exists only in a face bounded by intra-CC edges. Fig. 3 illustrates the configuration of the redundant intra-CC edges.

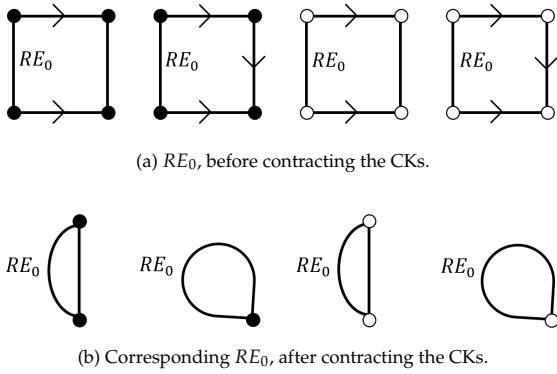


Figure 3: Configurations of the redundant intra-CC edges.

Definition 10 (Redundant Inter-CCs Edge (RE_1)). In an empty face, an inter-CCs edge incident to the vertex with lowest Idx is redundant iff:

- The empty face consists of only two inter-CCs edges.
- The empty face is bounded by inter-CCs edges and oriented intra-CC edges.

Fig. 4 illustrates all different configurations of the RE_1 edges before and after contracting the CKs.

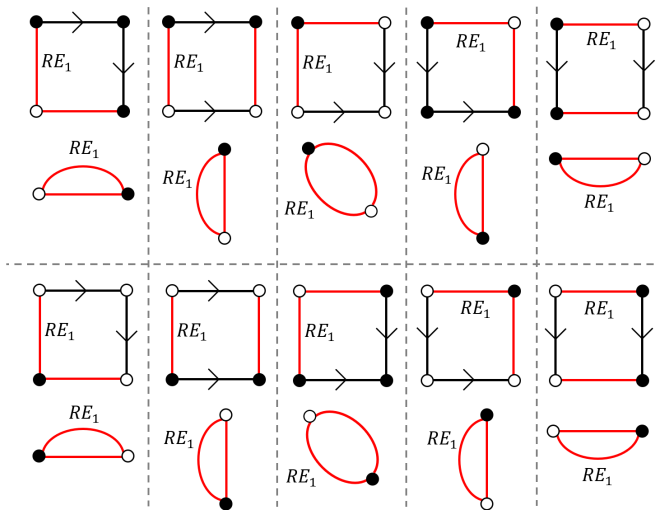


Figure 4: All different configurations of redundant inter-CCs edges

3.3. Second Step of Selecting the CKs

At the base level of the pyramid there are three types of the intra-CC edges:

1. The oriented edges that belong to the CKs.
2. The non-oriented redundant edges, RE_0 , were defined in Def. 9.
3. The remaining non-oriented intra-CC edges are defined as the *bridges*.

Definition 11 (Bridge). A **bridge** is a non-oriented intra-CC edge that bridges the gap between two contraction kernels of a connected component.

Note that the bridge is the edge of the equivalent contraction kernel (ECK) that is contracted after the two CKs are contracted.

Proposition 4. A bridge in a face of degree 4 at the base level of the pyramid is the vertical edge.

Proof. In the face of degree 4, there are two horizontal and two vertical edges. Assume the non-oriented bridge is the horizontal edge. However, due to Pro. 3 every horizontal intra-CC edge is oriented and therefore it cannot be a non-oriented intra-CC edge. \square

Proposition 5. A face of degree 4 at the base level of the binary pyramid does not have more than one bridge.

Proof. Assume a face of degree 4 contains two bridges. Since the bridges are vertical intra-CC edges, the oriented intra-CC edge must connect two different CCs which is in contradiction with the definition of the oriented edge (see Fig. 5-b). \square

Proposition 6. Two bridges at the base level of the binary pyramid are not incident to a same vertex.

Proof. Assume that two bridges are incident to the same vertex. Therefore, the horizontal common edge between their two corresponding faces must be the oriented intra-CC edge and the inter-CCs edge at the same time (see Fig. 5-c), contradiction. \square

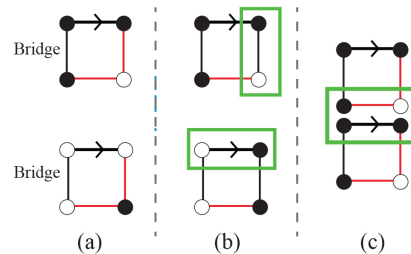


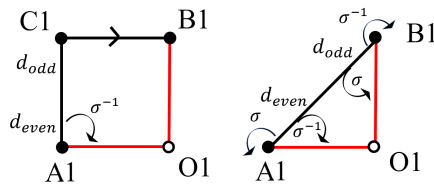
Figure 5: (a) The configurations of a bridge at the base level. (b) A face does not have two bridges. (c) Bridges are not incident to the same vertex

In order to select the CKs at the second step, the SCK function is performed over the bridges.

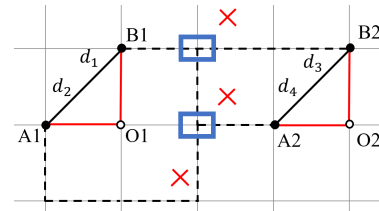
Definition 12 (inclusion edge). An inclusion edge is a non-empty self-loop inter-CC edge that preserves the topological inclusion relationship between two different CCs.

Note that if the inclusion relationships exists between two different CCs, the inclusion edge is one of the bridges that will be detected after the contractions of oriented edges. In Fig. 2 the inclusion edge is shown by a non-empty self-loop that is denoted by the letter **a** with the red color.

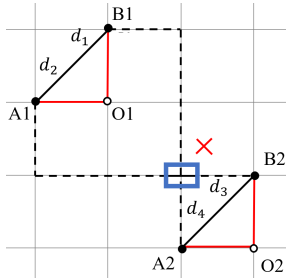
Proposition 7. All the redundant intra-CC edges are detected at the base level of the binary pyramid.



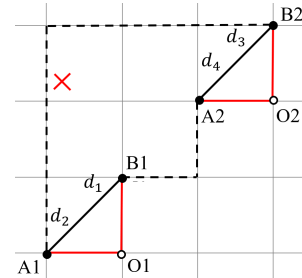
(a) The configurations of a bridge before and after the edge contraction.



(b) Contradiction to planarity of the graph G.



(c) Contradiction to planarity of the graph G.



(d) Contradiction to (5).

Figure 6: All redundant intra-CC edges, RE_0 , are at the base level of the pyramid.

Proof. The redundant intra-CC edges occur in a face bounded by only intra-CC edges. At an upper level, the remaining intra-CC edges are the bridges at the base level. However, since each bridge has the σ -related to a inter-CCs edge (Fig. 6a), therefore, there is no empty face containing only intra-CC edges at upper levels of the pyramid. Note that in the simple graph G , two bridges cannot be the σ -related of each other because this contradicts to planarity of the graph (Fig. 6b and Fig. 6c) or it contradicts to (5) that is shown in Fig. 6d. \square

The Proposition 7 states that there is no redundant intra-CC edge at an upper level of the pyramid. In fact, this is because of the important property of the defined total order over the indices of vertices where at the base level each non-surviving vertex only can be contracted into its right or down neighborhood vertex.

4. Fast Labeled Spanning Tree (FLST)

A CC in a binary graph pyramid is represented by a single surviving vertex at the top level of the pyramid. This vertex is the root of the tree spanning its receptive field at the base level [21]. In [22] it was shown that the combination of two (or more) successive reductions in an equivalent weighting function allows to calculate any level of the pyramid directly from the base. Kropatsch in [21] introduced the Equivalent Contraction Kernels (ECK) in the irregular graph pyramid and it was later used [23] in the minimum spanning tree (MST) segmentation.

In the binary pyramid, every spanning tree of a CC is the MST because the contrast (weight) of the intra-CC edges is zero. To drive the spanning tree of a CC, the previous common methods [14, 16, 11] need to select the CKs in n iterations where n is the height of the pyramid. In contrast, in the proposed method we only need two steps of selecting the CKs. Moreover, the SCK function is performed locally over each vertex. This means that the CKs are selected with parallel complexity of $O(1)$. Note that, it is assumed there

are sufficient processing elements available in order to do the parallel computations.

4.1. Independent Edges

To contract the CKs in a parallel manner, finding a set of independent edges plays the key role. Dependency of the edges differs based on what processing is going to be performed between a set of edges. In [19] two edges not sharing an endpoint are considered as *independent* edges. Using this definition all the CKs at the first selection can be contracted with parallel complexity bounded as follows:

$$O(\log_2(\delta(\text{CK}))) \leq \text{CKs contraction} \leq O(\log_3(\delta(\text{CK}))) \quad (10)$$

To determine the parallel complexity of contracting the CKs at the second step of selection, the dependencies between darts [6] is considered. Since in this step, each edge of the CK is a bridge at the base level, hence, there is an inter-CCs edge with a σ -relation incident to this edge. Therefore, all the CKs at the second selections are independent of each other and they will be contracted in parallel complexity $O(1)$.

5. Applications

To highlight the usefulness of the proposed method, two main applications are presented. In both application the parallel complexity is $O(\log(N))$ in a $N \times N$ -size input binary image.

5.1. Connected Component Labeling

Connected Component Labeling (CCL) is a fundamental task in analyzing binary images [24] where background and foreground are denoted by zero and one, respectively. A connected region is a group of pixels where all pairs of pixels are connected together. The role of the CCL is to assign a unique label to each CC. Common methods of CCL

[24, 25, 26] are linear; i.e., they search the binary image row by row in the raster-scan fashion. In contrast, using a hierarchical structure, within the bottom-up construction each pixel reaches its single surviving pixel (super-pixel) at top of the pyramid in a logarithmic number of steps. At this top-level of the pyramid, each of the super-pixels receives its unique label Idx . Afterwards, through the top-down propagation the vertices of the lower levels inherit the labels from the higher levels until all the pixels at the receptive field (base level of the pyramid) received their labels.

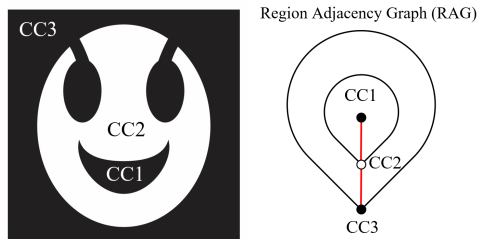


Figure 7: CCL by //ACC method.

The hierarchical method is called Parallel Pyramidal Connected Component (//ACC²) where the details can be found in [19]. The //ACC not only does the CCL task but also preserves the topological relations between the CCs. Fig. 7 shows how the //ACC encodes inclusion relationships between three CCs. Table 1 [19] shows the execution time of the //ACC method over three different categories of binary images; Random, MRI and Finger-print images. In addition, the execution time of the algorithm over different image-size is compared to the state-of-the-art methods; Spaghetti_RemSP, BBDT_RemSP, SAUF_UF, in [27]. The results in Fig. 8 encourage the //ACC method should be used in large images including more than one million pixels.

Table 1: Results for the different categories from (YACCLAB[28]).

Database Type	Random	MRI	Finger-print
size of Images	128×128	256×256	300×300
Num. of Images	89	1170	962
mean time (ms)	0.098	1.643	2.317
worst time (ms)	0.127	2.973	3.518

5.2. Distance Transform

The distance transform (DT) is another important fundamental operation that is applied to the binary image [1]. It is employed in a broad range of applications containing template matching [29, 30], image registration [31], map matching robot self-Localization [32], skeletonization [33], Line Detection in Manuscripts [34], Weather Analysis and Forecasting [35], etc. After applying the DT to a binary image, the result of the transform is a new gray-scale image whose foreground 1 pixels have intensities representing the minimum distance from the background 0 pixels.

²It is pronounced pac where the // and A stand for parallel and pyramidal.

³<https://waters-gateway.boku.ac.at/>

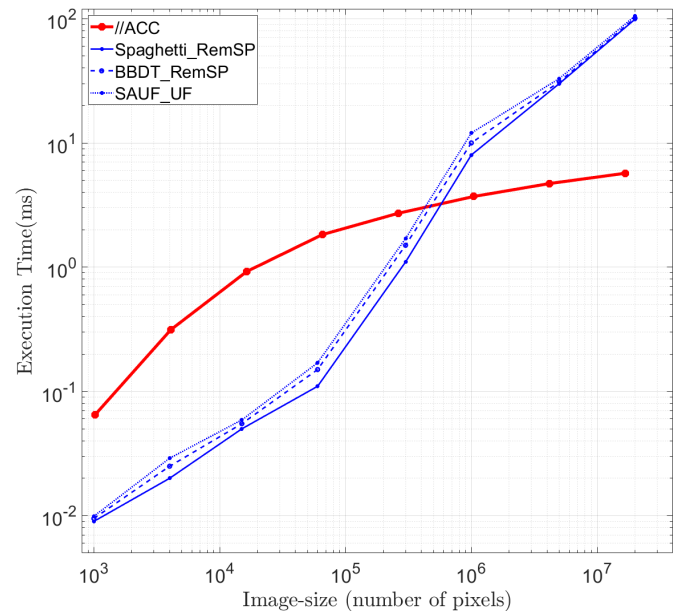


Figure 8: Illustration of the execution time (ms) over different image-sizes

In order to compute the DT, the common methods [1, 36], propagate the distances in linear sequential time. By contrast, using the hierarchical structure the distances can be propagated by a set of power-of-two numbers [20] where the parallel complexity is reduced into the logarithmic-time. The computation of DT with lower complexity makes the pyramid as a useful tool in analysing large binary images. In particular, currently we are working on the *Water's gateway to heaven* project³ dealing with high-resolution X-ray microtomography (μ CT) and fluorescence microscopy. The size of the images is more than 2000 in each of 3 dimensions where we use the saddle points of the DT to separate cells, which are visually difficult to be separated.

In the mentioned project above the input image is a labeled 2D cross slice of a leaf scan where it has six different labels illustrating different regions inside the leaf (Fig. 9a). The task of stomata is to control the amount of CO₂ that is entering the leaf. In order to do the photosynthesis, the CO₂ propagates through the airspace inside the leaf to reach the cells where it combines with water and sunlight. To model the procedure of the gas exchange in the leaf [37], we compute the geodesic distance transform (GDT) from the stomata through the airspace (Fig. 9b) to find out how long it takes to reach the necessary CO₂ concentration [20]. The use of pyramids would enormously speed up the computations of the DT in the large images of the project.

6. Conclusion

The paper presents a fast parallel method to select the equivalent contraction kernels in the irregular pyramid of a binary input image. It was shown that the first step of selecting the contraction kernels (CKs) at the base level is done with parallel complexity $O(1)$. These CKs are contracted with parallel $O(\log(\delta))$ complexity where the δ is the diameter of the maximum connected component (CC)

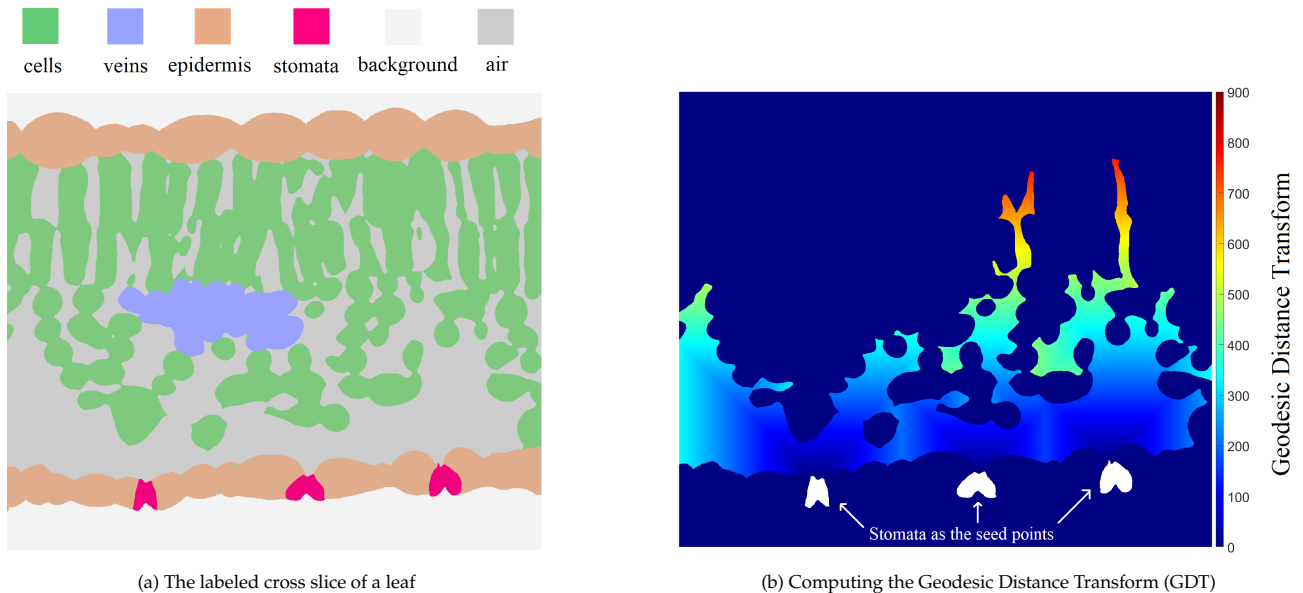


Figure 9: Computing the Geodesic Distance Transform in a multi-labeled image [20].

in the neighborhood graph of the image. By detecting the redundant edges (RE) the selection of CKs is performed in one parallel step. By defining the independent set of edges, we proved that all the selected CKs at the second step of selection are contracted in parallel complexity $O(1)$. The Fast labeled spanning tree (FLST) of the CCs is produced with parallel complexity $O(\log(\delta))$. Using the total order there is no random processing in construction of the pyramid and the resulting FLST is unique.

In addition, it was shown by employing the proposed FLST, that the fundamental operations in analyzing the binary image can be performed in lower parallel complexity. In particular, two main operations, connected component labeling (CCL) and distance transform (DT), were presented in detail. Finally, we presented how the proposed method can be useful in processing of the large images in practical real applications. For future works we plan to compute 3D distance transform in order to study the diffusion in the air space within a leaf.

Conflict of Interest The authors declare no conflict of interest.

Acknowledgment We acknowledge the Paul Scherrer Institut, Villigen, Switzerland for provision of beamtime at the TOMCAT beamline of the Swiss Light Source and would like to thank Dr. Goran Lovric for assistance. This work was supported by the Vienna Science and Technology Fund (WWTF), project LS19-013, and by the Austrian Science Fund (FWF), projects M2245 and P30275.

References

- [1] A. Rosenfeld, J. L. Pfaltz, "Sequential operations in digital picture processing", *Association for Computing Machinery*, vol. 13, no. 4, p. 471–494, 1966.
- [2] P. Meer, "Stochastic image pyramids", *Computer Vision, Graphics, and Image Processing*, vol. 45, no. 3, pp. 269–294, 1989.
- [3] Z. Pizlo, *Problem Solving, Cognitive Mechanisms and Formal Models*, Cambridge University Press, 2022.
- [4] M. C. Potter, B. Wyble, C. E. Hagmann, E. S. McCourt, "Detecting meaning in rsvp at 13 ms per picture", *Attention, Perception, & Psychophysics*, vol. 76, no. 2, pp. 270–279, 2014, doi:10.3758/s13414-013-0605-z.
- [5] J. A. Feldman, D. H. Ballard, "Connectionist models and their properties", *Cognitive science*, vol. 6, no. 3, pp. 205–254, 1982.
- [6] M. Banaeyan, W. G. Kropatsch, "Pyramidal connected component labeling by irregular graph pyramid", "2021 5th International Conference on Pattern Recognition and Image Analysis (IPRIA)", pp. 1–5, 2021, doi:10.1109/IPRIA53572.2021.9483533.
- [7] J.-M. Jolion, A. Rosenfeld, *A pyramid framework for early vision: multiresolutional computer vision*, vol. 251, Springer Science & Business Media, 2012.
- [8] W. G. Kropatsch, "Building irregular pyramids by dual graph contraction", *IEE-Proc. Vision, Image and Signal Processing*, vol. Vol. 142, no. No. 6, pp. pp. 366–374, 1995, doi:10.1049/ip-vis:19952115.
- [9] W. G. Kropatsch, H. Macho, "Finding the structure of connected components using dual irregular pyramids", "Cinquième Colloque DGCI", pp. 147–158, LLAIC1, Université d'Auvergne, ISBN 2-87663-040-0, 1995.
- [10] Y. Haxhimusa, W. G. Kropatsch, "Segmentation graph hierarchies", "Structural, Syntactic, and Statistical Pattern Recognition, Joint IAPR International Workshops on SSPR 2004 and SPR 2004", vol. LNCS 3138, pp. 343–351, Springer, Berlin Heidelberg, New York, 2004.
- [11] M. Cerman, I. Janusch, R. Gonzalez-Diaz, W. G. Kropatsch, "Topology-based image segmentation using LBP pyramids", *Machine Vision and Applications*, pp. 1–14, 2016, doi:10.1007/s00138-016-0795-1.
- [12] R. Klette, *Concise computer vision*, vol. 233, Springer, 2014.
- [13] R. Trudeau, *Introduction to Graph Theory*, Dover Books on Mathematics, Dover Pub., 1993.
- [14] L. Brun, W. G. Kropatsch, "Hierarchical graph encodings", O. Lézoray, L. Grady, eds., "Image Processing and Analysis with Graphs: Theory and Practice", pp. 305–349, CRC Press, 2012.
- [15] L. Brun, W. Kropatsch, "Introduction to combinatorial pyramids", "Digital and Image Geometry", pp. 108–128, Springer, 2001.
- [16] F. Torres, W. G. Kropatsch, "Canonical encoding of the combinatorial pyramid", "Proceedings of the 19th Computer Vision Winter Workshop", pp. 118–125, 2014.

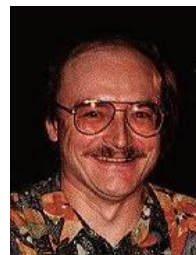
- [17] M. Banaeyan, D. Batavia, W. G. Kropatsch, "Removing redundancies in binary images", "International Conference on Intelligent Systems and Patterns Recognition (ISPR), Hammamet, Tunisia, March 24-25, 2022", pp. 221-233, Springer, 2022, doi:10.1007/978-3-031-08277-1_19.
- [18] B. A. Davey, H. A. Priestley, *Introduction to lattices and order*, Cambridge university press, 2002.
- [19] M. Banaeyan, W. G. Kropatsch, "Parallel $O(\log(n))$ computation of the adjacency of connected components", "International Conference on Pattern Recognition and Artificial Intelligence (ICPRAI), Paris, France, June 1-3, 2022", pp. 102-113, Springer, 2022, doi:10.1007/978-3-031-09282-4_9.
- [20] M. Banaeyan, C. Carratù, W. G. Kropatsch, J. Hladůvka, "Fast distance transforms in graphs and in gmaps", "IAPR Joint International Workshops on Statistical Techniques in Pattern Recognition (SPR 2022) and Structural and Syntactic Pattern Recognition (SSPR 2022), Montreal, Canada, August 26-27, 2022", p. in print, 2022.
- [21] W. G. Kropatsch, "Equivalent contraction kernels to build dual irregular pyramids", *Advances in Computer Science*, vol. Advances in Computer Vision, pp. 99-107, 1997.
- [22] P. J. Burt, E. H. Adelson, "The Laplacian pyramid as a compact image code", "Readings in computer vision", pp. 671-679, Elsevier, 1987.
- [23] Y. Haxhimusa, A. Ion, W. G. Kropatsch, "Evaluating hierarchical graph-based segmentation", "18th International Conference on Pattern Recognition", vol. II, pp. 195-198, IEEE Comp.Soc., 2006, doi:10.1109/ICPR.2006.511.
- [24] L. He, X. Ren, Q. Gao, X. Zhao, B. Yao, Y. Chao, "The connected-component labeling problem: A review of state-of-the-art algorithms", *Pattern Recognition*, vol. 70, pp. 25-43, 2017, doi:10.1016/j.patcog.2017.04.018.
- [25] L. He, Y. Chao, K. Suzuki, "Two efficient label-equivalence-based connected-component labeling algorithms for 3D binary images", *IEEE Transactions on Image Processing*, vol. 20, no. 8, pp. 2122-2134, 2011, doi:10.1109/TIP.2011.2114352.
- [26] U. H. Hernandez-Belmonte, V. Ayala-Ramirez, R. E. Sanchez-Yanez, "A comparative review of two-pass connected component labeling algorithms", "Mexican International Conference on Artificial Intelligence", pp. 452-462, Springer, 2011, doi:10.1007/978-3-642-25330-0_40.
- [27] F. Bolelli, S. Allegretti, L. Baraldi, C. Grana, "Spaghetti labeling: Directed acyclic graphs for block-based connected components labeling", *IEEE Transactions on Image Processing*, vol. 29, pp. 1999-2012, 2020, doi:10.1109/TIP.2019.2946979.
- [28] C. Grana, F. Bolelli, L. Baraldi, R. Vezzani, "YACCLAB - Yet Another Connected Components Labeling Benchmark", "2016 23rd International Conference on Pattern Recognition (ICPR)", pp. 3109-3114, Springer, 2016, doi:10.1109/ICPR.2016.7900112.
- [29] S. Prakash, U. Jayaraman, P. Gupta, "Ear localization from side face images using distance transform and template matching", "2008 First Workshops on Image Processing Theory, Tools and Applications", pp. 1-8, IEEE, 2008, doi:10.1109/IPTA.2008.4743786.
- [30] J. Lindblad, N. Sladoje, "Linear time distances between fuzzy sets with applications to pattern matching and classification", *IEEE Transactions on Image Processing*, vol. 23, no. 1, pp. 126-136, 2014, doi:10.1109/TIP.2013.2286904.
- [31] B. Hill, R. A. Baldock, "Constrained distance transforms for spatial atlas registration", *BMC bioinformatics*, vol. 16, no. 1, pp. 1-10, 2015, doi:10.1186/s12859-015-0504-5.
- [32] H. Sobreira, C. M. Costa, I. Sousa, L. Rocha, J. Lima, P. Farias, P. Costa, A. P. Moreira, "Map-matching algorithms for robot self-localization: a comparison between perfect match, iterative closest point and normal distributions transform", *Journal of Intelligent & Robotic Systems*, vol. 93, no. 3, pp. 533-546, 2019, doi:10.1007/s10846-017-0765-5.
- [33] C. Niblack, P. B. Gibbons, D. W. Capson, "Generating skeletons and centerlines from the distance transform", *CVGIP: Graphical Models and Image Processing*, vol. 54, no. 5, pp. 420-437, 1992.
- [34] M. Kassis, J. El-Sana, "Learning free line detection in manuscripts using distance transform graph", "2019 International Conference on Document Analysis and Recognition (ICDAR)", pp. 222-227, 2019, doi:10.1109/ICDAR.2019.00044.
- [35] D. Brunet, D. Sills, "A generalized distance transform: Theory and applications to weather analysis and forecasting", *IEEE Transactions on Geoscience and Remote Sensing*, vol. 55, no. 3, pp. 1752-1764, 2017, doi:10.1109/TGRS.2016.2632042.
- [36] R. Fabbri, L. D. F. Costa, J. C. Torelli, O. M. Bruno, "2D euclidean distance transform algorithms: A comparative survey", *ACM Computing Surveys (CSUR)*, vol. 40, no. 1, pp. 1-44, 2008, doi:10.1145/1322432.1322434.
- [37] M. Momayyezi, A. Borsuk, C. Brodersen, M. Gilbert, G. Théroux-Rancourt, D. Kluepfel, A. McElrone, "Desiccation of the leaf mesophyll and its implications for CO₂ diffusion and light processing", *Plant, Cell & Environment*, vol. 45, no. 5, pp. 1362 - 1381, 2022, doi:10.1111/pce.14287.

Copyright: This article is an open access article distributed under the terms and conditions of the Creative Commons Attribution (CC BY-SA) license (<https://creativecommons.org/licenses/by-sa/4.0/>).



MAJID BANAEBAN received his bachelor's degree in Computer Engineering from Isfahan University of Technology (IUT) in 2007. He has done his master's degree in Electrical Communication Engineering from Malek-Ashtar University of the technology (MUT) in 2010. Currently he is doing his PhD in Informatics at Vienna University of Technology (TUWIEN).

He is a member of Patter Recognition and Image Processing (PRIP) group under the supervision of Prof. Walter G. Kropatsch. He is working on hierarchical structure in pattern recognition, Irregular Graph Pyramid, Combinatorial and Generalized map.



WALTER G. KROPATSCH From 1990-2021 he was full professor at TU Wien. He received his diploma degree in Technical Mathematics from the Technical University in Graz. He then moved to Grenoble, France to get the Maître d'Informatique from the University of Grenoble. His PhD in 1982 was on the Registration of Satellite Images with Maps. In 1984 he was invited by Prof. Azriel Rosenfeld to spend a year at the Center for Automation Research of the University of Maryland.

The creation of the first group in Austria dealing with pattern recognition and image processing in 1990 was jointly coordinated with the Austrian Association of Pattern Recognition (AAPR), that he initiated and led from 1984 until 1995. Under his leadership the AAPR became a member of the International Association of Pattern Recognition (IAPR) in which he held several leading positions, 2004-2006 he was its president. In 1996 he organized the main conference of the IAPR, the International Conference of Pattern Recognition in Wien, Austria. His scientific research focuses on pyramidal representations of images since his collaboration with Azriel Rosenfeld in 1984/85. The current graph-based pyramids follow similar concepts with the advantage that

graphs are much more flexible data structures than the regular grids as currently used as architectures in deep learning. In his more than 400 scientific contributions many other concepts and applications have been addressed. He is

currently senior editor of the journal of Electronic Imaging, and associate editor the journal of the Visual Computer and of several special issues in Pattern Recognition and Pattern Recognition Letter.